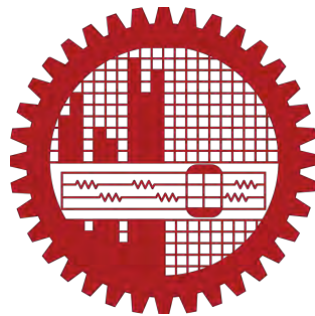


**DESIGN AND PERFORMANCE ANALYSIS OF SOLAR-TiO₂
IMMOBILIZED BED IN THE TREATMENT OF AZO DYE**

By

MD. RASHID-AL-MAMUN (0416022008F)

MASTER OF SCIENCE IN CHEMICAL ENGINEERING

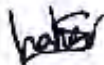


DEPARTMENT OF CHEMICAL ENGINEERING
BANGLADESH UNIVERSITY OF ENGINEERING AND
TECHNOLOGY (BUET)
DHAKA, BANGLADESH

AUGUST 29, 2020

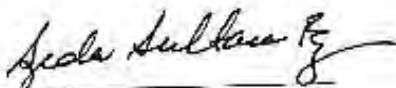
CERTIFICATION OF THESIS WORK

We the undersigned, glad to certify that **Md. Rashid-Al-Mamun**, candidate for the degree of Master of Science in Engineering (Chemical) has presented his thesis work title "**Design and Performance Analysis of Solar-TiO₂ Immobilized Bed in the Treatment of Azo Dye**", The thesis is acceptable in form and content. The student demonstrated satisfactory knowledge of the field covered by this thesis in an oral examination held in August 29, 2020.




Dr. Md. Shahinoor Islam
Associate Professor
Department of Chemical Engineering
BUET, Dhaka-1000.

**Chairman
(Supervisor)**




Dr. Syeda Sultana Razia
Professor and Head
Department of Chemical Engineering
BUET, Dhaka-1000.

**Member
(Ex-Officio)**



Dr. Ijaz Hossain
Professor
Department of Chemical Engineering
BUET, Dhaka-1000.

Member




Dr. Shakhawat Hossain Firoz
Professor and Head
Department of Chemistry
BUET, Dhaka-1000.

**Member
(External)**

CANDIDATE'S DECLARATION

I do hereby, declare that this thesis work or any part of it has not been submitted elsewhere for award of any degree or diploma.

Signature of the Candidate

A handwritten signature in black ink, appearing to be 'Rashid-Al-Mamun', is centered on a light gray rectangular background.

Md. Rashid-Al-Mamun

Student ID: 0416022008

August 29, 2020

ABSTRACT

Textile industry plays a vital role in the economic development of Bangladesh and around 6000 textile industries have been developed. Although it provides significant economic benefits, it also faces the social and environmental impacts associated with the generation of toxic wastewaters from its wet processing operations. Recently, advanced oxidation processes (AOPs) are considered as a highly attractive and competitive technology for the degradation of toxic compounds from industrial wastewater than conventional technology and make the technology more effective and efficient. In AOP, a strong oxidizing radical known as hydroxyl radical ($\cdot\text{OH}$) is generated that can react with toxic compounds in wastewater until mineralization. Among AOPs, the Solar- TiO_2 immobilized photocatalytic reactor is one of the most promising alternative technologies for the removal of toxic compounds from textile wastewater because the whole world is moving towards the application of renewable energy due to shortage of fossil fuel. Thus, the major objectives of this study were a synthesis of TiO_2 nanoparticles, design and construction of TiO_2 -immobilized reactors (with borosilicate glass, cement coated borosilicate glass, steel wire mesh) and investigation of the performance of these reactors in the degradation of methyl orange (MO) under solar irradiation.

TiO_2 nanoparticles were synthesized by sol-gel and thermal treatment methods. The physico-chemical properties of TiO_2 nanoparticle were characterized by various analytical and spectroscopic techniques such as UV-Vis, Fourier transform infrared spectroscopy (FT-IR), X-ray diffraction (XRD), Scanning electron microscopy (SEM) with EDX and Brunauer–Emmett–Teller (BET). The photocatalytic performance of MO dye with the help of immobilized- TiO_2 nanoparticles on borosilicate glass, cement coated borosilicate glass, and wire mesh in the presence of solar irradiation were investigated. The photocatalytic degradation of MO dyes was 97.8%, 88.6%, and 21.5%, respectively by using immobilized- TiO_2 on borosilicate glass, cement coated borosilicate glass and steel wire mesh with 5 h of contact time. The initial concentration and pH of MO dye were 10 ppm and 6.2, respectively. The photocatalyst doses were varied from 0.060 g to 0.150 g in all experiments. The result suggests that the solar- TiO_2 immobilized borosilicate glass reactor has high potential in the treatment of toxic compounds in textile wastewater. Based on that, the impacts of changing of different operational parameters such as dye concentration and oxidant H_2O_2 concentration on the performance of the borosilicate glass photoreactor was evaluated. The experimental results showed that removal rates were decreased with the increase of initial concentration of MO but increased with the increase of H_2O_2 oxidant concentration.

Dedicated to my parents

ACKNOWLEDGEMENT

Firstly, thanks to almighty Allah for giving me the strength and patience for completing this thesis work successfully.

It was a long journey (starting in April 2016) to finish the work. During this journey, I got encouragement from a wide range of people. I would like to express my sincere appreciation to my respectable teacher and research supervisor **Dr. Md. Shahinoor Islam**, Associate Professor, Department of Chemical Engineering, Bangladesh University of Engineering & Technology (BUET) for his guidance, prompting idea, laborious efforts, and dynamic encouragement throughout the progress of my research work.

I would like to thank **Dr. Kazi Bayzid Kabir, Dr. Md. Easir Arafat Khan, and Dr. Mohidus Samad Khan** for giving permission to use their laboratory equipment and for their continuous inspiration, help, particularly for valuable comments.

I would also like to thanks all the technicians and staff of Chemical Engineering Department for helping me with various essential equipment.

Finally, my thesis work could not be completed without the contribution from my parents, my elder brother, and my project partner **Shahina Kader** for their friendly attitude and helpful suggestions throughout the periods of this work. They continuously encouraged me for getting a higher degree. Their mental support and advice helped me the most for finishing this thesis carefully.

TABLE OF CONTENTS

	Page
	No.
<i>ABSTRACT</i>	i
<i>DEDICATION</i>	ii
<i>ACKNOWLEDGEMEN</i>	iii
<i>LIST OF FIGURES</i>	vii
<i>LIST OF TABLES</i>	x
CHAPTER 1	
INTRODUCTION	
1.1 Background	1
1.2 Scope of the study	4
1.3 Significance of the study	5
1.4 Objectives of the study	6
1.5 Outline of thesis	6
CHAPTER 2	
LITERATURE REVIEW	
2.1 Textile wastewater-a global scenario	8
2.2 Wastewater characteristics	8
2.3 Importance of dye removing from textile wastewater	9
2.4 Dye and selection of synthetic dye	10
2.5 Textile wastewater treatment processes	12
2.6 Advanced photochemical processes	16
2.7 Advance solar-TiO ₂ photocatalysis	19
2.7.1 Structure of TiO ₂ photocatalys	19
2.7.2 TiO ₂ as semiconductor photocatalyst under solar light	21
2.7.3 Strategies for improving TiO ₂ photoactivity	22
2.7.4 Mechanism and reaction kinetics of solar-TiO ₂ photocatalysis	22
2.8 Preparation technology of photocatalyst	25
2.9 Reactor design of photocatalyst	28
2.9.1 Immobilization of titanium dioxide (TiO ₂)	28
2.9.2 Immobilization procedures	29

2.10	Selection of radiation sources	29
2.11	Factors affecting the performance of photocatalytic reactor	31
2.12	Photocatalytic characterization and analytical techniques	37

CHAPTER 3

MATERIALS AND METHODOLOGY

3.1	Materials	42
3.1.1	Chemicals	42
3.1.2	Equipment and analytical instruments	42
3.2	Synthesis of TiO ₂ nanoparticles using sol-gel and heat treatment methods	42
3.2.1	Synthesis TiO ₂ nanoparticles with hydrolysis	43
3.2.2	Synthesis of TiO ₂ nanoparticles without hydrolysis	43
3.3	Characterization techniques of TiO ₂ nanoparticles	44
3.3.1	Ultraviolet-visible spectroscopy	44
3.3.2	Fourier transform infrared spectroscopy	45
3.3.3	Brunauer-Emmett-Teller Isotherm (BET) of TiO ₂ nanoparticles	45
3.3.4	Scanning electron microscopy (SEM)	45
3.3.5	X-ray diffraction (XRD)	46
3.4	Design and construction of TiO ₂ immobilized materials	47
3.4.1	Supporting materials for immobilization of TiO ₂	47
3.4.2	Immobilization of TiO ₂ on supporting materials	47
3.5	Experimental setup	53
3.6	Photocatalytic degradation of methyl orange under solar irradiation	53
3.6.1	Preparation of desired concentrated MO solution	54
3.6.2	Calibration curve	55
3.6.3	TiO ₂ -immobilized photocatalysis of MO under solar irradiation	55
3.6.4	Basic mathematical equations	57

CHAPTER 4

RESULTS AND DISCUSSION

4.1	Characterization of photocatalysts	58
4.1.1	Ultraviolet-visible spectroscopy (UV-Vis) of TiO ₂ nanoparticle	58
4.1.2	Fourier transforms infrared spectroscopy (FT-IR) of TiO ₂	61

	nanoparticle	
4.1.3	X-ray diffraction (XRD) of TiO ₂ nanoparticle	62
4.1.4	Scanning electron microscopy (SEM) of TiO ₂ nanoparticle	64
4.1.5	BET surface area analysis of TiO ₂ nanoparticle	67
4.2	Impact of solar irradiation on dye removal in the absence of photocatalyst	68
4.3	Effect of evaporation on dye degradation in the absence of photocatalyst	69
4.4	Photocatalytic activity assessment	70
4.4.1	Effect of thickness of TiO ₂ -immobilization on dye degradation	70
4.4.2	Reactors performance evaluation	73
4.4.3	Reaction kinetics study	76
4.5	Comparison of different reactor models and weight loss from different reactors	78
4.5.1	Comparison of reactors performance	78
4.5.2	Weight loss measurement	80
4.6	Impact of dye concentration and hydrogen peroxide addition on reactors performance	81
4.6.1	Impact of dye concentration	82
4.6.2	Impact of the addition of H ₂ O ₂ in the reactor	83
CHAPTER 5		
CONCLUSION		
5.1	Conclusion	85
REFERENCES		
87		
APPENDIX		
	Appendix A: BET isotherm of standard silica-aluminaa (SiO ₂ -Al ₂ O ₃), and TiO ₂ nanoparticles with and without hydrolysis	108
	Appendix B: Reaction kinetic study of pseudo-first-order, zero-order, and second-order	110

LIST OF FIGURES

		Page
		No.
Figure 2.1	Chemical structure of MO [80]	12
Figure 2.2	Structural phase of TiO ₂ nanoparticles [106]	20
Figure 2.3	Band gap energy of TiO ₂ nanoparticles [107]	20
Figure 2.4	Semiconductors and their band gap (eV) energy [111]	21
Figure 2.5	The photocatalytic degradation of organic compounds from textile wastewater in the presence of solar-TiO ₂ process [108]	24
Figure 2.6	Schematic diagram of TiO ₂ nanoparticles preparation by sol-gel method [109]	28
Figure 2.7	Total earth energy budget [134]	31
Figure 2.8	Explanation of band gap [148]	38
Figure 3.1	Heat treatment procedure from gel to TiO ₂ nanoparticle	43
Figure 3.2	Heat treatment procedure from gel to TiO ₂ nanoparticle without hydrolysis	44
Figure 3.3	Immobilizing materials (a) borosilicate glass, (b) white cement, and (c) steel wire mesh	47
Figure 3.4	(a) Circular borosilicate glass without TiO ₂ photocatalyst (b) TiO ₂ -immobilized borosilicate glass before treatment with 1 st , 2 nd , 3 rd , and 4 th layer (c) TiO ₂ -immobilized borosilicate glass after treatment with 1 st , 2 nd , 3 rd and 4 th layer	48
Figure 3.5	(a) Circular borosilicate glass without TiO ₂ photocatalyst (b) homogeneous cement layer (c) TiO ₂ -immobilized borosilicate glass with cement coating in before treatment with 1 st , 2 nd , 3 rd and 4 th layer (d) TiO ₂ -immobilized borosilicate glass with cement coating in after treatment with 1 st , 2 nd , 3 rd and 4 th layer	49
Figure 3.6	(a) Circular steel wire mesh without TiO ₂ photocatalyst (b) TiO ₂ -immobilized steel wire mesh in before treatment with 1 st , 2 nd , 3 rd and 4 th layer (d) TiO ₂ -immobilized steel wire mesh in after treatment with 1 st , 2 nd , 3 rd and 4 th layer	51
Figure 3.7	A set up of solar-TiO ₂ immobilized photocatalytic reactor	53
Figure 3.8	Chemical structure of MO	54
Figure 3.9	UV-Visible spectrum of an aqueous solution of MO at pH 6.20	54

Figure 3.10	Calibration curve of MO for dye degradation	55
Figure 4.1	UV-Vis spectra of TiO ₂ nanoparticles with and without hydrolysis preparation; (a) absorbance response and (b) reflectance response	59
Figure 4.2	Band gap energy of TiO ₂ nanoparticles prepared (a) by hydrolysis and (b) without hydrolysis	60
Figure 4.3	FT-IR analysis of TiO ₂ nanoparticle prepared with and without hydrolysis	62
Figure 4.4	XRD plot of TiO ₂ nanoparticle prepared with hydrolysis and without hydrolysis	64
Figure 4.5	(a) SEM image of TiO ₂ nanoparticle with hydrolysis, (b) Particle size analysis of TiO ₂ nanoparticles, (c) SEM image of TiO ₂ nanoparticle without hydrolysis, and (d) Particle size analysis of TiO ₂ nanoparticles without hydrolysis	65
Figure 4.6	EDX analysis (a) with hydrolysis at position 1, 2 and 3, (b) without hydrolysis at position 1, 2 and 3	66
Figure 4.7	Dye concentration under solar irradiation at open reactor in absence photocatalyst	69
Figure 4.8	Effect of evaporation at different reactor models	70
Figure 4.9	Concentration change of MO dye under solar irradiation (1 st , 2 nd , 3 rd , and 4 th layer of TiO ₂ immobilized reactors: 60 mg, 90 mg, 120 mg, and 150 mg, pH:6.2, initial MO dye conc.: 10 ppm) (a) borosilicate glass reactor, (b) cement coated borosilicate glass reactor and (c) steel wire mesh reactor	72
Figure 4.10	MO dye removal under solar irradiation (1 st , 2 nd , 3 rd , and 4 th layer of TiO ₂ immobilized reactors: 60 mg, 90 mg, 120 mg, and 150 mg, pH:6.2, initial MO dye conc.: 10 ppm) (a) borosilicate glass reactor, (b) cement coated borosilicate glass reactor and (c) steel wire mesh reactor	75
Figure 4.11	Pseudo-first-order reaction kinetics of MO dye removal in presence of solar irradiation (1 st , 2 nd , 3 rd , and 4 th layer of TiO ₂ immobilized reactors: 60 mg, 90 mg, 120 mg, and 150 mg, pH:6.2, initial MO dye conc.: 10 ppm) (a) borosilicate glass, (b) cement coated borosilicate glass and (c) steel wire mesh	77
Figure 4.12	Comparison of TiO ₂ -immobilized different reactors on a layer by layer	79

	(a) change of concentration and (b) change of dye removal	
Figure 4.13	Weight loss measurement from borosilicate glass, cement coated borosilicate glass, and steel wire mesh supporting materials (a) unit is g and (b) unit is percent	80
Figure 4.14	Impact of initial MO concentration on the removal efficiency (The third layer of TiO ₂ -immobilized coated borosilicate glass: 120 mg, pH: 6.2)	82
Figure 4.15	Impact of H ₂ O ₂ concentration on the removal efficiency (The third layer of TiO ₂ -immobilized coated borosilicate glass: 120 mg, pH: 6.2). (a) 10 ppm initial dye concentration with addition of 0.1 and 0.25 mL H ₂ O ₂ concentration, (b) 20 ppm initial dye concentration with addition of 0.1 and 0.25 mL H ₂ O ₂ concentration, and (c) 30 ppm initial dye concentration with addition of 0.1 and 0.25 mL H ₂ O ₂ concentration	84

LIST OF TABLES

		Page
		No.
Table 2.1	Typical characteristics of textile wastewater	9
Table 2.2	List of typical AOPs systems	15
Table 2.3	Advantage and disadvantages of different methods for TiO ₂ nanoparticle synthesis	26
Table 3.1	The weight of TiO ₂ immobilized on the borosilicate glass as layers	50
Table 3.2	The weight of TiO ₂ immobilized on the cement coated borosilicate glass as layers	50
Table 3.3	The weight of TiO ₂ immobilized on the steel wire mesh as layers	52
Table 4.1	The bandgap energy (eV) of the TiO ₂ nanoparticles prepared with hydrolysis and without hydrolysis	60
Table 4.2	FT-IR bands of TiO ₂ nanoparticle prepared with hydrolysis and without hydrolysis	61
Table 4.3	Summary of theoretical physicochemical properties of samples	64
Table 4.4	Summary of atomic and mass percentage of samples	67
Table 4.5	Surface area and pore volume measurement of composites	68
Table 4.6	Comparison of BET surface area among composites and components	68

CHAPTER 1

INTRODUCTION

This chapter represents the background and other relevant information on the current study. It states that the purpose of this research work concerning to present situation of the industry in Bangladesh. It also expresses the scope of application and significance of this type of research to remedy the industrial wastewater problem in the context of Bangladesh and Globally. The objectives of this research work have been discussed. Finally, the chapter represents the organization of the whole thesis.

1.1 Background

Environmental pollution has become a major concern in not only Bangladesh but also all over the world. It is caused by the disposal of various unwanted contaminants in the environment, which can cause serious damages to the living organisms and mankind. The sources of these unwanted contaminants are population growth, industrialization, urbanization, modernization, wash off plowed fields, construction and logging sites, eroded river banks, a rapid rise in transportation, inadequate and improper traffic management, poor sanitation systems, inefficient solid waste management, and natural disasters like earthquakes, tsunami and volcanic eruptions [1,2]. Researchers are trying to identify the contaminants that are disposed to the environment from various sources, their impacts on the environment, and the possible remediation techniques of these contaminants on the environment before disposal. Generally, environmental pollution is classified into five categories: air, water, soil, noise, and light pollution. Among these, water pollution is the most hazardous and dangerous [3,4].

Water can be polluted from many sources. Municipal, industrial, and agricultural sectors are the major contributors to water pollution [1]. The municipal wastewaters from homes, schools, offices, hospitals, and industries are discharged directly or indirectly into the surface water. Although the treatment processes of municipal wastewaters are well developed and simple, a very small fraction of these wastewaters is being treated in developing countries. This wastewater contains suspended solids, dissolved solids, oxygen-demanding materials, nutrients, and harmful bacteria. The sources of agricultural wastewater are cultivated lands, dairy farms, leaves and grass clippings, and livestock feedlots and pastures. Most of the constituents that are discharged from the agricultural sector are biodegradable (except pesticides and herbicides) that are removed by conventional treatment methods [5]. The most

important sector of water pollution is the industrial sector including textiles, dyeing, pharmaceuticals, plastics, leather, pulp and paper, sugar, petroleum, and metal works [6,7]. Among them, textile industries are found to be highly polluting industrial sector and a huge quantity of wastewater generated daily that are toxic and bio-persistent [8-9]. In Bangladesh, the textile industry is considered one of the largest manufacturing industries and it is the backbone of the economic development of the country for years. Around 6000 textile industries have been developed in Bangladesh and more than 5 million people (a majority of these people are women) are working there. Typically, this sector generates US 28.14 billion dollars and contributes around 20% of GDP by exporting 80% of its products [10].

Though the textile industry provides significant economic benefits, it also faces the environmental and social impacts associated with the generation of toxic wastewaters from its processing operations such as de-sizing, sizing, scouring, bleaching, mercerizing, dyeing, printing, finishing and other processes [11]. These wastewaters contain high BOD, COD, nitrogen, color, acidity, high suspended solids, high dissolved solids, surfactants, dyestuffs, heavy metals, and other soluble substances because of using various types of dyes to color their products [12-15]. To meet the color requirement, reactive and azo dyes which are highly water-soluble and toxic, are used. Around 10-20% of the used dyes are washed out with water as effluent which is hazardous (carcinogenic or mutagenic) and toxic to the environment [16,17]. It is reported that the produced textile wastewater can cause a serious impact on human health such as headaches, nausea, skin irritation, lungs problem, and congenital malformations. It also has an impact on the aquatic ecosystem by degrading the quality of the receiving water bodies and destroying the biodiversity of the surrounding environment [18,19]. Various treatment technologies have been developed for textile wastewater namely physical, chemical, and biological treatment [16,17]. Among physical processes, sedimentation, filtration (e.g. depth filtration and membrane), and adsorption are well-known processes that are applied for the treatment of textile wastewater. Sedimentation alone is not an effective treatment process. Membrane filtration is an effective process but frequent clogging of membrane from the foreign particles in wastewater is an issue and the process is highly cost-oriented. Adsorption is another effective treatment process; however, the adsorption does not indicate the real treatment of wastes and the process is costly. In adsorption, the contaminants transferred from the liquid phase to the solid surface of the used adsorbent. Therefore, the filtration and adsorption techniques are non-destructive due to the transfer of contaminants from the liquid phase to a solid surface that requires further

treatment [20,21]. The use of chemical coagulation processes is responsible for secondary pollution. The process produces a large amount of sludge, which is a concern to dispose. The biological treatment process is considered as the most economical and green treatment technology; however, because of the bio-persistence behavior of the azo dyes, it is not degraded from the application of the conventional biological treatment process. It has been reported that 11 of 18 azo dyes passed through the activated sludge process as untreated [22]. On the contrary, some traditional processes such as chlorination and ozonation are effective in destroying some classes of dyes [23,24]. The use of ozone can generate hydroxyl radicals ($\cdot\text{OH}$) that can oxidize a broad range of pollutants non-selectively and quickly and the process is known as advanced oxidation processes (AOPs). Advanced oxidation processes (AOPs) are considered as one of the most modern technologies that are capable of converting unwanted contaminants to harmless products. An inherent destructive nature is the actual advantage of AOPs. Literature investigated several AOPs such as Fenton, UV- H_2O_2 , UV- TiO_2 , solar- TiO_2 , O_3 -UV, and O_3 - H_2O_2 [25-27]. In recent years, researchers are considered photocatalytic AOPs for the treatment of industrial wastewater to make the processes cost-efficient, environmentally green, and most importantly sustainable. They reported that photocatalytic processes are innovative processes where the complex organic pollutants are completely destructed to CO_2 , water, and mineral acids [28].

At present, the development of the photocatalysis process has been focused on a wide range of research fields containing environmental and energy-related fields [29]. Recently, several approaches have been studied to increase the photocatalytic activity of TiO_2 for textile effluents treatment including metal doping (e.g. Fe, Cu, Al, Cr, Ag, Au, Pt, Pd, Zn, Bi, Mo, Co, Ni, Ce, etc.) [30-35], non-metal doping (e.g. N, C, S, F, I, B, etc.) and co-doping with metal/metal (Zn-Cu, Fe-Ni, Y-Dy, Cr-Co, Co-Ni, Ag-Mo, Zn-Eu, etc), metal/non-metal (Pt-N, Mn-P, Y-N, Mo-C, Cu-N, etc) and nonmetal/nonmetal (N-S, B-N, C-F, N-I, etc) with the semiconductor of TiO_2 [36-38]. The doping of metal/non-metals or co-doping with TiO_2 has been investigated under UV irradiation with suspension. The slurry suspension of traditional TiO_2 -based photocatalysis requires a subsequent filtration step to remove TiO_2 particles from water, which increases the treatment cost. Besides these, two more disadvantages are the difficulty of applying this method for continuous flow systems and the formation of agglomerates by TiO_2 particles which caused a loss of mass transfer and radiation transfer constraints [39,40]. To solve these problems, TiO_2 can be immobilized to various substrates such as glass materials (glass beads, glass plates, glass tube, reactor walls, and glass rings),

quartz, silica, silica gel, alumina, ceramics, stainless steel, alumina clays, activated carbon, fiberglass cloth, zeolites, polymeric material, rare earth oxides, magnesia, pumice stone, cellulose, etc. [41-43] that has greater interest to enhance the process engineering since it allows a straight forward separation and recovery of the catalyst from the process stream [44-46]. Among those substrates, glass is commonly used as the coating substrate due to its high transparency to the solar or UV radiation, good adherence to support TiO₂ powder without reduction of catalyst activity, resistance to high calcination temperature, chemical inertness with both catalyst and pollutant molecules, low cost, and resistance to corrosive environments [47]. The immobilized photocatalyst surface can be applied under solar or UV to degrade the textile dyes. The major problems of using UV irradiation are the cost and also have some negative aspects of using expensive UV light. Thus, this technique requires extensive improvement. Therefore, the solar light is an economical alternative for the UV radiation, and therefore, many types of research are being carried out on sunlight driven TiO₂ photocatalytic reactor [48,49]. The TiO₂ as a photocatalyst has a variety of applications because of having low cost, versatile, low operation temperature, biologically inert, low energy consumption, water insolubility, high photoactivity, high availability, low toxicity, high chemical stability, self-cleaning, suitable flat band potential, narrow bandgap and environmentally benign [50]. The successful and efficient application of photocatalysis depends on photocatalyst, pollutants, and sources of light. The TiO₂ photocatalyst is used for the effluent treatment of azo dye in wastewater in the presence of solar irradiation. Several studies applied to Solar-TiO₂ photocatalysts stated in the literature [51].

However, the application of this promising technique has not been considered in Bangladesh yet. Therefore, the current study will focus on achieving a greener process by using an immobilized TiO₂/solar-irradiation process for the treatment of azo dye. This paper sequentially represents the synthesis of TiO₂ nanoparticles, characterization of TiO₂ nanoparticles, TiO₂-immobilization on borosilicate glass, cement coated borosilicate glass, and steel wire mesh and apply these surfaces to degrade azo dye under solar irradiation. The reactor performance and optimization of reactor performance will be investigated based on dye removal by changing synthetic dye concentration and hydrogen peroxide dose.

1.2 Scopes of the Study

Textile industries play a vital role in the economic development of many developing countries including China, Bangladesh, Vietnam, India, Srilanka, etc. in the world and

therefore, it plays an important role to increase gross domestic products of these countries. These industries use different raw materials such as cotton, synthetic and woolen fibers; and chemicals including dyes. Approximately 10,000 different synthetic dyes are available in the market and worldwide. The annual production of these dyes is over 700,000 tons [52]. Nearly 200,000 tons of synthetic dyes are lost into the environment because of the inefficient dyeing process used in textile industries [53]. According to the World Bank estimation, about 17-20% of wastewater is generated from the textile dyeing and finishing treatment [12]. The wastewater is discharged to the environment from the industry after treatment using ineffective conventional treatment technology. This gives rise to an alarming environmental concern related to water pollution. The possible solution can be attached to the existing conventional wastewater treatment processes. The addition of AOPs such as noble photocatalytic treatment processes with conventional treatment seems to be the right step to make the system more efficient and effective.

This research was an attempt to synthesize TiO_2 nanoparticle for enhancing visible light photocatalytic performance. The photocatalyst will be able to degrade model textile azo dye (methyl orange) using immobilized borosilicate glass, cement coated borosilicate glass, and steel wire meshes reactors under solar irradiation. The current study will provide a preliminary direction towards a sustainable, greener, and comparatively economical solution for the treatment of textile wastewater.

1.3 Significance of the Study

Currently, the whole world is moving towards renewable energy applications where solar energy is considered to be of the highest potential. According to DoE (Department of Environment) requirements, all these industries must provide a road map to attain zero liquid discharge in three years. Presently, existing ETP technology in Bangladesh is not cost-effective and non-compliant with zero discharge requirements. The proposed novel technology requires a small footprint and can easily be installed by modifying the existing technology. This technology is highly efficient for the degradation of toxic compounds in textile wastewater. Thus, the proposed technology in addition to the existing technology can be able to remove contaminants effectively; and the treated effluent can be reused/recycled completely which will in turn lead to zero liquid discharge. The implementation of the new technology with the existing technology will secure the textile sector by developing sustainably and will assist to strengthen the respective job market. Therefore, it is expected

that the outcome from the current research will assist to improve the conventional wastewater treatment technology and will help to develop sustainable economic growth of the textile sector in Bangladesh.

1.4 Objectives of the Study

The main objective of this study was to investigate the performance of an immobilized TiO₂ photocatalytic reactor on the treatment of methyl orange dye in the presence of solar irradiation. The specific aims are listed below:

- Synthesis of TiO₂ nanoparticles by sol-gel technique along with the heat treatment method.
- Physical characterizations of TiO₂ nanoparticles using Fourier transform infrared spectroscopy (FT-IR, for the surface functional group), X-ray diffraction (XRD, for crystal structure), Scanning electron microscopy (SEM, for surface morphology) with EDX (for elemental analysis) and Brunauer–Emmett–Teller (BET, for the surface area).
- Design and construction of reactor by immobilizing TiO₂ on borosilicate glass, cement coated borosilicate glass, and steel wire mesh surfaces using heat treatment method.
- To study the reactor performance based on the photocatalytic degradation of methyl orange under solar irradiation.
- To optimize the reactor performance based on dye removal by changing the concentration of dye and hydrogen peroxide.

The possible outcomes of the immobilized TiO₂ based photocatalyst are (i) development of a new immobilized TiO₂-photocatalyst reactor and (ii) assistance to develop a sustainable scheme for the wastewater management and wastewater recycling in the textile sector.

1.5 Outline of the Thesis

The thesis paper has five distinct chapters. The outline of each chapter is given below:

Chapter 1: This is the introductory chapter of this thesis includes general information, background, scopes, significance, and objectives of research work.

Chapter 2: Chapter 2 includes a compilation of the relevant literature that has been reviewed for the study including textile wastewater scenario, wastewater characteristics,

dye degradation techniques, photocatalytic processes, advanced oxidation processes (AOPs), heterogeneous photocatalysis, reaction mechanism, photocatalyst synthesis techniques (sol-gel method), photocatalyst immobilization, radiation sources, factors affecting the photocatalytic activity, and characterization techniques.

Chapter 3: Chapter 3 presents the materials and methodology of the research. Initially, the sol-gel preparation technique of TiO₂ nanoparticle has been presented in the chapter. The subsection includes the characterization technique of TiO₂. Finally, the Chapter includes the immobilization of TiO₂ photocatalyst on the surface and application of the photocatalytic reactor to the degradation of methyl orange dye.

Chapter 4: Chapter 4 provides the results and discussion of the research work. Firstly, it describes all the characterization techniques employed in this research. Secondly, it includes the photocatalytic performance of methyl orange dye as immobilized-TiO₂ on borosilicate glass, cement coated borosilicate glass, and steel wire mesh and finally optimization and assessment of reactor performance based on dye removal.

Chapter 5: This Chapter includes the concluding remarks of the study.

CHAPTER 2

LITERATURE REVIEW

A well-known new technology of textile wastewater treatment is the photocatalysis process by using a solar-TiO₂ immobilized reactor in the last decade. Several researchers have been developed the process in the lab scale and are trying to install commercially. The Chapter represents a global scenario of textile wastewater treatment processes along with photocatalytic processes including solar-TiO₂. It also contains photocatalytic reaction mechanisms and kinetics, preparation techniques of TiO₂ nanoparticles, immobilization techniques of photocatalyst on the surface, and the factors that affect the photocatalytic reactor performance. Finally, the Chapter also includes the characterization technique of TiO₂ nanoparticle.

2.1 Textile Wastewater- A Global Scenario

Textile is one of the most important sectors in not only Bangladesh but also in the world and has a long history of many centuries. In Bangladesh, being a labor-abundant country started the process of industrialization by concentrating on labor-intensive products such as textiles and clothing. The textile industry consumes large amounts of potable and industrial water as processing water (90-94%) and a relatively low percentage as cooling water (6-10%). The recycling of treated wastewater has been recommended due to the high levels of contamination in dyeing and finishing processes (i.e. dyes and their breakdown products, pigments, dye intermediates, auxiliary chemicals, and heavy metals, etc.) [54,55]. Among those, dyes or color removal has been a matter of considerable interest during the last two decades [56,57]. In Europe, environmental legislation has necessitated increasingly green textile processing. This has, and is being achieved, through recycling of chemicals and water, production and use of biodegradable textile chemicals and dyes, as well as efficient effluent treatment [58]. According to U.S E.P.A, an average dyeing facility generates 1 to 2 million gallons of wastewater per day. About 10,000 different dyes and pigments are produced annually worldwide [59].

2.2 Wastewater Characteristics

The textile industry plays a vital part in the economy of several countries around the world [60]. A typical textile dyeing process consists of resizing, scouring, bleaching, dyeing, finishing, and

drying operations. The effluent generated from the textile processing industries is considered to be a very complex and inconsistent mixture of many pollutants, such as, a mixture of heavy metal ions (e.g., Cr, Al, Cu, etc.), suspended solids, dissolved solids, inorganic salts, dispersing agents, dyestuffs, and other toxic organic pollutants including polyvinyl alcohol, starches, various surfactants, organic-chlorine based pesticides, biocides as well as acidic and alkaline contaminants. Effluents discharged from textile industries are characterized by the low BOD, high COD, and variation of pH in the range of 2-12 [61,62]. Among those processes, dyeing is a fundamental operation during textile fiber processing. The dyeing process consumes large quantities of water for dyeing, fixing, and washing and produces a large volume of wastewater containing organic dyestuffs [63]. Over the last decades, the increasing demand for dyes by the textile industries has shown a high pollutant potential [61]. The typical characteristics of textile wastewater are summarized in Table 2.1.

Table 2.1: Typical characteristics of textile wastewater

Temp (°C)	pH (-)	Color (Pt-Co)	COD (mg/l)	BOD (mg/l)	TS (mg/l)	TSS (mg/l)	TDS (mg/l)	Ref.
35-45	6-10	50-2500	150-12000	80-6000	--	15-8000	2900-300	[64]
21-62	6.95-11.8	50-2500	150-30000	80-6000	6000-7000	15-8000	2900-3100	[65]
33-45	5.5-10.5	--	150-10000	100-4000	--	100-5000	1500-6000	[66]
35-45	6-10	50-2500	150-10000	100-4000	--	100-5000	1800-6000	[67]
35-45	7-9	50-2500	150-12000	80-6000	--	15-8000	2900-3100	[68]
35-45	6-10	--	1000-1500	300-500	--	200-400	8000-12000	[69]

2.3 Importance of Dye Removing from Textile Wastewater

Water is essential to animals and plants for their survival. Human beings use water for drinking, bathing, washing, culinary purpose, transportation, industrial and agricultural activities, etc. [70]. The day to day human activities and industrial revolution have influenced the flow and storage of water and the quality of available freshwater. Textile industries are using various dyes and pigments to color products. These industrial wastes are the main sources of water as well as environmental pollution because these contain a lot of non-biodegradable organic dyes. In dyeing processes, 10-15% of all dyestuffs are being lost directly to wastewater besides any pretreatment. The discharge of colored wastewater from these industries produces an eco-toxic

hazard and introduces the potential danger of bioaccumulation [71]. That's why the removal of organic dyes from water is the prime challenge to the present world.

2.4 Dyes and Selection of Synthetic Dye

Dyes are used to imparting color to textiles such that the coloring is not readily altered by washing, heat, light, or other factors to which the material is likely to be exposed. Most dyes are organic compounds. The dye is generally applied in an aqueous solution and may require a mordant to improve the fastness of the dye on the fiber [72]. A substance is referred to as a dye when it bears the following criteria [73]:

1. Dyes must have the desired color to match the object to be dyed.
2. It must be able of being fixed to the fabrics or supports directly or indirectly with the help of certain reagents known as mordant.
3. The color must be fast to light when fixed to the supports and resistant to soap and water.

By forming covalent bond or complexes with salts or metals, the dyes can be adhered to compatible surfaces by solution through the mechanical retention or physical adsorption [74]. There are two types of dyes, one is a natural dye and another is the synthetic dye.

2.4.1 Natural Dyes

The common natural sources of these dyes are the vegetables, trees, plants, lichens, and few insects. The main ingredients of dyes are natural fibers that are mainly come from the two distinct origins; one is the vegetable origin and another is the animal origin. There has a strong affinity between the animal origin and natural dyes including silk, mohair, and wool that are usually used. Similarly, strong affinity is also observed between the plant origin includes jute, cotton, hemp, flax or linen, ramie, etc. and natural dyes [75]. Mordant such as salts (iron, copper, alum, tin salts), vinegar, tannin, natural alum, ammonia, etc. are used to bind the natural dyes. Mordant is a substance used in fabrics by forming an insoluble compound. These can adsorb on natural fiber and react with the dye to generate a less soluble form. Notice that the natural dye cannot be applied directly to cotton without pretreatment with the mordant.

2.4.2 Synthetic Dyes

Nowadays, synthetic dyes are the most widely used dyes in the textile industry. Synthetic dyes are used as a replacement for natural dyes. According to the chemical structure of their particular chromophoric group, the synthetic dyes are named such as triphenylmethane, diphenylmethane, xanthene, oxazine compounds, etc. [76]. Among these chemical structures, the azo dyes are one of the most popular varieties of synthetic dyes. Now a day, 90% of dyeing units are using the azo dyes because it can easily be synthesized. The major portion of the synthetic dyes can be divided into groups like cationic, anionic, and non-ionic [77]. The synthetic or organic dyes are used in the textile dyeing process have a high chemical, photolytic stability.

2.4.3 Azo Dyes

One of the major problematic dyes is considered to be azo dyes. The azo dye has shown countless detrimental consequences on the environment [78]. It typically resists bio-degradation due to its fused aromatic ring structure. In addition to that, it can easily be reduced to toxic amines due to the presence of an azo group. These amines along with existing azo dyes are carcinogenic and easily participate in the human food cycle. The chemical's participation can lead to allergies, dermatitis, malignant tumors, and cancer. Beyond all these concerns, LD50 value for aromatic azo dyes varies between 100 and 2000 mg/kg body weight. A person can easily consume it, whose water and food cycle are infected by azo dye wastewater. To date, in the existing marketplace, about 50-70% of the available dyes are azo dyes [79]. Azo dyes are being classified into three departments like mono-azo dye, di-azo dye, and tri-azo dye. This classification is done based on the presence of the number of azo bonds. Unfortunately, numerous sorts of azo dyes have been found hazardous for the ecosystem. To some extent, an azo dye is lethal for humans due to the formation of aromatic amines which is carcinogenic [80,81].

2.4.4 Methyl Orange

One of the most widespread types of model azo dye is methyl orange (MO). MO is a regularly used as water-soluble azo dye and anionic in nature. The chemical formula of MO is $C_{14}H_{14}N_3NaO_3S$. There is a presence of $-N=N-$ as shown in the molecular structural arrangement represented in Figure 2.1.

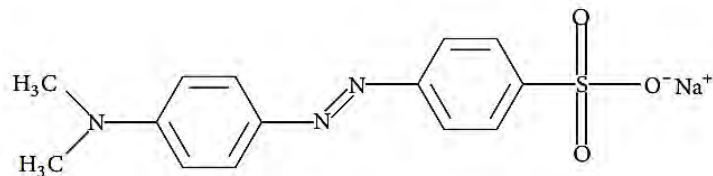


Figure 2.1: Chemical structure of MO [80].

MO obstructs the diffusion of light even at a very low concentration. The obstruction causes an adverse effect on the photosynthesis process and results in ecosystem disruption. A great deal of effort has been executed on examining the decomposition of methyl orange azo-dye. Recently, MO degradation using photocatalyst has received massive interest from environmental scientists. The quest is to find the best photo-catalytic reactions mechanism to enhance the photocatalytic degradation of MO [80,81].

2.5 Textile Wastewater Treatment Processes

The liquid is discharged from the industry containing unwanted contaminants depends on the types of chemicals used in the industry and the applied treatment process on the wastewater. The treatment processes are classified as [16,17]:

- i) Physical methods
- ii) Chemical methods
- iii) Biological methods

2.5.1 Physical Methods

In physical methods, the contaminants from wastewater are separated by applying mechanical force (filtration), a physical force like Vander walls force (adsorption), and gravitational force (sedimentation) are well-known processes that are applied for the treatment of textile wastewater [82]. The physical unit operations involved here are adsorption, floatation, filtration, gravity settling, mixing and sedimentation, screening, gas transfer, and volatilization. Sedimentation is not effective for the removal of very fine and highly colloidal impurities from water including clay particles, gels, and emulsions. This removal can be greatly increased by the addition of certain chemical compounds in water [83]. The most well-established operation is the filtration process which involved in the treatment of potable water for achieving supplemental removals of

suspended solids from wastewater [84]. Among filtration, the membrane filtration removes all types of dye, recovery, and reuse of chemicals and water. But the disadvantages of membrane filtration are high running cost, concentrated sludge production, and dissolved solids are not separated in this process [85]. Another is the adsorption process that has particular advantages of good removal efficiency of a wide variety of dyes, leaving no fragments in the wastewater [86]. But the limitation of the process is very expensive and cost-intensive regeneration is required [87].

2.5.2 Biological Methods

Biological treatments are considered reproduction, artificially, or otherwise of self-purification phenomena existing in the natural environment. There are different biological treatments performed in aerobic or anaerobic or combined anaerobic/aerobic conditions. The processing, quality, adaptability of microorganisms, and the reactor type are decisive parameters for removal efficiency [88]. The biological treatment process for the decolorization of industrial effluents is ambiguous, different, and divergent [89]. The most currently used biodegradation involves aerobic microorganism which utilizes molecular oxygen as reducing equivalent acceptor during the respiration process. But biodegradation in anaerobic environment conditions (anoxic and hypoxic environments) also occurs and the survival of microorganisms is possible by using sulfate, nitrates, and carbon dioxide as electron acceptors [90]. The advantage of the aerobic process is the partial or complete decolorization for all classes of dyes but the limitation is the expensive treatment [91]. On the contrary, the advantage of the anaerobic process is resistant to a wide variety of complex colored compounds and also biogas produced that is used for steam generation. But the disadvantage of the anaerobic process is the longer acclimatization phase [92].

2.5.3 Chemical Methods

Chemical methods are those where contaminants are degraded chemically by using a chemical to react with the contaminants. This type of treatment is used when the biological treatments are not efficient. Usually, it is used as a pre-treatment step to biological treatment. The more popular use of such treatment processes is to degrade non-biodegradable and/or toxic contaminates. The coagulation-flocculation is a widely used chemical method in the industry. However, the process

generates a huge amount of sludge that needs to address further. Chemical disinfection is another widely used method that is applied after biological treatment. The chemical methods can be classified into two broad categories and those are:

- 1) classical oxidation treatment
- 2) advanced oxidation processes

2.5.4 Classical Oxidation Treatment

In the classical oxidation treatment process, an oxidant is added to the water that contains contaminants. The oxidants oxidize the organics in wastewater and mineralize the chemicals. There are various types of oxidizing agents including chlorine, oxygen, hydrogen peroxide, and ozone that are used in textile wastewater treatment.

- 1. Chlorine:** Chlorine represents a strong and cheap oxidizing agent that can be used efficiently for wastewater treatment. But the disadvantages of applying chlorine are low selectivity, requires high dosage, and chlorogenic byproducts formation.
- 2. Oxygen:** Oxygen is considered as a moderate oxidizing agent due to its low cost operating conditions that make it an attractive choice.
- 3. Hydrogen peroxide:** Hydrogen peroxide is one of the most proposed oxidizing agents recommended for a large variety of systems. It can be applied alone or with a catalyst.
- 4. Ozone:** Ozone is a strong oxidizing agent, which has the same advantage as oxygen and peroxide. The most problem in an application such as treatment is the difficulty of ozone production and the instability of ozone.

2.5.5 Advanced Oxidation Processes (AOPs)

Advanced oxidation processes refer to a set of chemical treatment procedures that are designed to remove organics and sometimes inorganic materials in water and wastewater by oxidation through reactions with hydroxyl radicals ($\cdot\text{OH}$). The organic compounds that are discharged from the industry pose severe problems in biological treatment systems due to their resistance to biodegradation and toxic effects on microorganisms. As a result, the use of alternative treatment technologies aiming to mineralize or transform refractory molecules into others which could be further biodegraded is a matter of great concern. Thus, AOPs have been used for the treatment of wastewater containing recalcitrant organic compounds such as dyes, pesticides, surfactants,

coloring matters, pharmaceuticals, and endocrine-disrupting chemicals. Moreover, they have been successfully used as pretreatment methods to reduce the concentrations of toxic organic compounds that inhibit biological wastewater treatment processes. There are two types of AOPs, these are homogeneous and heterogeneous systems. The heterogeneous system is the most widely used process for the treatment of textile wastewater [93,94]. In AOPs, the hydroxyl radicals ($\cdot\text{OH}$) are effective in destroying organic chemicals because they are reactive electrophiles (electron preferring) which react rapidly and non-selectively with nearly all electron-rich organic compounds. They have an oxidation potential of 2.33 eV and exhibit faster rates of oxidation reactions comparing to conventional oxidants such as H_2O_2 or KMnO_4 . The major types of advanced oxidation processes are listed in Table 2.2.

Table 2.2: List of typical AOPs systems

With Irradiation	Without Irradiation
Homogeneous systems	
O_3 /ultraviolet (UV)	$\text{O}_3/\text{H}_2\text{O}_2$
H_2O_2 /UV	$\text{O}_3/\text{OH}\cdot$
Electron beam	$\text{H}_2\text{O}_2/\text{Fe}^{2+}$ (Conventional Fenton)
Ultrasound (US)	
H_2O_2 /US	
UV/US	
$\text{H}_2\text{O}_2/\text{Fe}^{2+}$ /UV-Photo-Fenton	
Heterogeneous systems	
TiO_2/O_2 /UV/Solar	Electro-Fenton
$\text{TiO}_2/\text{H}_2\text{O}_2$ /UV	

The major advantages of AOPs in the wastewater treatment are (i) non transferring of pollutants from the one phase to another, (ii) able to couple with other physicochemical and biological processes, (iii) capable of eliminating organic compounds effectively in an aqueous phase, (iv) rapid reaction rates, and (v) able to remove heavy metals as a precipitate of $\text{M}(\text{OH})_x$ [95].

2.6 Advanced Photochemical Processes

The principle of the photochemical reaction is the addition of energy such as UV or solar light as a form of radiation that can be absorbed by an organic compound in textile wastewater to reach an excited state. Most of the cases, this radiation energy is sufficient for breaking the aromatic ring. Different investigations indicate that several organic contaminants can be decomposed partially or totally into harmless substances or more biodegradable substances through oxidation based on solar light [96].

In the photochemical reactions, the main step is the generation of the hydroxyl radical by photolysis of the water according to the following reaction:



When the hydroxyl radical $\cdot OH$ gets electronic radiation, it generates a huge quantity of intermediate products, which leads to considerable effect in increases the rate of photo-oxidation kinetics of the contaminants, and thus, this makes the process is valid for all types of effluents even with low contaminant concentration contaminate. The photochemical treatment has a good effect on solving the problem of refractors compound [97].

2.6.1 O₃/UV

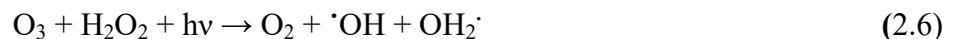
Ozone combined with UV results in a net enhancement of dye degradation due to ozone decomposition and H₂O₂ formation:



Another advantage of ozone and UV is a substantial reduction in the amount of ozone required as compared to a system using O₃ alone. The disadvantage of this process is the high operating cost.

2.6.2 O₃/H₂O₂/UV

The addition of H₂O₂ in the O₃/UV can accelerate the decomposition of ozone, which results in an increase in the rate of $\cdot OH$ generation [98].



2.6.3 UV/H₂O₂ Process

In the UV/H₂O₂ process, light is absorbed by a molecule that can increase the molecule's ability to lose or gain electrons and excited. This excitation state of molecules is highly reactive with ([•]OH) radical. The photocatalysis involves the photolysis of hydrogen peroxide in the presence of ultraviolet light. The most accepted mechanism for this H₂O₂ photolysis is the rupture of the O-O bond by the action of ultraviolet light forming two hydroxyl radicals shown in below [99].



There are some difficulties in photocatalysis of H₂O₂ in the presence of UV, and these are:

- Requires a low wavelength (below 200-400 nm) to make the process.
- Aromatic organic compounds require higher light concentration that increases the cost of photocatalysis.
- Not applicable to in situ treatment.

In the UV/H₂O₂ process, require an acidic pH that can be performed by addition of acid. The method of irradiation is not limited to the UV light and can be extended to natural sunlight. This may require longer processing time, but that may be outweighed by the convenience of using natural light. Chemicals that can be treated with this technique include aromatic hydrocarbons, substituted aromatic hydrocarbon, phenols, alkanes, alkynes, ethers, and ketones, both in their substituted and non-substituted forms.

The rate of the aqueous H₂O₂ photolysis was found to be pH-dependent and increases when alkaline conditions are used, probably because at 253.7 nm, the anion peroxide H₂O₂ has higher molar absorption coefficient (240 vs 18.6 M⁻¹cm⁻¹) [100,101]. After that the ([•]OH) radical can attack to the hydrogen peroxide leading to the following sequence of equations:



The above reactions produce different radicals that react with organic contaminants to degrade. This system has the advantage that if it works with ozone, it provides cheaper and faster hydroxyl radicals, which makes the ozone a good selection with H₂O₂. The reaction of ([•]OH) radical with an organic substrate can be executed in three different ways:

With hydrogen abstraction:



With electrophilic addition:



With electron transfer:

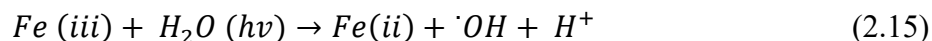


The recombination of radicals should also be taken into account:



2.6.4 UV/Fe (III)

UV/Fe (III) is considered one of the most common treatment processes in textile wastewater in the presence of UV light. Fe (III) acts as photocatalyst in the presence of UV irradiation photocatalyst has been studied [102]. In the photocatalytic process, the photocatalyst is not only the absorbed UV photons lead to organic matter degradation but also undergoes a photo-redox reaction that produces more hydroxyl radicals.

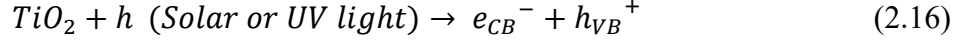


It has been studied that degradation of nitro-benzene by UV/Fe (III), reduced 80% of nitro-benzene during 60 min irradiation time [103].

2.6.5 TiO₂/UV/Solar

TiO₂ has widely been used as a heterogeneous photocatalyst for the degradation of organic dye compounds from the effluent of the textile industry. Thus, great attention has been devoted to the TiO₂ in photocatalysis of wastewater treatment. The advantage of TiO₂ as photocatalyst is that the reactions do not suffer the drawbacks of photolysis reactions in terms of the production of intermediate products because organic pollutants are usually completely mineralized to non-toxic substances such as CO₂, HCl, and water [104].

In irradiation, photons and electrons on the TiO₂ surface are excited in the conduction band thus positive holes are formed in the valance band. The holes and electrons can either recombine or generate thermal energy. A powerful hydroxyl radical is produced by reaction with holes and electron donors in the solution which can oxidize the organics on the surface. The holes can also oxidize the substrate by direct electron transfer. In brief, the photogeneration of radical species in the TiO₂/UV/Solar system can be described as follows [105].



There are different types of inorganic oxidants such as O_3 , H_2O_2 , BrO_3^- , $S_2O_8^{2-}$ and ClO_4^- have been proposed to increase the efficiency of TiO_2 /Solar/UV treatments. These oxidants increase the number of trapped electrons, which prevents recombination of ($\cdot OH$) radical and generate oxidizing radicals that can enhance the photocatalytic degradation of dye in textile wastewater.

2.7 Advanced Solar- TiO_2 Photocatalysis

Treatment of textile wastewater using titanium dioxide (TiO_2) photocatalysis has been started from the last decade and reached attention to the researchers because of its versatile application. The variety of applications of TiO_2 as a photocatalyst has been taken place because of low operating temperature, biologically inert nature, low energy consumption, water insolubility, ease availability and photoactivity, less toxicity, high chemical stability, suitable flat band potential, narrow bandgap and environmentally benign. The successful and efficient application of photocatalysis depends on the quality of photocatalyst, nature of pollutants, and source of light, which should be in close contact with each other [50].

2.7.1 Structure of TiO_2 Photocatalyst

Titania or Titanium (IV) oxide (TiO_2) is an n-type semiconductor. It exists in three forms in generally like as anatase, rutile, and brookite is given in Figure 2.2. Rutile is a common form of TiO_2 which is stable at high temperatures, while the anatase phase is stable at low temperatures. The brookite phase is rare, unstable, and uncommon and that does not show catalytic behaviors.

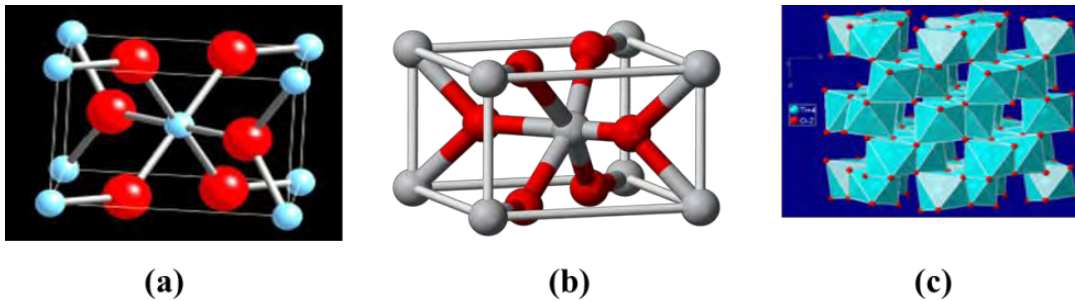


Figure 2.2: (a) Anatase phase of TiO₂, (b) Rutile phase of TiO₂, and (c) Brookite phase of TiO₂ [106].

TiO₂ crystalline structure affects photocatalytic activity. Anatase phase has the best photocatalytic activity of TiO₂ semiconductor because of its energetic separation capacity between the valence and conduction band in the presence of solar radiation [106]. In solar radiation, TiO₂ semiconductor absorbs photon energy from solar radiation and causes the molecular charge separation and excitation. The bandgap energy of TiO₂ photocatalyst (3.03 eV for rutile and 3.2 eV for anatase) is less compared to other semiconductors like as ZnO (3.35 eV) and SnO₂ (3.6 eV). The conduction and valence band energies of anatase TiO₂ photocatalyst are -0.1 V and +3.1 V, respectively. The bandgap energy level of TiO₂ photocatalyst is shown in Figure 2.3 [107].

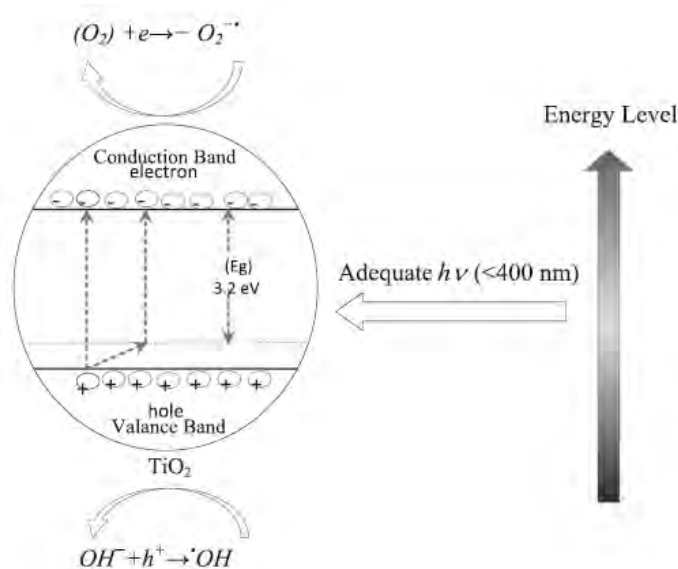


Figure 2.3: Band gap energy level of TiO₂ nanoparticles [107].

2.7.2 TiO₂ as Semiconductor Photocatalyst under Solar Light

The photocatalytic heterogeneous wastewater treatment processes which use various groups of solid semiconductors such as oxides (TiO₂, CeO₂, ZnO, ZrO₂, Fe₂O₃, WO₃, and V₂O₅) and sulfides (ZnS, CdS). However, many of these semiconductors have enough bandgap energies which need to overcome for the photocatalytic chemical reactions as shown in Figure 2.4. Although the metal oxides are less powerful catalysts (higher bandgap energies) than the noble metals, these are more suitable as photocatalytic semiconductors because of their resistive behavior to deactivation and poisoning [108,109]. It is reported that titanium TiO₂ is the most effective and efficient as a semiconductor photocatalyst under solar light. It is because of having high stability and high ultraviolet absorption of TiO₂ that allows in the photocatalytic degradation of chemicals in water and air. The TiO₂ nanoparticles are usually integrated into thin films or immobilized on a surface and doped with other materials to avoid free nanoparticles in water [110].

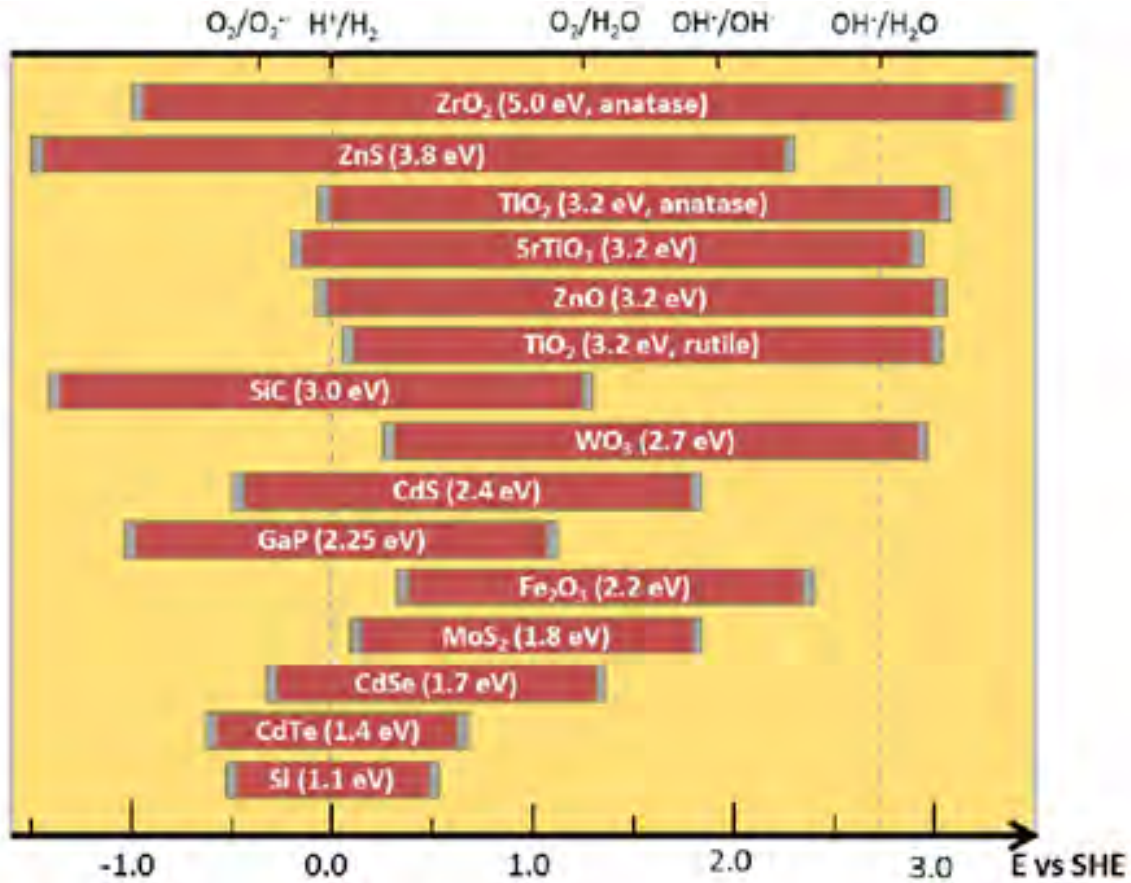


Figure 2.4: Semiconductors and their band gap (eV) energy against standard hydrogen potential [111].

2.7.3 Strategies for Improving TiO₂ Photoactivity

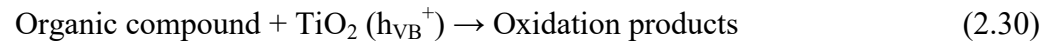
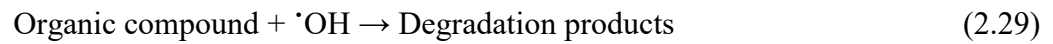
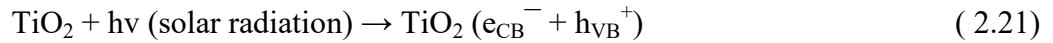
The major factors affecting the TiO₂ photocatalytic performance are pore volume, size, specific surface area, density, crystalline phase, pore structure, and bandgap energy. The properties of TiO₂ except the bandgap energy can be improved by morphological modification during the synthesis. It is reported that the overall efficiencies of TiO₂ can be enhanced significantly by controlling the semiconductor morphology [29]. The widely used TiO₂ morphology is mono-dispersed nanoparticles where the diameter is controlled to contribute to the benefits associated with the smaller crystallite particles [112]. TiO₂ nanoparticles have higher bandgap energy to generate photons [•]OH radical and thus, chemical modification (doping) has been applied to reduce the bandgap energy. The chemical modification not only reduces the bandgap energy but also shifts the photocatalytic activity to visible light active (VLA). Moreover, the introduction of the doping concept can modify the other physical properties such as surface morphology which can increase the photoactivity of the TiO₂ photocatalyst.

One of the major disadvantages of TiO₂ photocatalysis is the recombination of the photo-generated electron (e_{CB}^-) and hole (h_{VB}^+). This step decreases the quantum yield and causes energy wasting. Therefore, the recombination of the e^-h^+ process would be inhibited by using efficient photocatalysis. It is reported that the addition of dopants such as metal and non-metal can counter the recombination problem between the electrons and holes by increasing the charge separation. The advantages of doping for photocatalytic degradation are: (i) increased photoactivity and thus, complete degradation within a very short time (ii) reuse of photocatalyst (iii) required a smaller amount of photocatalyst (iv) required less energy [113]. Therefore, the photocatalytic activity of TiO₂ can be increased by doping or co-doping of different metals and nonmetals with TiO₂ nanoparticles for the treatment of textile wastewater.

2.7.4 Mechanism and Reaction Kinetics of Solar-TiO₂ Photocatalysis

The Solar-TiO₂ treatment process is an indirect but effective heterogeneous photocatalytic process, which uses energy from solar radiation to break down various organic and inorganic substances in the wastewater. The photocatalytic degradation process has five steps as stated below [114,115]: (i) the mass transfer of organic pollutants from the liquid phase to the TiO₂ surface; (ii) adsorption of the organic pollutants onto the photon activated TiO₂ surface; (iii) photocatalysis reaction on the TiO₂ surface (iv) desorption of organic pollutants (intermediate)

from the TiO₂ surface; and (v) the mass transfer of the organic pollutants (intermediate) from the interface region to the bulk fluid. The overall process is involved with the generation of very powerful non-selective hydroxyl radicals ($\cdot\text{OH}$) to destroy hazardous organic compound adsorbed on the TiO₂ surface. The produced ($\cdot\text{OH}$) radical has the highest oxidation potential of 2.80 V and the highest relative oxidation power 2.06 V respectively [116]. The mechanism started by equations (2.21) to (2.31) below is widely accepted to describe the photodegradation of organic compounds by the TiO₂ photocatalytic process. [81]:



When TiO₂ nanoparticles are irradiated with solar light, a photogenerated hole is produced Eq. (2.21). As a result, the photogenerated holes undergo an oxidation reaction with OH⁻ or H₂O and thus, generate hydroxyl radicals Eq. (2.22)-(2.23). This $\cdot\text{OH}$ radical is principally responsible for the degradation of organic species. As shown in Eq. (2.24), and efficient electron trap oxygen is used, which prevents the recombination of electrons and photogenerated holes. Eq. (2.25)-(2.28) represents the other reactions of solar-TiO₂. If oxygen is limited, the rapid recombination of photo produced electrons and holes in TiO₂ lowers the efficiency of photocatalytic reactions. In the process, the charge carriers h_{VB}^+ and e_{CB}^- can recombine or h_{VB}^+ can be scavenged by oxidizing species such as OH⁻, H₂O, organic compounds, and e_{CB}^- by reducing species such as O₂ in the solution. Mainly these combinations lead to the formation of hydroxyl radicals ($\cdot\text{OH}$), hydroperoxyl radicals (HOO \cdot), and superoxide radical anions (O₂ \cdot^-) on the surface of TiO₂ that are capable to destroy a large variety of organic compounds (toxic and non-toxic) and biological

agents [117,118]. The mechanism of the degradation of organic compounds under the Solar-TiO₂ process from textile wastewater has been explained in Figure 2.5.

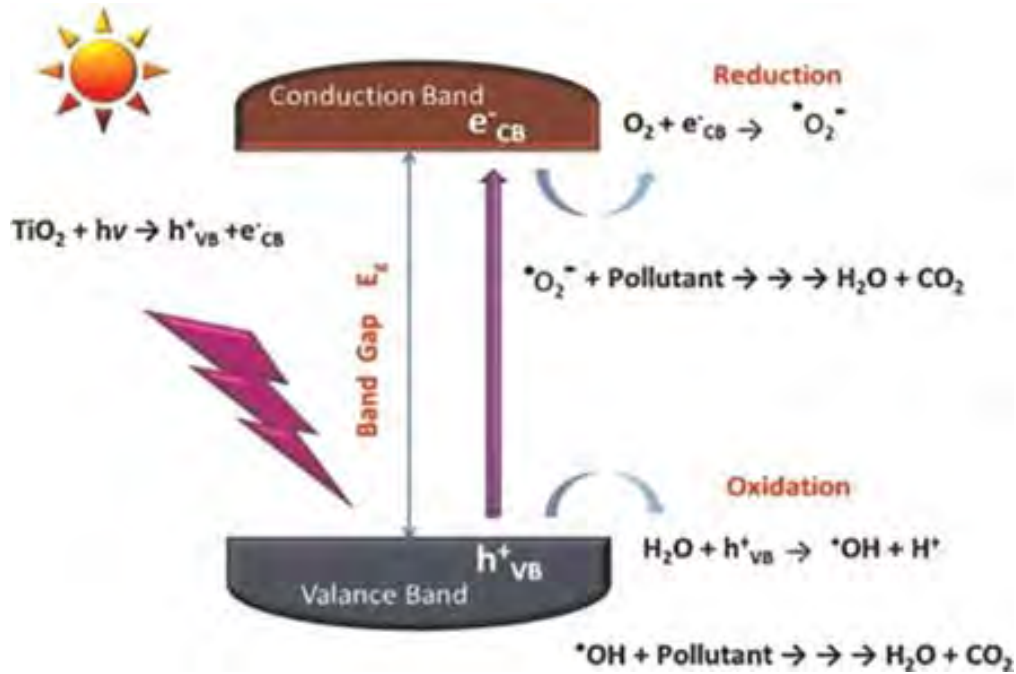


Figure 2.5: The photocatalytic degradation of organic compounds from textile wastewater in the presence of solar-TiO₂ process [108].

In photocatalytic studies, first-order kinetics is found sufficient to model the photo mineralization of organic compounds. It is reported that first-order kinetics is only valid for low concentration dye. One of the most favorable models to describe the dye degradation reaction is Langmuir–Hinshelwood (LH) kinetic model [119].

$$r = -\frac{dc}{dt} = k_r \theta_x = \frac{k_r KC}{1+KC} \quad (2.32)$$

According to L-H model represented by Eq. (2.32), the photocatalytic reaction rate (r) is proportional to the fraction of surface coverage by the organic substrate (θ_x), k_r is the reaction rate constant, C is the concentration of dye and K is the Langmuir adsorption constant.

L-H model depends on several assumptions, which include:

- i. The reaction system should be in dynamic equilibrium
- ii. The reaction should be surface-mediated
- iii. The competition for photocatalyst's active site is negligible

Literature studied that the real K-value is significantly smaller [119]. This is explained by the differences in adsorption and desorption phenomena during the dark and illuminated period. Considering all these assumptions the Eq. (2.32) can be converted to a typical pseudo-first-order model. The pseudo-first-order model is represented by Eq. (2.33).

$$C = C_0 e^{-kt} \quad (2.33)$$

Where C_0 is initial concentration, t is time and k is an apparent first-order rate constant.

2.8 Preparation Technology of Photocatalyst

In photocatalysis, the photocatalyst is the most important part and is mostly dependent on its synthesis technique. TiO_2 is most commonly used and it is preferred nano-sized particles compared with the larger size TiO_2 particles. There are two most important characteristics of nanoparticles that make it more preferable to textile wastewater applications. These are (i) the quantum confinement at the nanoscale that associated with the transport of hole and electron from bulk surface materials and (ii) high surface to volume ratio that ensures the reaction rate enhancement due to its high reactant interaction with the active sites. The catalyst should have properties of high absorption capacity, non-scattering, incident irradiation, and production of charge carriers by bandgap excitation for photocatalytic degradation [109].

2.8.1 Synthesis Techniques of TiO_2 Nanoparticles

Various techniques are applied for the preparation of TiO_2 nanoparticles or thin films of TiO_2 including sol-gel method, chemical precipitation method, hydrolysis, spray deposition method, chemical vapor deposition, sputtering, micro-emulsion method, aerosol-assisted chemical vapor deposition, hydrothermal method, electro-deposition, flame combustion method, microwave-assisted hydrothermal synthesis, thermal plasma, solvothermal method, and sonochemical method, etc. [120]. Each of the above techniques has certain advantages or disadvantages based on characteristics of final product TiO_2 nanoparticles or thin-film can be differing from method to method is given in Table 2.3. Various operating conditions such as anatase rutile phase ratio, surface area, pore-volume, pore density, particle size, hydroxyl group content surface, band gap energy of TiO_2 can be depended on the reaction conditions such as the molar composition of reactants, precursor compound, fuel, reaction temperature, hydrolyzing agent, reaction time, presence of a gas atmosphere and calcination temperature [121].

Table 2.3: Advantage and disadvantages of different methods for TiO₂ nanoparticle synthesis [109, 122-124]

Method	Advantage	Disadvantage
Sol-gel method	<ol style="list-style-type: none"> 1. It is a cheap and low-temperature technique. 2. Capable of control chemical composition, porosity, and texture. 3. Good mixing & small quantity of dopants needed. 4. Suitable homogeneity, reliability & purity than raw materials. 5. Better product from the special properties of the gel. 6. Easy maintenance and performance in laboratory. 	<ol style="list-style-type: none"> 1. High fabrication cost. 2. Not suitable to attach the substrate. 3. Long-period deposition. 4. High-temperature calcination.
Hydrothermal method	<ol style="list-style-type: none"> 1. Ability to high-quality crystal. 2. Good control capacity. 3. Simple and elegant mode of operation. 	<ol style="list-style-type: none"> 1. Unable to observe crystal growth. 2. The high cost of autoclaves required.
Chemical precipitation method	<ol style="list-style-type: none"> 1. Proved to be a relatively simple and effective method. 2. Gives a permanent and immediate result. 3. The implementation and monitoring process is easy. 4. Low-temperature method. 	<ol style="list-style-type: none"> 1. Expensive process for treatment. 2. May generate a silt product. 3. Requires operation and maintenance of the unit. 4. Not applicable to all cases.
Chemical vapor deposition	<ol style="list-style-type: none"> 1. Good adhesion and compatibility. 2. Capable of multi-layer fabrication. 3. Develops pure, uniform, and reproducible with high or low rates. 4. High texture capability. 	<ol style="list-style-type: none"> 1. High cost. 2. Associated with contamination and safety requirements. 3. Higher reaction temperature. 4. Lower deposition rate.
Electro-	<ol style="list-style-type: none"> 1. Good control of the deposition of a layer. 	<ol style="list-style-type: none"> 1. Time-consuming and

deposition	<ol style="list-style-type: none"> 2. Good adhesion on the substrate. 3. Able to coat complex objects. 4. Lower operating cost. 	<ol style="list-style-type: none"> expensive. 2. Have limitations on the size and strength of electro-deposition. 3. A continuous process layout is more difficult.
Thermal plasma	<ol style="list-style-type: none"> 1. Higher deposition rates. 2. Temperature-sensitive. 3. The lower temperature required. 4. Uniform, low porosity, and good adhesion. 	<ol style="list-style-type: none"> 1. Toxic byproducts generate. 2. Particle and chemical contamination. 3. Higher equipment cost.

2.8.2 Sol-gel Technique

Among all methods, the sol-gel technique is a very simple and elegant method of TiO₂ nanoparticle preparation [121]. In the sol-gel process, a sol or colloidal suspension is formed by a precursor of metal alkoxide (TTIP) through the hydrolysis and polymerization reactions. Then the loss of solvent due to complete polymerization is performed and the liquid colloidal suspension or sol converts into the solid gel phase. The sol can be converted into either particle such as nanoparticles, or film into a desired pot with the required size such as fibers, membrane, glasses, glass sheets, steel balls, ceramics, steel wire mesh, etc. The sol is mostly used as nanoparticles in different application fields. The TiO₂ nanoparticles are synthesized by sol-gel where thermal treatment method that consists of four steps; hydrolysis, condensation, polymerization, and calcination, has been modified [109]. The produced Ti-O-Ti chains prefer low hydrolysis rates, low content of water, and excess titanium precursors in the reaction mixture. The preparation of TiO₂ nanoparticles by sol-gel with a modified thermal heat treatment technique is shown in Figure 2.6 [109].

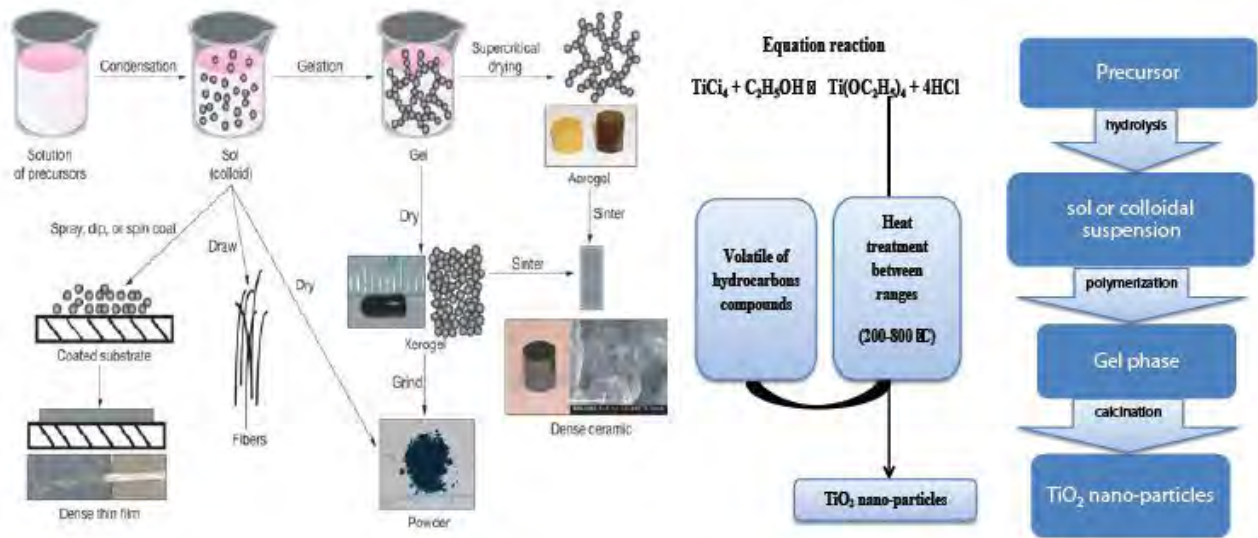


Figure 2.6: Schematic diagram of TiO₂ nanoparticle preparation by the sol-gel method [109].

2.9 Reactor Design of Photocatalyst

Reactor design is an important part of photocatalysis. The photocatalytic activity of dye is mostly dependent on the photocatalytic reactor design. The photocatalytic steps are entirely controlled by the essential governing factors stated below:

- i. Light absorption mechanism
- ii. A stipulation of active surface sites
- iii. Charge carrier dynamics

2.9.1 Immobilization of Titanium Dioxide (TiO₂)

In textile wastewater treatment, the photocatalysis is performed in two configurations; one is suspension and the other is immobilization. In suspension, the nano-sized photocatalyst is used in the reactor as suspended particles that eventually dispersed into the solution in the reactor. This reactor configuration provides uniform distribution of photocatalyst with the increase of high surface area to volume ratios. But the mass transfer is the limitation of this configuration. Besides these, it has several disadvantages such as filtration and recycling of TiO₂ are required, and loosing of TiO₂ may contribute to higher cost [119, 125]. The second reactor configuration is the immobilization of the catalyst onto the support. This configuration is getting rid of the above difficulties. In immobilization, the photocatalyst can be immobilized on any type of supportive materials including glass, glass beads, polymeric substrates, silica, quartz materials, perlite

granules, volcanic porous stones, clay aggregates, ceramic spheres, porcelain grade tiles, and black sand as well as to the glass tubes that surround the light source in the reactor [126]. The immobilization of photocatalyst on supportive materials can reduce the active surface area because the catalyst is used in continuous operation due to fouling. But it can be used several times in the photocatalytic degradation of organic compounds in textile wastewater treatment [127].

2.9.2 Immobilization Procedures

There are various procedures for immobilization such as heat treatment, spin-coating; dip coating, electrophoretic coating, and spray coating have been developed. Among those, the heat treatment is the most common and widely used technique for immobilization. The immobilization is followed by high-temperature treatment for a better bond to the supporting materials. Dip coating is the easiest of all the coating methods and produces non-uniform films that require several dipping cycles [128]. The immobilized film is produced by dip-coating is not mechanically robust and can be easily wiped off or damaged in the reactor during the photocatalytic experiment. On the contrary, the other coating produced by different methods is relatively stable but could be difficult to produce at larger scales [129]. It is essential to choose a preparation and immobilization technique compatible with the support and required film configuration in the reactor during experimental performance analysis.

2.10 Selection of Radiation Sources

In photocatalysis, light must be absorbed on the molecules. There are two radiation sources for photocatalysis in textile wastewater treatment. These are ultraviolet and solar radiation. There are various types of ultraviolet radiation sources that are described below. At present, most of the researchers are focusing on the application of renewable energy sources.

2.10.1 The Mercury Arcs: The most widely used source of ultraviolet and visible light for conventional photochemical study with steady illumination is the mercury arcs [130]. Three basic types of arcs are as follow; (i) the low pressure or resonance lamp, (ii) the medium pressure arc, and (iii) the high-pressure mercury arc.

2.10.2 Resonance lamps: Cadmium (Cd)-vapour resonance lamp has been used for the photosensitized luminescence of many substances. This source emits radiation mainly at 326.1 and 228.8 nm. Sodium (Na) vapor resonance lamps are available commercially, and lamps using the other alkali metals can be either purchased or constructed easily. They usually offer little interest in photochemical use since the electronic transition involved is of such small energy. Zinc (Zn) resonance lamps and inert-gas resonance lamps have been built and used successfully [131].

2.10.3 Discharge lamps: Various ingenious designs of discharge lamps for short-wavelength ultraviolet are described in the current literature. A windowless source from a low-pressure discharge in hydrogen is very rich in the 800-200 nm region. High-intensity noble-gas discharges have been described using low pressures of Krypton (116.5, 123.6 nm). Hot-cathode low pressure discharges using hydrogen, helium, argon, or nitrogen provide radiation in the 50-165 nm region [132].

2.10.4 The vacuum ultraviolet region: In gas phase photochemistry, the vacuum ultraviolet region is the most important because highly energetic processes can occur in this process that involving photoionization and higher excited states. The light source used in this process as synchrotron radiation. The radiation is also produced in bursts, with pulse lengths as short as 100 ps so that time-resolved experiments are possible.

2.10.5 Solar Radiation: Solar radiation is the form of electromagnetic radiation received from the sun as in the wavelength range of the measuring instrument. Pyranometer is the device that is used for measuring solar radiation. The unit of solar radiation is the power per unit area (W/m^2). Solar radiation is often integrated over a given period to report the radiant energy emitted into the surrounding environment (J/m^2), during that period. This integrated solar irradiance is called solar irradiation, solar exposure, solar insolation, or insolation. Irradiance may be measured in space or at the Earth's surface after atmospheric absorption and scattering. Irradiance in space is a function of distance from the Sun, the solar cycle, and cross-cycle changes. Solar radiation depends on various factors such as weather, time, distance, and sun's position. It affects plant metabolism and animal behavior [133]. The total earth energy budget is shown in Figure 2.7. There are several applications for solar radiation including energy generation from solar power plants, cooling and heating loads of buildings, weather forecasting,

climate modeling, and wastewater treatment. In wastewater treatment, TiO_2 requires photo-excitation with light at wavelengths exceeding the bandgap of the active anatase phase (3.2 eV), that is, the light at wavelength slower than 387 nm, which is in the UV range. However, the UV range in sunlight represents only 5–8% of the solar spectrum at sea level, and only a small fraction of sunlight can be used because TiO_2 as a photocatalyst absorbs only the UV spectral range [134]. Addressing the need for more sustainable technologies using photocatalysts that can be activated by natural sunlight is the goal of this and other research.

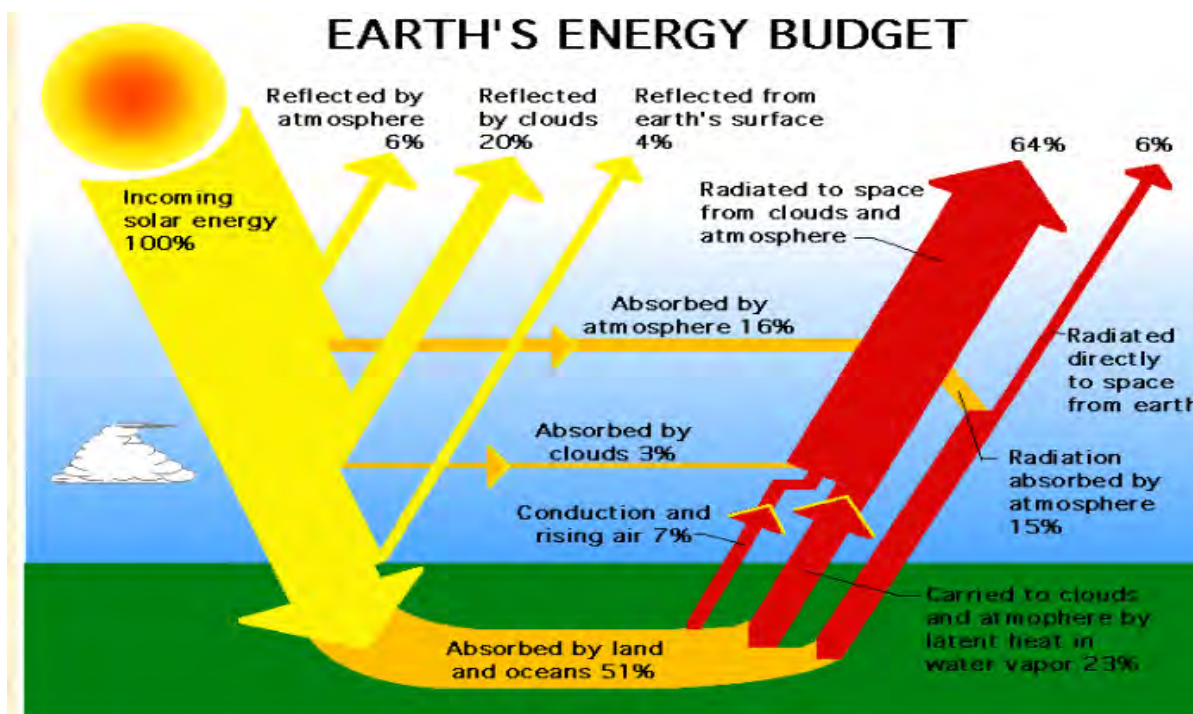


Figure 2.7: Total earth energy budget [134].

2.11 Factors that Affecting the Performance of Photocatalytic Reactor

The photocatalytic degradation efficiency of textile wastewater is highly dependent on various numbers of operational parameters that regulate the photocatalytic reaction rates of the organic molecules with TiO_2 under solar irradiation [119]. These are solar light intensity, catalyst loading, dissolved oxygen, airflow rate, temperature, pH, initial dye concentration, and irradiation time [50]. The performance of the photocatalytic reaction rate is mostly dependent on the above operating conditions. The effect of operating conditions of the process performance is represented in the following sections.

2.11.1 Solar Light Intensity

Light intensity regulates the electron-hole formation rate in a photochemical reaction as well as photocatalysis initiation. Solar light intensity depends on the weather and time that controls the contaminants' degradation efficiency of photocatalyst particles [135]. Usually, a higher intensity of light generates a higher amount of electron-hole pairs on the catalyst surface where the adsorption of the contaminants took place. As the adsorption of contaminants takes place on the photocatalyst surface, the decomposition/degradation of the contaminants proceeds by the holes and free radicals, which are generated on the surface. The extent of radiation absorbed by the photocatalyst determines the photocatalyst reaction rate. However, the nature or form of light never changes the reaction pathway [136]. In general, the intensity of solar radiation is the sum of photon absorption by the catalyst. Photon absorption of catalyst increased by increasing solar light intensity which rise the generation of electron-hole pair. Moreover, the kinetics of the photocatalytic reaction is affected by light intensity.

2.11.2 Effect of Air Flow Rate

The rate of airflow through the process, up to a certain value, has a positive impact on contaminants removal from the process. Thus, the decrease of airflow rate causes generates a lower number of bubbles and less mixing i.e. less mass transfer between contaminants and photocatalyst. On the other hand, a higher flow rate generates more bubbles because of obtaining a higher rate of mass transfer as well as promote the adsorption of contaminates on the TiO₂ catalyst [137].

2.11.3 Effect of Feed Flow Rate

The reaction rate is inversely proportional to the feed flow rate through the reactor. As the feed flow rate increased, the retention time for the contaminants to come in contact with the photocatalyst decreased. It is reported that the degradation of indole was affected by the adsorption of indole on the surface of TiO₂ with the increase of flow rate. The degradation of indole was decreased from 93% to 58% as the flow rate was increased from 0.5 to 4.03 mL/s [138].

2.11.4 Effect of Temperature

Temperature is an important factor for any photocatalytic reaction. The photocatalytic reaction rate is increased with the increase of temperature. As the temperature increased, the number of cavitation bubbles increased, which helps to promote the formation of free radicals ($\cdot\text{OH}$). Thus, the increase of temperature enhances the oxidation rate at the catalyst interface. Moreover, it also hinders the electron-hole recombination. However, with the increase of temperature, the organic adsorption capacities of photocatalyst are decreased; and thus, decrease the photocatalytic reactor performance [139]. Therefore, the optimum temperature range for the photodegradation of organics is 20-80°C as suggested by the literature. At extremely low temperatures (<20°C), the reaction rate is very low although the adsorption of organics on photocatalyst is increased. On the other hand, at extremely high temperatures (>80°C) the adsorption rate of organics on the catalyst surface is very less compared with the reaction rate on the catalyst surface and thus, less degradation of organics was observed [140].

2.11.5 Effect of Dissolved Oxygen

The adsorption of organics on the TiO_2 catalyst does not affect by the oxygen concentration because oxidation and reduction reactions take place at different locations [136]. Electron and holes are generated by the photoreactions taking place on the photocatalyst surface, and separated by dissolved oxygen with the ($\cdot\text{OH}$) radical production. In a study, the dissolved oxygen meter was placed in the tank and showed different oxygen concentrations had a great impact on dye degradation [141]. Therefore, it is suggested that the reaction rate of photocatalyst can be controlled by changing the oxygen concentration on the catalyst surface. Pure oxygen is more effective to increase the reaction rate as compared with air [137].

2.11.6 Effect of pH

pH always plays an important role in the degradation of organics by the photocatalytic process because it determines the surface charge and the size of aggregates [142]. The wastewater pH may vary significantly, which affects the ionization and surface charge of the photocatalyst. Various factors that influence the degradation rate of dyes are the type of dye, surface properties of TiO_2 , and type of application [143]. At lower pH, the degradation rate is low and at higher pH the degradation rate increases to a greater extent. The pH has the greatest effect on the oxidation

kinetics of dye degradation. With increasing pH, the oxidation kinetics increases but the order is not changed at higher pH. From the literature, it should be noted that the degradation rates of some dyes from the treatment textile wastewater were increased with the decrease of pH [81]. Under the acidic or alkaline condition, the surface of TiO₂ can be protonated or deprotonated, respectively, according to the following reactions:



Thus, in acidic medium (pH<6.9), the TiO₂ surface will remain positively charged due to the strong adsorption of dye into the TiO₂ particles with corresponding to their electrostatic attraction and negatively charged in alkaline medium (pH>6.9) due to increase *TiO*⁻ basic groups into the TiO₂ surface that affect the rate of adsorption. TiO₂ has higher oxidizing activity at lower pH but at very low pH, excess H⁺ can decrease the reaction rate [144].

2.11.7 Effect of Irradiation Time

The photocatalytic reaction follows pseudo-first-order reaction kinetics generally. Moreover, the photocatalytic reaction has a proportional relationship with irradiation time. But after sometimes it shows an inverse relationship with irradiation time due to evaporation. Thus, the reaction rate of dye is increased until evaporation starts. With the increase of evaporation of water, the degradation rate of original dye compounds decreases as the concentration of dye increased with irradiation time. As the time increase, more and more intermediate products such as small chain aliphatic compounds are produced and these aliphatic compounds react with hydroxyl free radical that causes the slow kinetics of dye degradation after the certain reaction time. The deposition of strong by-products on the photocatalyst active sites causes the deactivation of the catalyst, which reduces the catalyst activity for the photocatalytic reaction with the original dye compounds [142].

2.11.8 Effect of Contaminant or Initial Dye Concentration

A photo-catalytic degradation rate largely depends on the substrate concentration or initial dye concentration. The increase of initial dye concentration decreases the reaction rate and removal efficiency. At higher dye concentration, the absorbance of solar irradiation by dye molecules becomes much more significant for degradation. Generally, it is studied that up to a certain limit,

the degradation rate is increased with the increase of dye concentration then decreases degradation rate with increasing the dye concentration due to the penetration light obstacle [81]. The TiO₂ photocatalyst surfaces inhibit the direct contact between the photogenerated hole and dye molecules with an increase of the initial dye concentration that decreases the active surface area [145]. In photocatalytic degradation of high concentration of dyes that enhancing the demand of oxidizing species ([•]OH). The adsorption of the contaminants takes place on the surface of the catalyst. The photocatalytic process depends on the available reaching number of photons as well as reactant adsorption on the photo-catalyst surface. Therefore, the formation of hydroxyl free radicals is important for the photocatalytic process [137]. However, the number of active sites on the catalyst surface remains constant for fixed light intensity, irradiation time, pH, and catalyst loading.

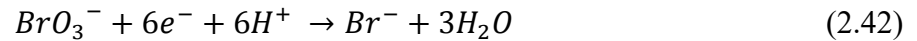
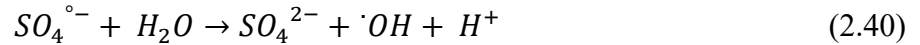
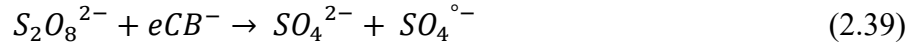
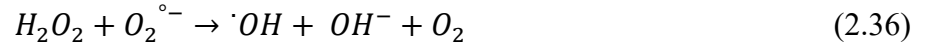
2.11.9 Effect of TiO₂ Load

The photocatalytic degradation process is affected by the amount of TiO₂. The prime photoreaction rates have a proportional relationship with the mass of the catalyst in the solution. With an increase of catalyst mass, the active sites of catalyst and reaction sites on the catalyst surface in the solution increase, and thus, more ([•]OH) radical is generated. However, a large quantity of the catalyst may cause rising in turbidity and decreases the radiation intensity of solar light. The light penetration is decreased with the increase of turbidity in the suspension which is increased with catalyst loading. Besides, there is some possibility to enhance particle-particle interactions in suspension. These may reduce the electron density on the catalyst surface and the density of available reactive sites [25]. At lower TiO₂ loading, the reaction extent is controlled by photonic adsorption due to their limited surface area; while at higher loading; photonic adsorption is affected by light scattering of the particles. Thus, the photocatalytic degradation rates increase up to an optimum mass with TiO₂ loading corresponding to an increase of photon absorption and after that, the rates decrease to a constant value. The excess TiO₂ loading causes the formation of light scattering by the suspended particles that reduce the reaction rate. The threshold optimum TiO₂ loading varies based on the type of application of the photocatalytic process. It mostly depends on the irradiation method, types of photocatalyst, geometry, pollutant concentration, nature of the dye, photoreactor, and the overall operating conditions [81,143]. The removal efficiency depends on (i)increase of absorb area of dye molecules on the surface, (ii)

increase of the density of catalyst particles, and (iii) increase of the active sites on the surface. To avoid excess usage of catalyst and to ensure maximum absorption of photons, an optimum catalyst dose should be obtained. Hence, the catalyst with an optimized range is strongly recommended to apply for the photocatalytic process.

2.11.10 Effect of Oxidant

There are various oxidants including H_2O_2 , BrO_3^- and $S_2O_8^{2-}$ are added to TiO_2 catalyst that has a great influence on the degradation of organic compounds such as (i) to increase the hydroxyl radical concentration, (ii) to prevent the hole-electron recombination, and (iii) to generate other oxidizing elements ($O_2^{\circ-}$, $SO_4^{\circ-}$) to enhance the degradation of intermediate compounds. In photocatalytic reaction, the intermediate oxidants perform dual functions such as strong oxidants and electron scavengers. These intermediate products can inhibit the hole-electron recombination of the TiO_2 surface according to the following equations [81].



The addition of peroxide acts as an oxygen supplier that increases the reaction rate. The effect of H_2O_2 on the degradation of textile wastewater is significant. The oxidation rates have become increase e increasing with the addition of H_2O_2 since more hydroxyl radicals could be generated by removing surface trapped electrons [146]. However, the oxidative conversion of photocatalytic efficiency would be uniformly increased by the addition of H_2O_2 . As a result, hydroxyl radicals are produced from the oxidation of hydroxide ions are given in the reactions. On the contrary, the $S_2O_8^{2-}$ influences the mineralization rate despite being decreasing the pH of the dye solution [81]. It takes place in two different ways including (i) enhances the charge separation by scavenging persulphate ion in conduction band electron and (ii) sulfate radical anion ($SO_4^{\circ-}$) can be generated from $S_2O_8^{2-}$ from both the photolytically and thermally in the TiO_2 aqueous solution. To enhance the photocatalytic degradation rate, the use of BrO_3^- as an

oxidant is an efficient electron acceptor. It increases the decolorization efficiency of dyes in textile wastewater. This rate can be increased due to the reaction between conduction band electron and BrO_3^- by scavenging effect. But excess addition of BrO_3^- shows small enhancement that has great effects on TiO_2 activity [147].

2.12 Photocatalyst Characterization and Analytical Techniques

According to the literature, for photocatalyst characterization, various analytical methods are used. These analytical techniques are also able to provide the desired accurate-precise understanding of nanoparticles. Some of the universally reliable and splendid analytical techniques available for photocatalyst analysis are stated below:

1. Ultraviolet-Visible (UV-Vis) Absorption Spectroscopy
2. Fourier Transform Infrared Spectroscopy (FT-IR)
3. Field Emission Scanning Electron Microscopy (FESEM)
4. Energy Dispersive X-ray Spectroscopy (EDX)
5. X-Ray Diffraction Spectroscopy (XRD)
6. BET Surface Area Analysis

2.12.1 Ultraviolet-Visible (UV-Vis) Absorption Spectroscopy

UV-Vis absorption spectroscopy is a common tool in absorption/adsorption study, particularly in dye removal. It is absorption spectroscopy in the UV region of electromagnetic radiation (EMR). Owing to different electronic structures, molecules may absorb radiation at different wavelengths, with different intensities varying upon concentration and thus, can be used to identify and calculate their concentration in a solution. The absorption of UV or visible radiation corresponds to the excitation of outer electrons. There are three types of electronic transition among which transitions involving σ , π , and n electrons are more simple and easy to explain. Molecules containing π or non-bonding electrons can absorb UV-Vis light to result in various electronic excitations e.g. $\sigma - \sigma^*$, $\pi - \pi^*$, $n - \pi^*$ etc. With the difference in bandgap energy, different excitation requires different amounts of energy leading to UV-Visible light absorption at different wavelengths. Thus, different compounds with a difference in their electronic structure, rise to excite to by absorption of UV-Vis light at characteristic wavelength [148].

Bandgap energy is an important measurement that refers to the energy difference between the valence and conduction band. It is measured when an electron jumps from a valence band to conduction band; a specific minimum amount of energy is required for the transmission of an electron from point 1 to 2. A diagram illustrating the bandgap is shown in Figure 2.8.

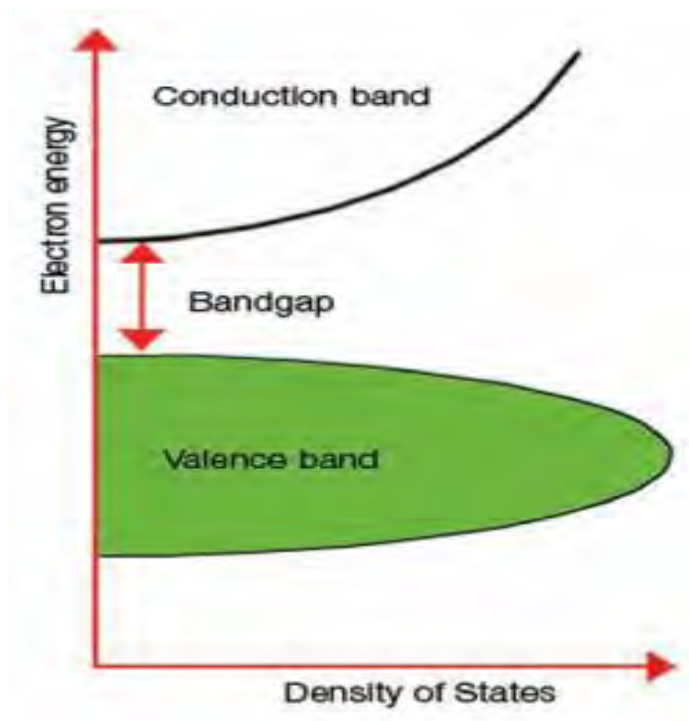


Figure 2.8: Explanation of bandgap [148].

2.12.2 Fourier Transform Infrared Spectroscopy (FT-IR)

FTIR is one of the most common and widely used spectroscopic techniques employed for determining structure or to identify the functional groups of compounds on the surface. It is based upon characteristic absorption of Fourier transform infrared radiation (FT-IR) of molecules. The fundamental measurement obtained in FTIR is an infrared spectrum, which is a plot of measured intensity versus wavenumber of FT-IR for a solid, liquid, or gas sample. FT-IR involves the energy region of EMR corresponding to the wavenumber of $14000 \sim 4 \text{ cm}^{-1}$. It can be divided into near-infrared region ($14000 \sim 4000 \text{ cm}^{-1}$), mid-infrared region ($4000 \sim 400 \text{ cm}^{-1}$) and far-infrared region ($400 \sim 4 \text{ cm}^{-1}$). The commonly used region for FTIR is ($4000 \sim 400 \text{ cm}^{-1}$) because the absorption radiation of most functional groups and bonds in organic and inorganic materials is within this region. Only the molecules which have a dipole moment that changes as a

function of time can interact with FT-IR and thus, called FT-IR active. Molecules with different structure even with the same bond at different chemical environments vibrate at different frequencies and thus, make it enable to distinguish them from FTIR. FTIR of a sample may be affected by various structural parameters. Structural factors include the nature of the bonds (single/double/triple), the mass of the atoms constituting bond, nature of hybridization, mode of vibration, resonance, type of isotope, solvent, etc. [149]. The most common method of sample preparation for IR involves mixing the finely ground solid sample with powdered KBr and pressing the mixture under high pressure. Under pressure, KBr melts and seals the compound into a matrix. The resultant mixture is a KBr pellet which can be inserted into a holder of the spectrometer. This method is known as the mull technique. FTIR is advantageous based on its distinguished properties such as high scan speed, high resolution, high sensitivity, a wide range of applications, a large amount of structural information, non-destructiveness.

2.12.3 Field Emission Scanning Electron Microscopy (FESEM)

Field emission scanning electron microscopies is a modern form of the SEM, which can be used in the examination of materials, revealing external morphology (texture), imaging crystalline structure, and observed the orientation of materials on the surface of the sample [150]. The term ‘SEM’ is substituted by ‘FESEM’ with the use of Field Emission Gun (FEG) instead of Thermionic Emission Gun (TEG) as an electron emitter gun. SEM uses a focused beam of high-energy electrons to generate a variety of signals at the surface of a solid specimen.

The backscattered electrons and secondary electrons are commonly used for imaging samples among all the signals. The secondary electrons are the most useful for showing topography and morphology. In this application, data are collected over a selected area of the surface of the sample, and a 2-dimensional black-white image is generated that displays spatial variations in these properties. Areas ranging from approximately 1 cm to 5 microns in width can be imaged in a scanning mode using conventional SEM techniques (magnification ranging from 20X to approximately 500000X, the spatial resolution of 50 to 100 nm). There are various advantages of SEM including its wide array of applications, the detailed two-dimensional and topographical imaging, and the versatile information garnered from different detectors. SEMs are also easy to operate with the proper training and advances in computer technology and associated software have made the operation user-friendly.

2.12.4 Energy Dispersive X-ray Spectroscopy (EDX)

Energy Dispersive X-ray Spectroscopy (EDX) is a microanalysis technique used to identify the elemental composition and chemical characterization of materials. EDX systems are commonly used in conjunction with Electron Microscopy instruments (Scanning Electron Microscopy (SEM) or Transmission Electron Microscopy (TEM)), where the imaging capability of the microscope identifies the specimen of interest [151]. When the sample is bombarded by the SEM's electron beam, electrons are ejected from the atoms comprising the sample's surface. The resulting electron vacancies are filled by electrons from a higher state, and an X-ray is emitted to balance the energy difference between the two electrons' states. The X-ray energy being characteristic of the element from which it was emitted, the identity of elements, and their relative abundance can be marked by detecting this x-ray radiation. EDX offers the advantages of quick 'first look' compositional analysis. When used in "spot" mode, a user can acquire a full elemental spectrum within a few seconds. Supporting software makes it possible to readily identify peaks, which makes EDX a great survey tool to quickly identify unknown phases before quantitative analysis. EDX can also be used in semi-quantitative mode to determine chemical composition by a peak-height ratio relative to a standard.

2.10.5 X-Ray Diffraction Spectroscopy (XRD)

XRD is one of the most powerful, reliable, non-destructive techniques for the qualitative and quantitative analysis of the crystalline materials, in the form of powder or solid. XRD is based on the constructive interference of monochromatic X-rays and a crystalline sample. These X-rays are generated by a cathode ray tube, filtered to produce monochromatic radiation, collimated to concentrate, and directed toward the sample. The interaction of the incident rays with the sample produces constructive interference (and a diffracted ray) when conditions satisfy Bragg's Law. This law relates the wavelength of electromagnetic radiation to the diffraction angle and the lattice spacing in a crystalline sample [152]. These diffracted X-rays are then detected, processed, and counted. By scanning the sample through a range of 2θ angles, all possible diffraction directions of the lattice are attained due to the random orientation of the powdered material. Conversion of the diffraction peaks to d-spacing allows identification of the mineral because each mineral has a set of unique d-spacing. Typically, this is achieved by comparison of d-spacing with standard reference patterns. The value of d-spacing is obtained from Bragg's law-

$$2d \sin\theta = n\lambda \quad (2.43)$$

Where d is an interlayer spacing, θ is the X-ray angle of incidence (and of diffraction) measured concerning the crystalline planes, n is an integer value and λ is the wavelength of the incident beam. Crystallite size of crystals are calculated from Scherrer formula-

$$D = \frac{k\lambda}{\beta \cos\theta} \quad (2.44)$$

Where D is the crystallite size, k is a dimensionless shape factor (typical value 0.9), λ is the X-ray wavelength, β is the line broadening at halfway of the maximum intensity (FWHM) and θ is the Bragg angle (in degrees). Sample preparation is one of the most important steps in a successful XRD analysis. Typically, samples are ground to achieve a good S/N ratio, avoid spottiness, and minimize preferred orientation. The ideal samples are crystalline powders. XRD offers many advantages over other available techniques in sample analyses and those are (i) it is a powerful and rapid technique for identification of an unknown mineral, (ii) it requires a small amount of sample preparation time, (iii) data interpretation is relatively straight forward, etc.

2.10.6 BET Surface Area Analysis

The physisorption technique is one of the most common methods used to measure surface area, pore-volume, pore size, and its statistical distribution. The technique uses an inert gas as adsorbate, especially nitrogen. The process of adsorption and desorption is carried out with different amounts of nitrogen. The corresponding readings in terms of pressure or thermal conductivity are measured. The recorded measurements are used in gas adsorption equation models to estimate microstructure characteristics like porosity. According to literature, the Brunauer–Emmett–Teller (BET) multi-point model is one of the finest available techniques [153].

CHAPTER 3

MATERIALS AND METHODOLOGY

This chapter represents the materials and methodology of the study. The TiO₂ nanoparticle synthesis technique has been studied carefully to meet the stated research objectives. The Chapter contains TiO₂ nanoparticle synthesis by sol-gel and thermal heat treatment method, the photocatalytic reactor design and detailed experimental procedures.

3.1 Materials

3.1.1 Chemicals

The major reagents and chemicals were used for experiments in the laboratory include the precursor titanium (IV) isopropoxide (C₁₂H₂₈O₄Ti) (Sigma-Aldrich, 97%), absolute ethanol (C₂H₅OH) (Tradia, USA), methyl orange (Sigma-Aldrich, dye content 85%), nitric acid (HNO₃, 65% extra pure) (Sigma-Aldrich), sodium hydroxide (NaOH) (Merck, Germany), hydrofluoric acid (HF, 48% extra pure) (Sigma-Aldrich), and hydrogen peroxide (H₂O₂) (Sigma-Aldrich, 30%). Doubly distilled water was used as a solvent to prepare most of the solution in this work.

3.1.2 Equipment and Analytical Instruments

The major equipment/instruments were performed for analysis in the laboratory include the UV-Visible spectrophotometer (UV-Vis) (DR-6000, DR-4000, UV-2600, Shimadzu, Japan), Fourier transform infrared spectroscopy (FT-IR) (FT-IR-470, Shimadzu, Japan), Scanning electron microscope (SEM) (JSM-6700F, JEOL, Japan), X-ray diffraction (XRD) (PANalytical Empyrean Series 2 X-ray Diffraction), Brunauer–Emmett–Teller isotherm (BET), Digital balance (Precisa, Switzerland), Micro oven/Drier (Germany), Muffle furnace (Navertherm, England), and Magnetic stirrer (China).

3.2 Synthesis of TiO₂ Nanoparticles using Sol-Gel and Heat Treatment Methods

3.2.1 Synthesis TiO₂ Nanoparticles with Hydrolysis

All reagents were of analytical grade and were used as received without further purification. TiO₂ nanoparticle was synthesized via sol-gel method using Titanium (IV) isopropoxide (TTIP, Sigma Aldrich), distilled water, and absolute ethanol (Tadia, USA) as the starting materials. To

synthesis TiO_2 , Titanium (IV) isopropoxide ($\text{C}_{12}\text{H}_{28}\text{O}_4\text{Ti}$), absolute ethanol, and water were mixed in a molar ratio of $\text{TTIP}:\text{C}_2\text{H}_5\text{OH}:\text{H}_2\text{O}=1:7.14:4$ [154]. Nitric acid (HNO_3) and sodium hydroxide (NaOH) was used to adjust the pH at 3 and to restrain the hydrolysis of the solution [155]. The obtained solution was stirred on a magnetic stirrer for 180 min at room temperature. Then the solution was aging up to 12 hours to obtain the gel. The gel was dried at 90°C , 100°C , and 110°C for 1 hour at each condition to evaporate water and organic materials to the maximum extent [156]. Then the dried powder was calcinated at 400°C and 500°C for 2 h at each condition to achieve desired TiO_2 nanoparticles (ramp 6.6°C to rise 400°C and holding 2 hours, then ramp 3.3°C to rise 500°C and holding 2 hours and finally forced cooling to obtain room temp within 1 hour) [157]. The heat treatment procedure from gel to TiO_2 nanoparticles is shown in Figure 3.1. Finally, the TiO_2 nanoparticles were ground. The approximate amount of 1.80 ± 0.05 g TiO_2 nanoparticles was obtained from the above proportion of reagents.



Figure 3.1: Heat treatment procedure from gel to TiO_2 nanoparticle; (a) Sol-gel of TiO_2 after 12-hour aging (b) Heat treatment of 1 hour at 90°C (c) Heat treatment of 1 hour at 100°C (d) Heat treatment of 1 hour at 110°C and (e) Heat treatment of 4 hours at 400°C and 500° in a muffle furnace.

3.2.2 Preparation of TiO_2 Nanoparticles without Hydrolysis

All the reagents used are of analytical grade and no further purification is done before use. TiO_2 nanoparticle is prepared via the sol-gel method using Titanium (IV) isopropoxide (TTIP, Sigma Aldrich) and absolute ethanol (Tadia, USA) as the starting materials. The sol-gel synthesized TiO_2 was obtained by dissolving TTIP in absolute ethanol at a molar ratio of $\text{TTIP}:\text{C}_2\text{H}_5\text{OH}=1:7.14$. The three drops of nitric acid (HNO_3) (2.0 M) were added to the solution to obtain pH 3. The rest of the synthesis process is exactly similar as we mentioned in section 3.2.1. The heat

treatment procedure from gel to TiO₂ nanoparticles is shown in Figure 3.2. Finally, the synthesized TiO₂ nanoparticles were ground. The approximate amount of 4.8123 ± 0.05 g TiO₂ nanoparticles was obtained from the above proportion of reagents.



Figure 3.2: Heat treatment procedure from gel to TiO₂ nanoparticle without hydrolysis.

3.3 Characterization Techniques of TiO₂ Nanoparticles

3.3.1 Ultraviolet-Visible Spectroscopy (UV-Vis)

The UV-Vis spectral analysis of the sample solutions was performed using a double beam spectrophotometer (Spectrophotometer, UV mini-1800, Center for Advance Research Studies (CARS) at the University of Dhaka). Water was used as a solvent in the UV-Vis spectroscopic analysis of TiO₂ nanoparticle adsorption. The reference aqueous solutions were also used for preparing the adsorbate solutions at certain pH 6.0. The determination of the amount of TiO₂ nanoparticles adsorbed by an adsorbent was done by spectroscopy in the visible region (200-800 nm) [158]. The 1 mg sample of TiO₂ nanocomposite is dissolved in 10 ml distilled water. The UV-Visible spectrum of TiO₂ was obtained for 10 μ M solutions in the range of 250 nm to 600 nm. The maximum absorbance was 0.797, which was obtained at 464 nm and photometric measurements were carried out at 464 nm.

The bandgap energy is an important part of semiconductor nanoparticle. The bandgap of the semiconductors has been found to be particle size-dependent. The bandgap increases with decreasing particle size and the absorption edge are shifted to higher energy (blue shift) with decreasing particle size [159]. After heat treatment, the intensities of absorption peaks of TiO₂ film increased and the peak position slightly shifted to a higher wavenumber, because of the formation of TiO₂. [160]. The bandgap energy can be determined by employing Kubelka-Munk function and Tauc's plot is stated in the Eq. (3.1).

$$(\alpha hv)^{1/2} = A(hv - E_g) \quad (3.1)$$

Where α is the absorption coefficient (cm^{-1}), A is a constant which is independent of photon energy, and hv (eV) is the energy of excitation. The calculation of the bandgap can be performed by plotting $(\alpha hv)^{1/2}$ versus hv and extrapolating of the absorption edge to zero [161].

3.3.2 Fourier Transform Infrared Spectroscopy (FTIR)

FT-IR spectra of TiO_2 nanoparticle was recorded on an FT-IR spectrometer (Spectrophotometer, FT-IR 8400S Shimadzu, Center for Advance Research Studies (CARS) at University of Dhaka) in the region of $4000\text{-}400 \text{ cm}^{-1}$. FT-IR spectra of the solid samples were frequently obtained by mixing and grinding a small number of materials with dry and pure KBr crystals [162]. Grinding of nanoparticles was performed in a mortar by a pestle. The powdered mixture was then compressed in a metal holder under a pressure of 8-10 tons to make a pellet. The pellet was placed in the path of the FT-IR beam for measurements.

3.3.3 Brunauer–Emmett–Teller Isotherm (BET) of TiO_2 Nanoparticles

Brunauer–Emmett–Teller (BET) analysis represents the specific surface area (m^2/g) and total pore volume (cm^3/g) of catalyst. BET explains the physical adsorption and desorption of gas molecules on a solid surface and desorption data are used to analyze the adsorption/desorption capacity of solids. Nitrogen (N_2) is the most commonly employed gaseous adsorbate used for surface probing by BET methods. All the samples were dried at 200°C for 30 minutes. The moisture-free samples were analyzed sequentially by nitrogen adsorption and desorption methods. Different compositions of nitrogen (15%, 30%, 50%, and 95%) were used to experiment. The respective parameters of thermal conductivity were calculated using 48 Pulse Chemi Sorb 2705 (Micromeritics) [163]. The BET analysis was conducted at the boiling temperature of N_2 (77 K). The BET model is represented by the Eq. (3.2).

$$\frac{1}{v[(p^0/p) - 1]} = \frac{c-1}{v_m c} \left(\frac{p}{p^0} \right) + \frac{1}{v_m c} \quad (3.2)$$

3.3.4 Scanning Electron Microscopy (SEM)

TiO_2 nanoparticle was prepared and treated for their surface morphology. For this purpose, SEM was adopted. The SEM images were found from instruments of model JSM-6700F (JEOL,

Japan). In the former device, the dried powders of these samples were dispersed on a conducting carbon glued strip and the sample-loaded strip was then mounted to a chamber that evacuated to $\sim 10^{-3}$ to 10^{-4} torr. In the latter machine, a very thin gold layer (\sim few nanometers thick) was sputtered on the sample additionally to ensure the conductivity of the sample surface. The sample was then placed in the main SEM chamber to view its surface in both cases [164]. The systems were computer interfaced and thus, provide recording of the surface images in the computer file for its use as hard copy. The EDX is also performed to analyze the quantity of components based on the atomic weight percentage. EDX systems were commonly used in conjunction with electron microscopy instruments (Scanning electron microscopy) by using the method of JSM 7100F, JEOL, where the imaging capability of the microscope identifies the specimen of TiO₂ nanoparticle which was studied.

3.3.5 X-ray Diffraction (XRD)

PANalytical Empyrean Series 2 X-ray Diffraction system was operated at the wavelength of 32.297 nm (Cu K α wavelength), 40 mA, and 40 keV. XRD diffractograms were acquired at 25°C over a 2θ range of 5–90° with a step size of 0.020° and a step time of 1s. Powder form TiO₂ nanoparticle was used for their X-ray diffraction pattern. The powder samples were pressed in a square aluminum sample holder (40 mm \times 40 mm) with a 1 mm deep rectangular hole (20 mm \times 15 mm) and pressed against an optical smooth glass plate. The average crystalline size of the TiO₂ photocatalyst was calculated according to the Debye-Scherrer formula [165].

$$D = \frac{0.9\lambda}{\beta \cos \theta} \quad (3.3)$$

The phase composition of the samples can be calculated from equation [166]:

$$X_R = 1 - [1 + 1.26 \left(\frac{I_R}{I_A}\right)^{-1}]^{-1} \quad (3.4)$$

Where X_R is the weight fraction of rutile in the mixture, and I_R and I_A are the peak intensities of the rutile (1 1 0) and anatase (1 0 1) diffractions respectively.

The upper surface of the sample was labeled in the plane with its sample holder. The sample holder was then placed in the diffractometer. The corresponding results of the sample in terms of intensity against 2θ were observed from the computer. All the other samples were analyzed using the above protocol without any notable change.

3.4 Design and Construction of TiO₂ Immobilized Reactors

3.4.1 Supporting Materials for Immobilization of TiO₂

In our research work, the borosilicate glass, cement (white cement), and steel wire mesh were used as supporting materials where TiO₂ nanoparticle was immobilized. These supporting materials were purchased from the local market. The supporting materials are shown in Figure 3.3.



Figure 3.3: Immobilizing materials (a) Borosilicate glass, (b) White cement, and (c) Steel wire mesh

3.4.2 Immobilization of TiO₂ on Supporting Materials

The TiO₂ nanoparticle powder can be immobilized on the borosilicate glass, cement, and steel wire mesh by various methods including heat treatment, bond formation, doping, etc. In this work, we used the heat treatment method because, in this method, we don't need any binder such as colloidal SiO₂, acrylic emulsion, and polymer compounds.

At first, the supporting materials such as borosilicate glass plate and steel wire mesh were cleaned with distilled water and then it is pretreated with HF solution (1 M) overnight and washed with NaOH solution (0.1 M) for 2 h to increase the number of (⁻OH) groups on the surface for ensuring a good fixation of TiO₂ photocatalyst on a borosilicate glass plate and steel wire mesh [167]. Five milliliters (5 mL) of suspension containing 0.060, 0.090, 0.120, and 0.150 g TiO₂ nanoparticle powder is prepared using ethanol as solvents. The suspension was stirred by using a glass rod for 10 min to improve the dispersion of TiO₂ photocatalyst in the solvent [168]. The suspension was poured on a borosilicate glass plate, cement coated glass plate, and steel wire mesh and then placed in room temperature for 1 hour. After that, it was placed in an oven at 110°C for 1 hr. After drying, the glass plate, cement coated glass plate, and wire mesh were calcinated at 500°C for 120 min and washed with distilled water for the removal of weakly

attached TiO₂ particles [47]. This thermal treatment ensured the removal of the organic (ethanol) load and facilitated inters connection (sintering) of TiO₂ nanoparticles. TiO₂ deposition process was carried out for 1, 2, 3, and 4 times to increase the amount of TiO₂ photocatalyst loading on the surface of the glass plate which was represented as a first, second, third and fourth layer, respectively. Several plates with 1, 2, 3, and 4 layers of TiO₂ photocatalyst dispersed in ethanol were prepared.

3.4.2.1 Preparation of TiO₂-Immobilized on Borosilicate Glass

A borosilicate glass sheet was purchased and cut into circular shapes of the desired size of 45.00 cm². The TiO₂ suspension was prepared with the 0.060 g into the required amount of ethanol and it was stirred about 10 min. Then the slurry of TiO₂ was poured onto the borosilicate glass to form the first layer by using calcination of 500°C of 2 h. Similarly, second, third, and fourth layers were formed with the addition of an amount of 0.0900 g, 0.1200 g, and 0.1500 g TiO₂ suspension, respectively. The total weight of the first, second, third, and fourth layers of TiO₂ nanoparticles immobilized on borosilicate glass before and after treatment is given in Table 3.1. The first, second, third, and fourth layers of TiO₂ on borosilicate glass before and after treatment are shown in Figure 3.4.

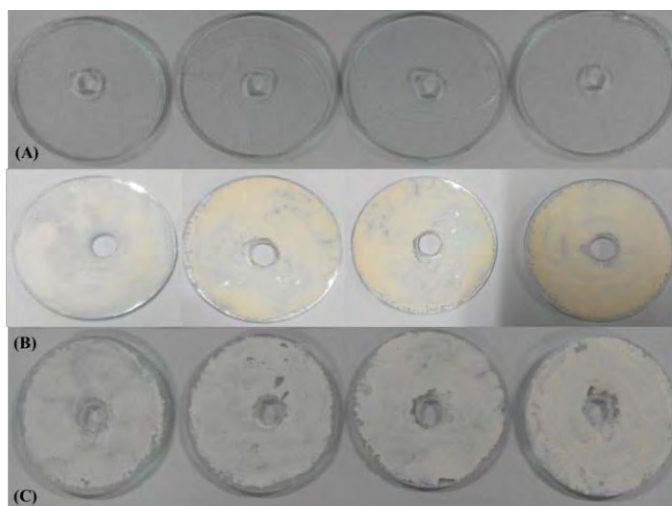


Figure 3.4: (a) Circular borosilicate glass without TiO₂ photocatalyst (b) TiO₂-immobilized borosilicate glass before treatment with 1st, 2nd, 3rd, and 4th layer (c) TiO₂-immobilized borosilicate glass after treatment with 1st, 2nd, 3rd, and 4th layer

3.4.2.2 Preparation of TiO₂-Immobilized on Cement Coated Borosilicate Glass

The Borosilicate glass sheet was cut in a circular shape of size of 45.00 cm². The white cement was purchased from the local market and a cement layer was formed over the borosilicate glass with the amount of 0.0700 g white cement and the required amount of deionized water. It is kept at room temperature over 1 hr and then placed in an oven at 110°C for 2 hrs. After that, it was calcinated at 500°C for 2 hrs. The TiO₂ suspension was prepared with the 0.060 g into the required amount of ethanol and stirred about 10 min. Then the slurry of TiO₂ was poured into the borosilicate glass with cement layer to form the first layer by using calcination at 500°C of 2 hours. Similarly, second, third, and fourth layers were formed with the addition of 0.0900 g, 0.1200 g, and 0.1500 g TiO₂ in suspension, respectively. The total weight of first, second, third, and fourth layer TiO₂ nanoparticles with cement coated before and after treatments are given in Table 3.2. The images of the first, second, third, and fourth layers of TiO₂ on borosilicate glass with cement layer before and after treatment are shown in Figure 3.5.

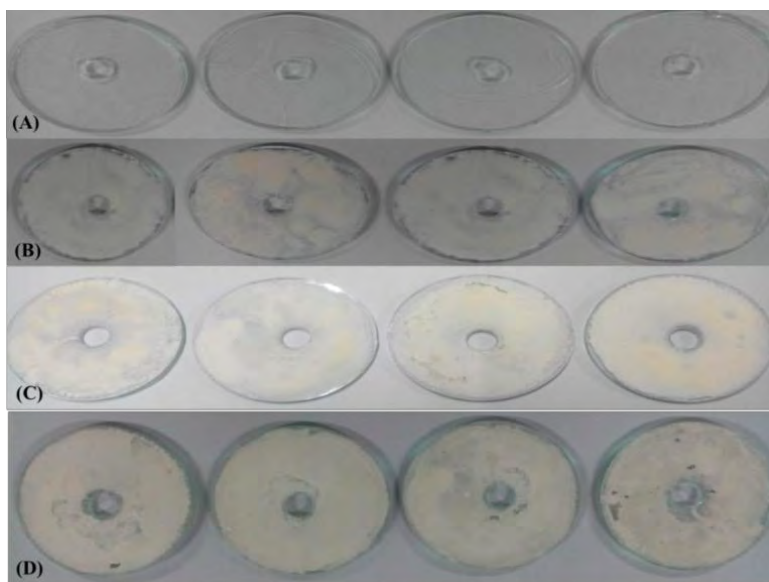


Figure 3.5: (a) Circular borosilicate glass without TiO₂ photocatalyst (b) Homogeneous cement layer (c) TiO₂-immobilized borosilicate glass with cement coating in before treatment with 1st, 2nd, 3rd and 4th layer (d) TiO₂-immobilized borosilicate glass with cement coating in after treatment with 1st, 2nd, 3rd and 4th layer.

Table 3.1: The weight of TiO₂ immobilized on the borosilicate glass as layers

No	TiO ₂ catalyst	Wt. of glass (g)	Wt. of glass + TiO ₂ (g)	1 st layer (g)	2 nd layer (g)	3 rd layer (g)	4 th layer (g)	Wt. of glass after treatment		
								Wt. of glass	Wt. of TiO ₂	Wt. loss TiO ₂
1.	60 mg	13.724	13.784	0.059	-	-	-	13.778	0.054	0.006
2.	90 mg	13.373	13.434	13.4599	0.086	-	-	13.451	0.078	0.008
3.	120 mg	12.306	12.364	12.397	12.425	0.119	-	12.406	0.100	0.019
4.	150 mg	13.329	13.393	13.422	13.455	13.480	0.151	13.469	0.140	0.012

Table 3.2: The weight of TiO₂ immobilized on the cement coated borosilicate glass as layers

No	TiO ₂ catalyst	Wt. of glass (g)	Wt. of cement (g)	Wt. of TiO ₂ (g)	1 st layer (g)	2 nd layer (g)	3 rd layer (g)	4 th layer (g)	Wt. of glass after treatment		
									Wt. of glass	Wt. of TiO ₂	Wt. loss TiO ₂
1.	60 mg	13.392	13.463	13.527	0.063	-	-	-	13.514	0.050	0.0133
2.	90 mg	13.716	13.789	13.819	13.878	0.088	-	-	13.870	0.080	0.008
3.	120 mg	13.272	13.340	13.402	13.430	13.459	0.118	-	13.448	0.107	0.011
4.	150 mg	13.121	13.196	13.259	13.288	13.320	13.348	0.152	13.323	0.126	0.025

3.4.2.3 Preparation of TiO₂-Immobilized on Steel Wire Mesh

A steel wire mesh was purchased from the local market and cut into circular shapes to the desired size of 45.00 cm². Then the required amount of TiO₂ was dissolved in ethanol to prepare a solution. The wire mesh was dipped into TiO₂ solution and kept in the environment to dry and weight was measured. Then it was kept at room temperature over 1 hr and in an oven at 110°C for 2 hrs. After drying, it was calcined at 500°C for 2 hrs. First, second, third, and fourth layers of TiO₂ deposition on the steel wire mesh were formed with the amount of 0.060 g, 0.0900 g, 0.1200 g, and 0.1500 g TiO₂ suspension, respectively. The total weight of TiO₂ immobilized steel wire mesh before and after treatment is given in Table 3.3. The images of the first, second, third, and fourth layers of TiO₂ on steel wire mesh layer before and after treatment are shown in Figure 3.6.

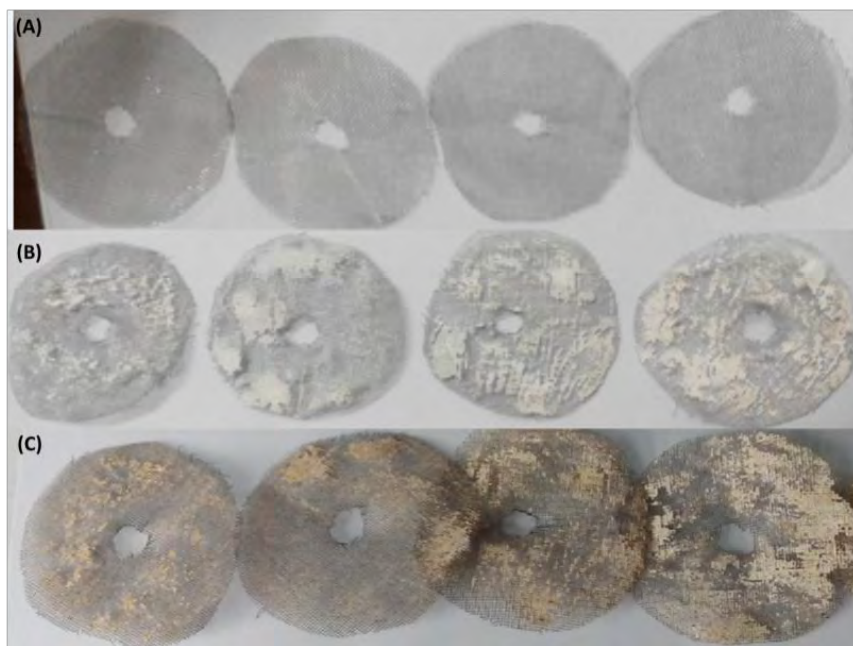


Figure 3.6: (a) Circular steel wire mesh without TiO₂ photocatalyst (b) TiO₂-immobilized steel wire mesh in before treatment with 1st, 2nd, 3rd, and 4th layer (c) TiO₂-immobilized steel wire mesh in after treatment with 1st, 2nd, 3rd, and 4th layer.

Table 3.3: The weight of TiO₂ immobilized on the steel wire mesh as layers

No	TiO ₂ catalyst	Wt. of wire mesh (g)	Wt. of glass + TiO ₂ (g)	1 st layer (g)	2 nd layer (g)	3 rd layer (g)	4 th layer (g)	Wt. of glass after treatment		
								Wt. of glass	Wt. of TiO ₂	Wt. loss TiO ₂
1.	60 mg	0.612	0.673	0.061	-	-		0.628	0.045	0.016
2.	90 mg	0.617	0.706	-	0.089	-		0.638	0.067	0.021
3.	120 mg	0.625	0.743	-	-	0.118		0.647	0.096	0.021
4.	150 mg	0.615	0.762	-	-	-	0.146	0.643	0.119	0.027

3.5 Experimental Set-up

The solar-TiO₂ immobilized experiments were carried out using batch reactors containing a TiO₂-immobilized surface. Three types of supporting materials such as borosilicate glass, borosilicate glass with cement coating, and stainless steel wire mesh were used to immobilize TiO₂. Experiments and analysis were performed according to developed methods based on the removal of dye concentration, color, and with or without the addition of oxidant hydrogen peroxide. The experimental set-up of MO degradation by using TiO₂-immobilized supported materials are shown in Figures 3.7.

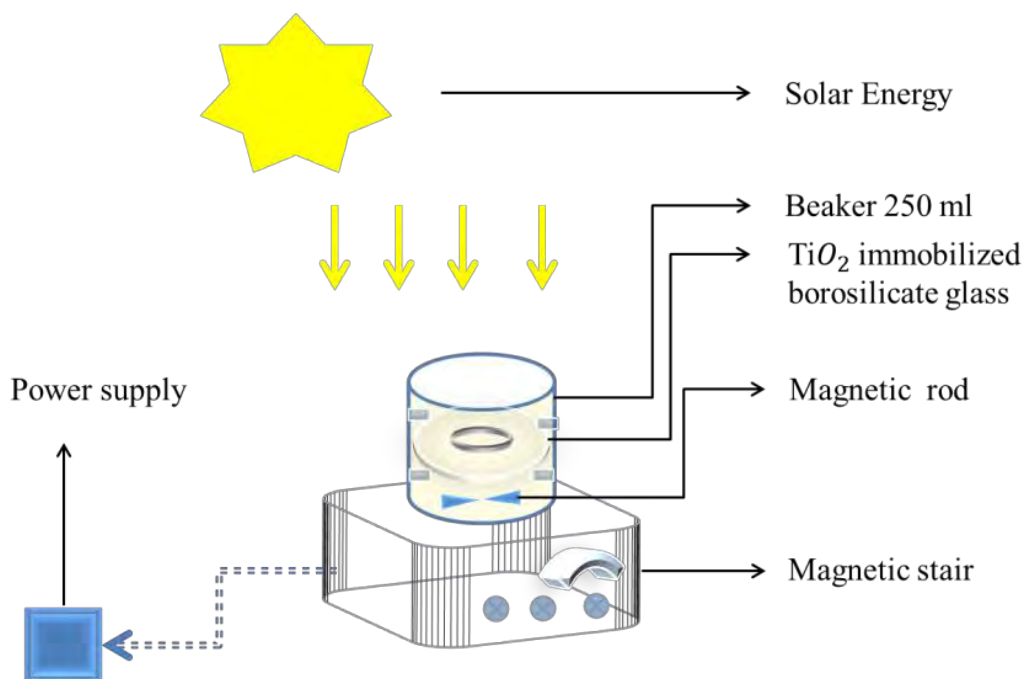


Figure 3.7: A set-up of solar-TiO₂ immobilized photocatalytic reactor

3.6 Photocatalytic Degradation of Methyl Orange under Solar Irradiation

The photocatalytic degradation of MO dye under solar irradiation has been divided into four major parts stated below:

- i. Preparation of desired concentrated MO solution
- ii. Calibration curve
- iii. Photocatalytic decomposition of MO dye using TiO₂-immobilized photocatalyst reactor under solar irradiation
 - a. Study of the effect of dose

- b. Study of the effect of dye concentration
- c. Study of the effect of hydrogen per-oxide concentration
- iv. Basic mathematical equations

3.6.1 Preparation of desired concentrated MO solution

0.1 g powder MO was dissolved in 1 L double distilled water to prepare 100 ppm MO solution.

With the help of these stock solutions, dilute solutions of various concentrations were prepared by using the formulae:

$$S_1V_1=S_2V_2 \quad (3.5)$$

The chemical structure and typical UV-Visible spectral feature of MO are represented in Figure 3.8 and Figure 3.9 respectively.

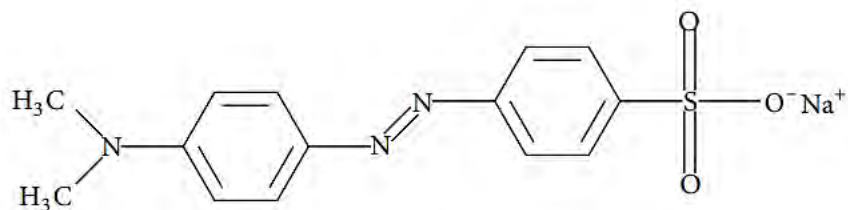


Figure 3.8: Chemical structure of MO

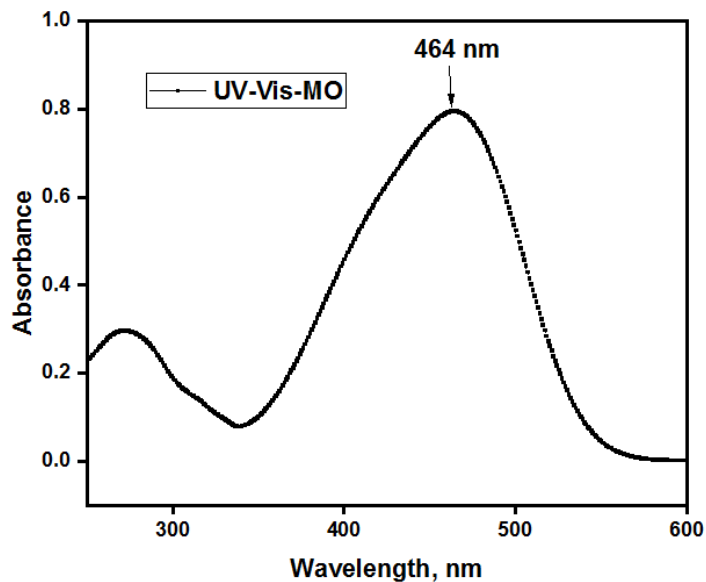


Figure 3.9: UV-Visible spectrum of an aqueous solution of MO at pH 6.20

3.6.2 Calibration Curve

The molar absorption coefficient of the MO solutions was determined from a plot of absorbance against concentration (calibration curve) using Beer-Lambert law. To have data for this plot, five different MO solutions of concentrations viz. 5, 10, 15, 20, 30 ppm were prepared and their absorbance value was determined without any further treatment. Each and every sample including a blank was placed in SHIMADZU UV-2600 UV-VIS Spectrophotometer. The corresponding absorbance peak value was recorded at a wavelength of 464 nm at room temperature with the pH 6.20 (water was used as reference). The recorded absorbance peak values against MO concentrations were plotted in the calibration curve is shown in Figure 3.10.

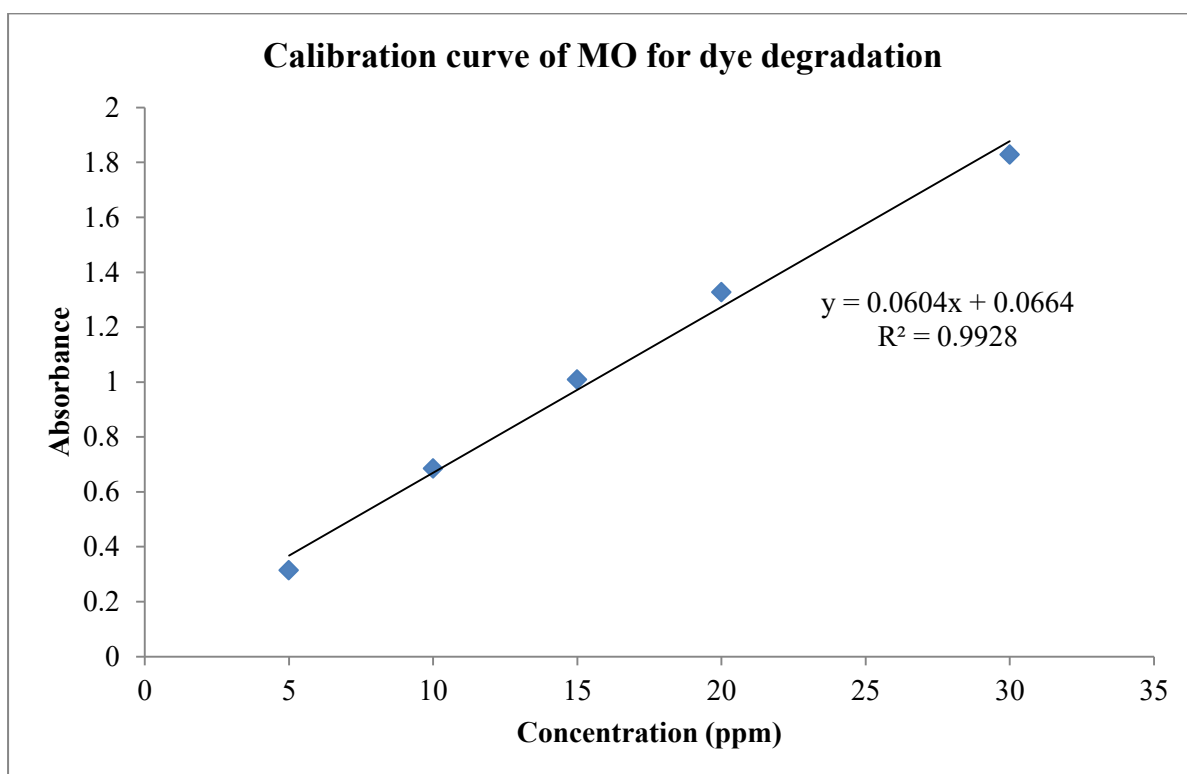


Figure 3.10: Calibration curve of MO for dye degradation

3.6.3 TiO₂-Immobilized Photocatalysis of MO under Solar Irradiation

A photocatalytic batch reactor consists of a 250 mL beaker and TiO₂-immobilized surface which may contain a TiO₂-immobilized borosilicate glass or TiO₂-immobilized cement coated borosilicate glass or TiO₂-immobilized stainless steel wire mesh. 3 sets of such reactors were operated together to investigate a comparative performance of those 3 surfaces. Initially, a 125

mL of dye solution at a fixed concentration (e.g. 10 ppm) and a fixed pH was placed into each of 3 sets of reactors. Then the reactors were placed under solar light source on a magnetic stirrer. The magnetic stirring speed was maintained at medium speed throughout the study to ensure uniform mixing. The batch studies were carried out from 10.00 am to 3.00 pm at the surrounding temperature. At the end of preset time intervals, samples were withdrawn and the changes in concentration of dye solution were analyzed by using a UV-Vis spectrophotometer. The photocatalytic degradation of dye was evaluated for each reactor to investigate the performance of TiO₂-immobilized borosilicate glass, TiO₂-immobilized cement coated borosilicate glass and TiO₂-immobilized stainless steel wire mesh. The impact of pH, photocatalyst dosage, and initial dye concentration was evaluated from the experiment. The pH was regulated by adding incremental amounts of either dilute HNO₃ or NaOH to the solution.

3.6.3.1 Study of the Effect of Dose

To understand the dose-effect, the experiment was conducted with five different amounts of samples viz. 60 mg, 90 mg, 120 mg, and 150 mg which were added with 125 mL 10 ppm, 20 ppm, and 30 ppm of MO solution and were allowed to interact for the equilibrium time interval of 10.00 am to 3.00 pm.

3.6.3.2 Study of the Effect of Dye Concentration

The effect of dye concentration, experiment was conducted with three different dye concentrations viz. 10 ppm, 20 ppm and 30 ppm which was formulated 125 mL MO solution containing pH 6.2 was allowed to contact with dose with the time interval of 10.00 am to 3.00 pm. The different dye concentrations of the MO solution were prepared by the addition of distilled water.

3.6.3.3 Study of the Effect of Hydrogen Per-oxide (H₂O₂)

The effect of hydrogen peroxide (H₂O₂) was unraveled by experimenting 0.1 mL and 0.25 mL which was applied 125 mL of MO solution containing 10 ppm, 20 ppm and 30 ppm containing the natural solution of pH 6.2. In each case, 120 mg of the samples were added and allowed to interact for the equilibrium time of 10.00 am to 3.00 pm. The different oxidant concentrations were prepared by the addition of the H₂O₂ solution.

3.6.4 Basic Mathematical Equations

The dye degradation (%) was used as the indicator to evaluate and compare the photocatalytic performances of the TiO₂ immobilized borosilicate glass, cement coated borosilicate glass and steel wire mesh.

The percentage (%) degradation was determined by using the following equation [169]:

$$\% \text{ Degradation} = \frac{C_0 - C_t}{C_0} \times 100 \quad (3.6)$$

Where C_0 = initial concentration of dye solution, C_t = concentration of dye solution after irradiation.

The kinetics of the degradation of MO dye by photocatalytic reaction were studied for zero-order, first-order and second-order with respect to dye degradation with time [170]. The integrated form of expressions for kinetic models are presented as follows Eqs. (3.7-3.9)

Zero order kinetics:

$$C_t - C_0 = k_0 t \quad (3.7)$$

First order kinetics:

$$\ln \left(\frac{C_0}{C_t} \right) = k_1 t \quad (3.8)$$

Second order kinetics:

$$\frac{1}{C_t} - \frac{1}{C_0} = k_2 t \quad (3.9)$$

Where k_0 ($\text{mgL}^{-1} \cdot \text{min}^{-1}$), k_1 (min^{-1}) and k_2 ($\text{Lmg}^{-1} \cdot \text{min}^{-1}$), represent the apparent kinetic rate constants of zero, first and second order reaction kinetics, respectively. C_0 and C_t are the initial dye concentration and dye concentration at time t (min), respectively [170].

CHAPTER 4

RESULTS AND DISCUSSION

In this Chapter, the results and discussion of the study have been presented systematically. The Chapter includes results and discussion on the characterization of TiO₂ photocatalyst and the photocatalytic degradation of MO dye in the presence of solar irradiation.

4.1 Characterization of Photocatalysts

The analytical techniques used in this research work for characterization of TiO₂ photocatalyst were UV-Vis Spectroscopy, Bandgap energy measurement, Fourier Transform Infrared Spectroscopy (FT-IR), X-ray Diffraction (XRD), Scanning Electron Microscopy (SEM), and Brunauer–Emmett–Teller Isotherm (BET) analysis. It is well established that morphological and structural parameters such as crystalline structure, bandgap position, surface area, particle size, and pore volume which implies the lack of impurities, defects, or amorphous domains, strongly affect the photocatalytic activity of a semiconductor [171,172]. This section includes the instrumental results obtained from the experiment.

4.1.1 Ultraviolet-Visible Spectroscopy (UV-Vis) of TiO₂ Nanoparticle

In Ultraviolet-Visible Spectroscopy (UV-Vis), the absorption and reflectance spectrum of TiO₂ nanoparticles prepared with hydrolysis and without hydrolysis were recorded to study the optical property of photocatalyst in the wavelength range of 200 nm to 600 nm as shown in Figure 4.1. The absorption spectrum of TiO₂ nanoparticles (Fig. 4.1) revealed a single and broad intense absorption around 270 nm due to charge transfer from the valance band to the conduction band [173]. In hydrolysis, it was observed that the reflectance spectrum of TiO₂ nanoparticles slightly increased at a wavelength of less than 240 nm without hydrolysis and thus consequently decreased the band gap values which maximized the electron-hole recombination during the photocatalytic degradation of MO [158]. It was demonstrated that the hydrolysis absorption edge shifted towards a longer wavelength than without hydrolysis. The absorbance spectrum of TiO₂ nanoparticles prepared with hydrolysis and without hydrolysis clearly indicates that the characteristics of the particles were different.

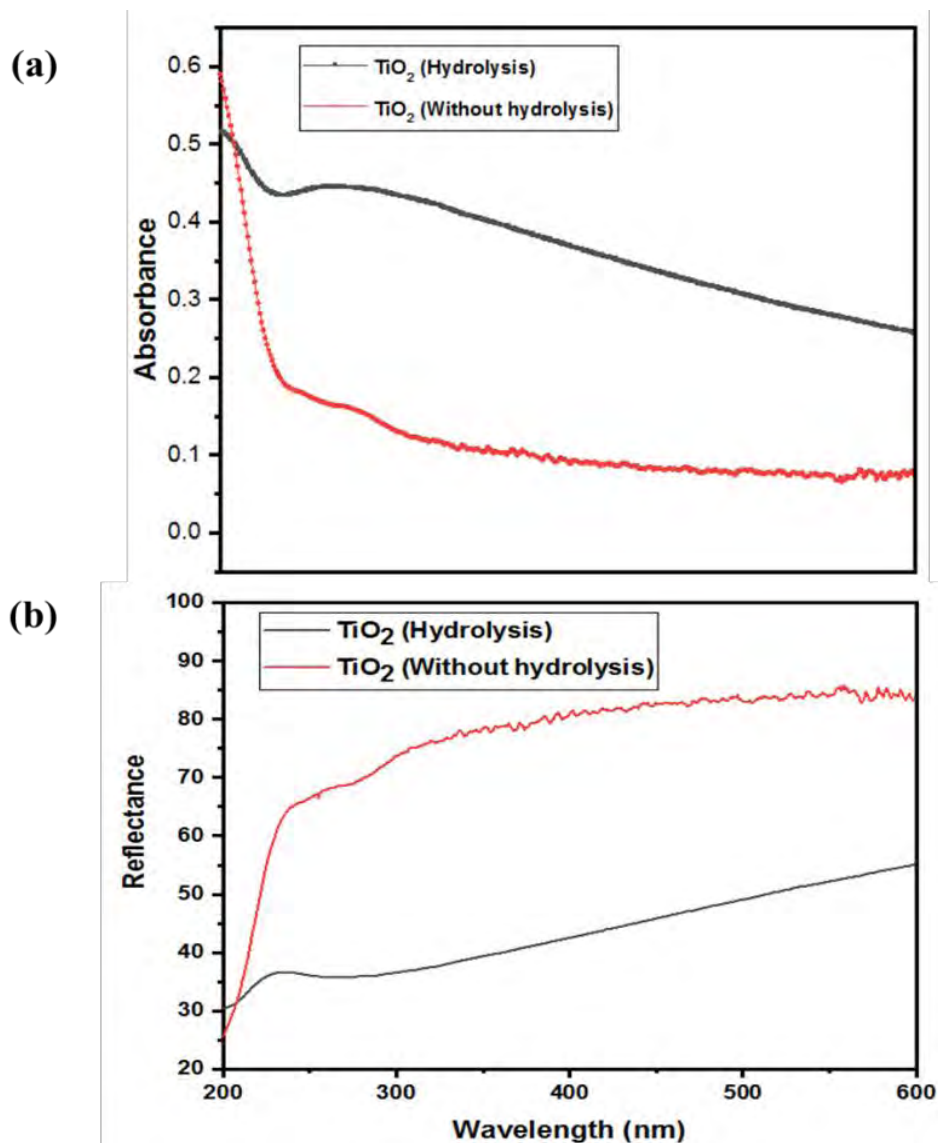


Fig. 4.1: UV-Vis spectra of TiO₂ nanoparticles with and without hydrolysis preparation; (a) absorbance response and (b) reflectance response

The bandgap energy (E_g) of semiconductor photocatalyst is very important in measuring electronic structure since it states that the amount of energy to be absorbed to generate the electron-hole pair. It was reported that the E_g of TiO₂ nanoparticles depends on the absorbance data and the electronic transition of semiconductors [174]. The E_g of TiO₂ nanoparticles were calculated by using Tauc plots which is a graphical representation of Kubelka-Munk formulism (Table 4.1).

Table 4.1: The bandgap energy (eV) of the TiO₂ nanoparticles prepared with hydrolysis and without hydrolysis by using Kubelka-Munk equation.

Sample	Method	Bandgap, E _g (eV)
TiO ₂	Sol-gel with hydrolysis	3.06
TiO ₂	Sol-gel without hydrolysis	5.29

The E_g values of TiO₂ were found 3.06 eV and 5.29 eV for hydrolysis and without hydrolysis, respectively is shown in Figure 4.2. The E_g in without hydrolysis shows higher due to cause by the quantum size effects, absorption edge that is shifted to higher energy (blue shift), and not using a solvent (H₂O) [175-177]. This indicates that more energy is required to generate e/h pair and thus considered as less active photocatalyst than nanoparticles with hydrolysis. According to the literature, the typical band gap energy of TiO₂ nanoparticles for pure anatase phase is 3.2 eV and for pure rutile phase is 3.0 eV [178]. The bandgap was reduced by the incorporation of ethanol and solvent (H₂O) into the reaction medium. However, TiO₂ nanoparticles having smaller bandgap can be suitable for photocatalytic applications [175].

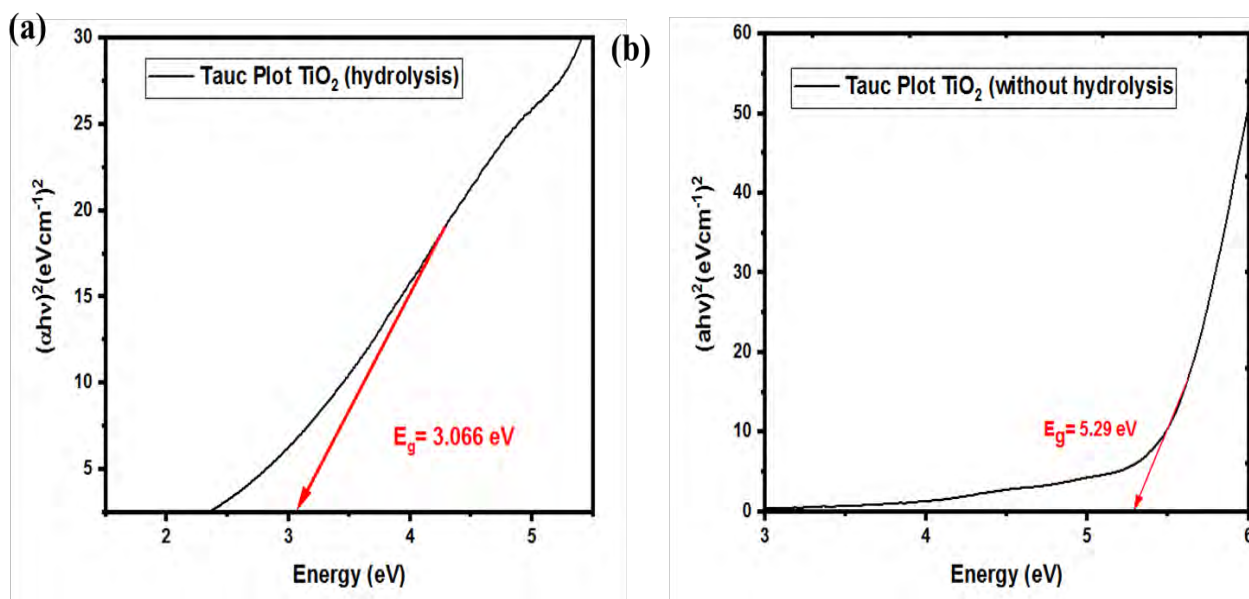


Figure 4.2: Band gap energy of TiO₂ nanoparticles prepared (a) by hydrolysis and (b) without hydrolysis

4.1.2 Fourier Transform Infrared Spectroscopy (FT-IR) of TiO₂ Nanoparticle

The FT-IR spectra of the TiO₂ nanoparticles prepared with hydrolysis and without hydrolysis were recorded in the range of 4000-400 cm⁻¹. Figure 4.3 shows the spectra and the extracted functional groups from spectra are shown in Table 4.2.

Table 4.2: FT-IR bands of TiO₂ nanoparticle prepared with hydrolysis and without hydrolysis

TiO ₂ nanoparticle with hydrolysis		TiO ₂ nanoparticle without hydrolysis	
Frequency (cm ⁻¹)	Functional groups	Frequency (cm ⁻¹)	Functional groups
3462	O-H (alc./water)	3462	O-H (alc./water)
1724	C=O (carbonyl)	1726	C=O (carbonyl)
1635	C=C (sp ² hybrid)	1635	C=C (sp ² hybrid)
1357	Ti=O (Stretching)	1359	Ti=O (Stretching)
1224	C-O-C (epoxy)	1222	C-O-C (epoxy)
1064	Ti-O-Ti (Stretching)	1093	Ti-O-Ti (Stretching)
1020	Ti-O-Ti (Stretching)		
904	Ti-O-Ti (Stretching)		
825	Ti-O-Ti (Stretching)		

In hydrolysis, the weak absorption bands were attributed between 700-800 cm⁻¹ that represents the stretching vibrations of (Ti–O–Ti) bonds in the TiO₂ lattice structure while no effective absorption bands were found in that position containing without hydrolysis. It was reported that the higher surface content of (Ti-O-Ti) species subsequently enhance the dispersion and photocatalytic performance of dye [179]. The strong absorption bands were observed in both cases to be the frequency region of 800-1000 cm⁻¹ corresponds to (Ti-O-Ti) bonding which confirms the formation of titanium metal complex. The broad intense band below 1000 cm⁻¹ was attributed due to (Ti-O-Ti) stretching vibrations that have been reported [162]. The typical vibrations centered around 3462 cm⁻¹ with corresponding groups which identify the broad bands of (O-H) group that refers to alcohol and carboxylic acid groups. The peak was observed at 1635 cm⁻¹ corresponding shows stretching vibrations of (–C=C–) bond alkenes that indicating the presence of sp² hybridized carbon along with a contribution from bending vibration of (O-H) bond resulting higher intensity. The sharp peaks were observed at 1357 cm⁻¹ and 1359 cm⁻¹ show stretching vibrations of (Ti=O) bonds [180]. Similarly, the peak observed at 1222 cm⁻¹

shows the epoxy group (C-O-C) bond formation in the spectra of TiO₂ nanoparticles without hydrolysis.

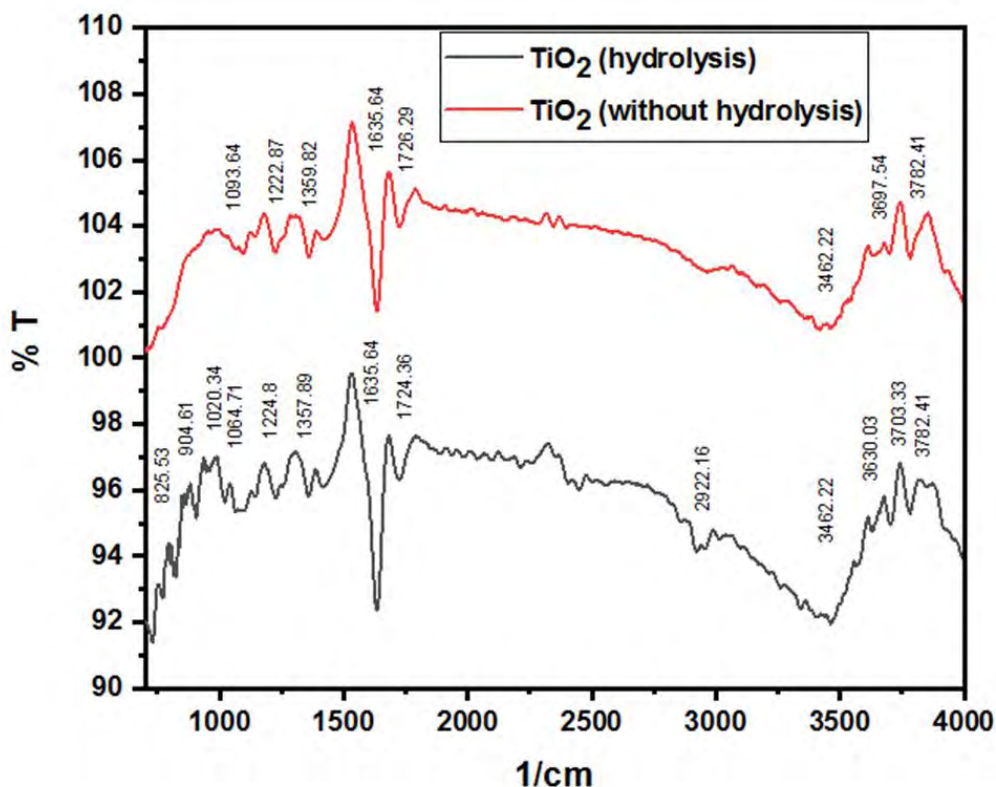


Figure 4.3: FT-IR analysis of TiO₂ nanoparticle prepared with and without hydrolysis

4.1.3 X-ray Diffraction (XRD) of TiO₂ Nanoparticle

The proper crystal structure is very important for TiO₂ photocatalyst. XRD is used to determine the crystal phase composition, intensity, and average crystalline size of TiO₂ nanoparticles prepared with hydrolysis and without hydrolysis, and the spectra are shown in Figure 4.4. The TiO₂ nanoparticles prepared with hydrolysis and without hydrolysis were calcined at 500°C. In hydrolysis preparation, it can be observed (Figure 4.4) that the 2θ peaks in XRD spectra were at 25.04°, 37.83°, 47.87°, 53.72°, 54.92°, 62.57°, 68.66°, 70.09°, and 74.87° corresponding to the reflection from {101}, {004}, {200}, {105}, {211}, {204}, {116}, {220} and {215} crystal planes which indicates that the TiO₂ nanoparticles were dominated by anatase crystal [176]. The anatase phases were confirmed by {101}, {004}, {200}, {211}, and {204} diffraction peaks [161]. The patterns reveal that the effects of calcination temperatures on the phase change of TiO₂ nanoparticle. According to the literature, the anatase phase was observed for TiO₂ NPs

calcined at 400°C and 500°C [181]. The anatase phase was usually exhibited the best photocatalytic behavior, while the rutile phase was the most stable [182]. This was formed due to electron transport from the valence band to the conduction band in the anatase phase and thus, results in the increase of photocatalytic activity for dye removal [183,184]. The factors that increase this separation time increase the electron and hole pair's longevity, and eventually photocatalytic activity increases for dye degradation [185,186]. Electron transport to the conduction band of the rutile phase, which is adjacent to the anatase phase can be effective in the durability and longevity of electron and hole pairs. However, if the percentage of anatase is higher than rutile, it shows higher photocatalytic activity [186]. The presence of the rutile phase in adjacent to the anatase phase in small quantities acts such as a structural defect or impurity and causes high photocatalytic activity [187]. It has been established that the photocatalytic activity of TiO₂ strongly depends on its crystal structure. For instance, anatase-phase TiO₂ crystallites were generally found to be more active than rutile [188]. It can be observed from Figure 4.4 for TiO₂ nanoparticles prepared from without hydrolysis that the 2θ peaks in XRD spectra were at 25.32°, 27.46°, 36.09°, 37.78°, 41.25°, 44.08°, 48.09°, 54.32°, 55.12°, 56.65°, 62.78°, and 69.01° corresponding to the reflection from {101}, {110}, {101}, {004}, {111}, {210}, {200}, {105}, {211}, {220}, {022} and {301} crystal planes, respectively indicating the TiO₂ nanoparticles were dominated by rutile crystal. A rutile peak (110) was marked in corresponds to the anatase phase due to calcined at 500°C and without solvent (H₂O) in preparing nanoparticles. It was observed that the diffraction anatase peak intensity becomes stronger and narrower the peak width that reveals the larger grain size. Furthermore, the presence of the anatase phase adjacent to the rutile phase in small quantities acts as a no structural defect or impurity and causes lower photocatalytic activity [187]. Based on the rough estimation obtained from XRD data, the average crystalline size of the TiO₂ photocatalyst according to the Debye-Scherrer method was calculated to be found 11.03 nm and 18.08 nm for hydrolysis and without hydrolysis respectively. The peak intensities from the XRD analysis were used to calculate the theoretical physicochemical properties of TiO₂ nanoparticles are provided in Table 4.3. The crystalline size was reduced due to the lattice distortion. The smaller crystalline size represents higher photocatalytic activity when the dye only absorbs the incident visible light that enhances the overall yield [189]. Besides, lattice parameters such as a, c, and d_{hkl} were determined for both samples (Table 4.3) and massive differences were observed in hydrolysis

with respect to without hydrolysis. However, the smaller crystalline size in hydrolysis is an indication of increased surface area as we observed from BET analysis and can have a higher photocatalytic activity to the degradation of dye under the incident visible light [190].

Table 4.3: Summary of theoretical physicochemical properties of TiO₂ nanoparticles

SI No.	Samples	Methods	Crystalline Size (nm)	d_{hkl} (Å)	Lattice Parameter (Å)	
					a	c
1.	TiO ₂	Sol-gel with hydrolysis	11.03	3.52	3.78	9.50
2.	TiO ₂	Sol-gel without hydrolysis	18.08	8.10	1.74	57.08

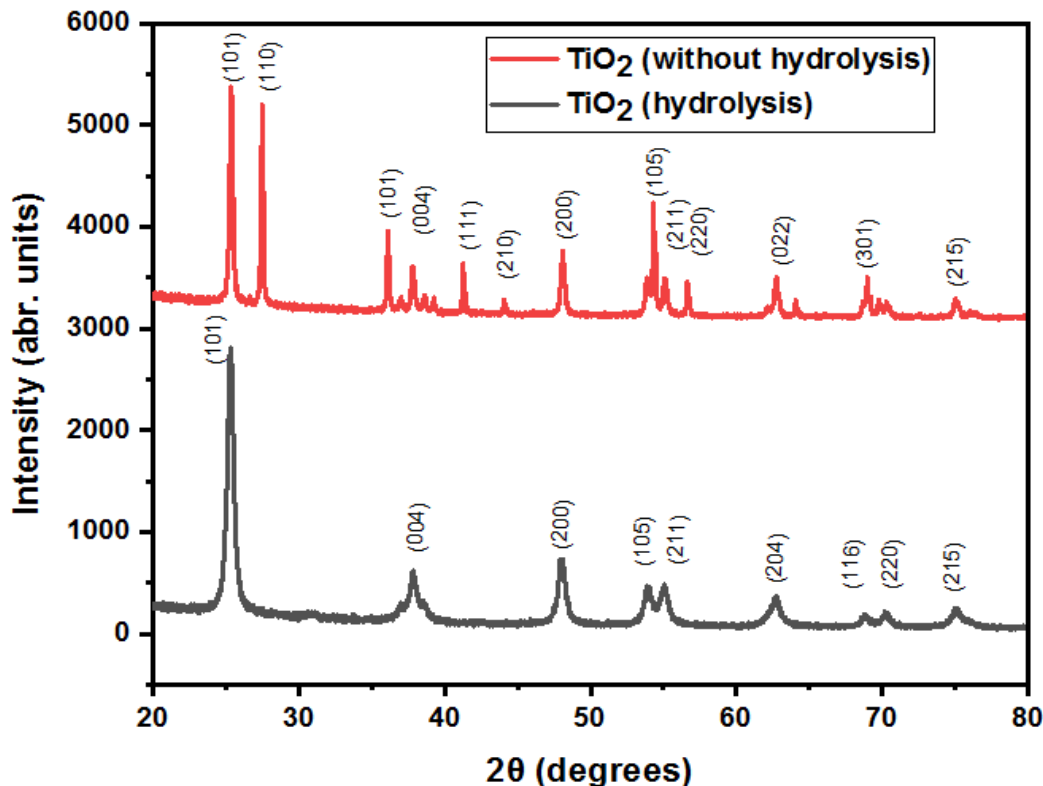


Figure 4.4: XRD plot of TiO₂ nanoparticle prepared with hydrolysis and without hydrolysis

4.1.4 Scanning Electron Microscopy (SEM) of TiO₂ Nanoparticle

SEM is a powerful analytical technique in the identification of materials, revealing external morphology (texture), crystalline structure, size, and orientation of materials making up the

sample. SEM images also show the relatively smooth surface and thickness of the sample. The nanoscale SEM images of TiO₂ nanoparticles were taken. Figure 4.5 shows the SEM images of TiO₂ nanoparticle prepared by hydrolysis and without hydrolysis. For TiO₂ nanoparticle prepared by hydrolysis, porous bulk structure with uniform spherical particle distribution was observed, while non-uniform particle distribution was observed for TiO₂ without hydrolysis (Fig 4.5a-b). The more rugged and rough surface was observed for TiO₂ with hydrolysis than TiO₂ without hydrolysis, which is consisted with the higher surface area as observed from BET surface area analysis. The estimated average TiO₂ nanoparticles size was around to be 4-5 nm and 6-7 nm for hydrolysis and without hydrolysis respectively. It has been reported that the particle size increases with an increase in calcination temperature because of the agglomeration of a smaller particle at high temperatures [162]. Low temperature leads to better boundaries between nanoparticles. Consequently, the morphology of the TiO₂ nanoparticles was changed to the sphere. The spheres consist of many small spherical crystals of TiO₂ crystals due to agglomeration [191]. However, substantial aggregation of the particles was also confirmed by SEM images.

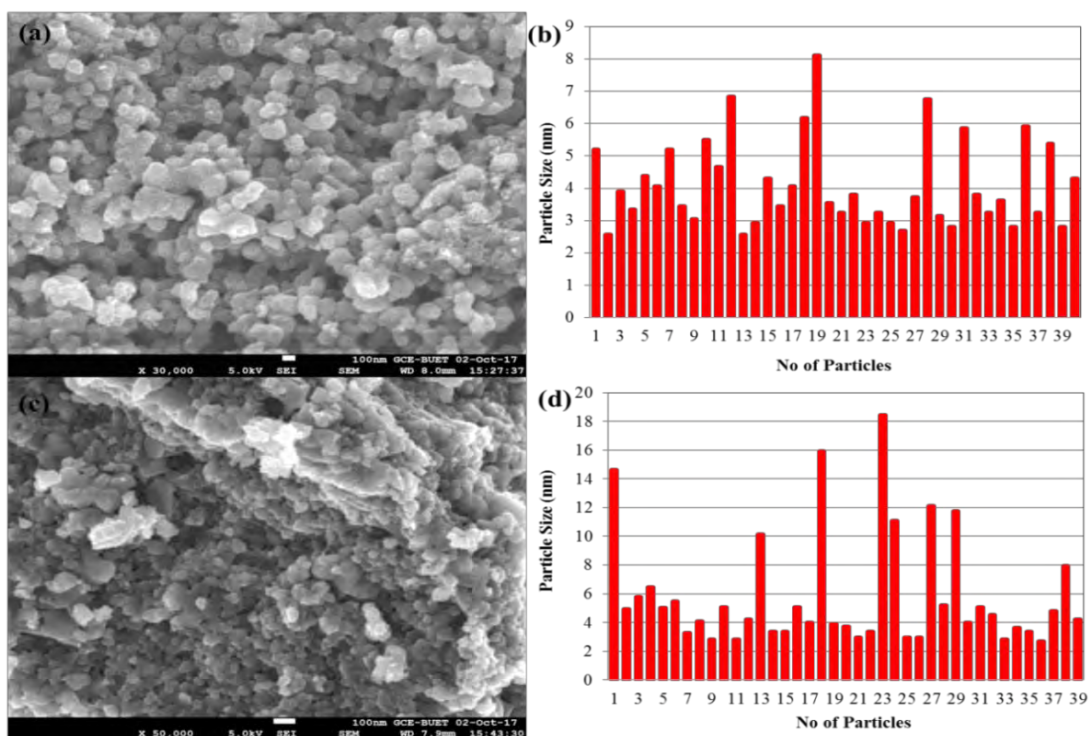


Figure 4.5: (a) SEM image of TiO₂ nanoparticle with hydrolysis, (b) Particle size analysis of TiO₂ nanoparticles, (c) SEM image of TiO₂ nanoparticle without hydrolysis, and (d) Particle size analysis of TiO₂ nanoparticles without hydrolysis.

The presence of TiO₂ nanoparticles prepared with hydrolysis and without hydrolysis was analyzed by the EDX spectrum. Figure 4.6 depicts the quantitative analysis of the TiO₂ nanoparticle. It confirms the presence of carbon, oxygen, and titanium [192]. The EDX mapping of the synthesized TiO₂ nanoparticles with and without hydrolysis is shown in Figure 4.6.

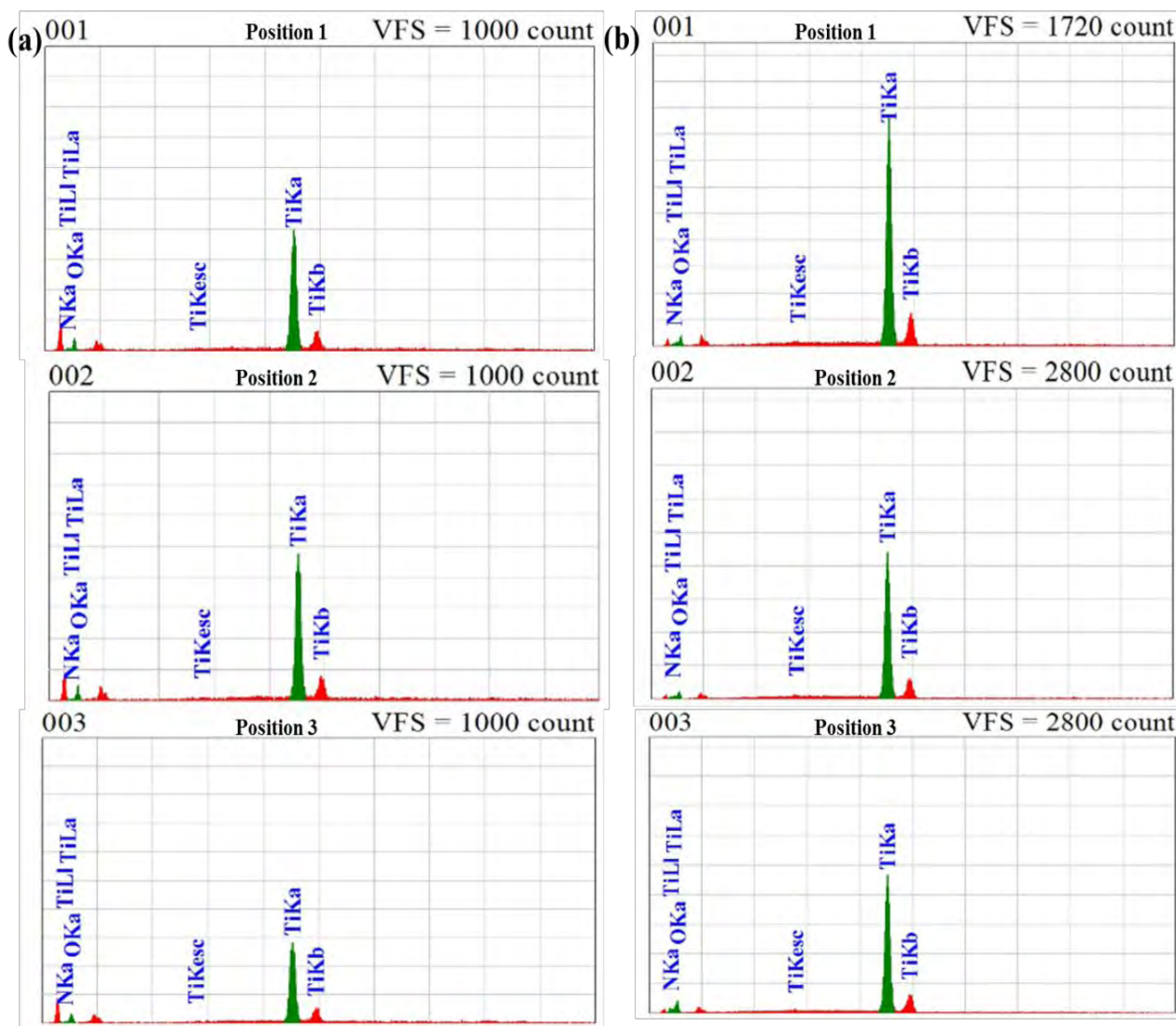


Figure 4.6: EDX analysis of TiO₂ nanoparticle (a) with hydrolysis at positions 1, 2, and 3, (b) without hydrolysis at positions 1, 2, and 3.

The average atomic (mass) percentages of Ti and O in TiO₂ prepared with hydrolysis were 77.75% and 22.25% (91.27% and 8.73%), respectively. Similarly, the average atomic (mass) percentages of Ti and O in TiO₂ prepared without hydrolysis were 85.91% and 14.01% (94.77%

and 5.20%), respectively. The summaries of atomic and mass percentage of TiO₂ nanoparticles prepared with hydrolysis and without hydrolysis were given in Table 4.4.

Table 4.4: Summary of atomic and mass percentage of samples (a) hydrolysis, (b) without hydrolysis

(a)	Sample Point	Fitting Coefficient	Ti (atm. %)	O (atm. %)	Ti (mass %)	O (mass %)
	1.	0.2657	78.76	21.24	91.74	8.26
	2.	0.2307	77.37	22.63	91.10	8.90
	3.	0.2957	77.11	22.89	90.98	9.02
	Average	0.2640	77.75	22.25	91.27	8.73

(b)	Sample Point	Fitting Coefficient	Ti (atm. %)	O (atm. %)	Ti (mass %)	O (mass %)
	1.	0.1342	89.49	10.51	96.23	3.77
	2.	0.1342	87.29	12.71	95.36	4.64
	3.	0.1276	80.94	18.81	92.72	7.20
	Average	0.1320	85.91	14.01	94.77	5.20

4.1.5 BET Surface Area Analysis of TiO₂ Nanoparticle

The surface area and pore volume analysis of TiO₂ nanoparticles synthesized with hydrolysis and without hydrolysis was carried out by an N₂ adsorbate based adsorption-desorption mechanism. The experimental values were calculated using the BET adsorption method and are summarized in Table 4.5. The specific surface area and pore volume of TiO₂ nanoparticles were increased in hydrolysis as compared to without hydrolysis. For instance, about 67 times the higher surface area was obtained for TiO₂ nanoparticles synthesized with hydrolysis than without hydrolysis. It was observed that the surface area decreased with increasing the crystal size. This was formed due to increasing temperature and densification (inadequate solvent) and thus an increase in average particle size [193]. The increase of surface area can be very useful for contaminants to penetrate through and carry out the desired degradation reactions as it implies larger contact surfaces exposed to the reagents. Similarly, the increase of pore volume can also be considered as an increase in mesopore volume [194].

Table 4.5: Surface area and pore volume measurement of composites

SI No.	Sample	Sol-gel method	Surface area (m ² /g)	Pore Volume (cm ³ /g)
1.	TiO ₂	Hydrolysis	81.48±4.96	0.2298
2.	TiO ₂	Without hydrolysis	1.20±0.16	0.0034

The experimental results from the BET surface studies reflected the crystallite sizes determined by XRD. It was accepted in heterogeneous photocatalysis process, higher surface area and pore volume can be useful in the formation of photogenerated electron-hole pairs. The heterogeneous photocatalytic activity can be influenced greatly by the surface area and pore volume [195].

A comparison between the surface area and pore volume of semiconductor TiO₂ nanoparticles with literal values are shown in Table 4.6. Among those, the proposed study shows that the surface area and pore volume of TiO₂ nanoparticles prepared by sol-gel and heat treatment method with hydrolysis was very high.

Table 4.6: Comparison of BET surface area among composites and components

SI No.	Sample	Method	BET (m ² /g)	Surface Area	Pore Volume (cm ³ /g)	Reference
1.	TiO ₂	Sol-gel	32.22		0.0564	[196]
2.	TiO ₂	Sol-gel	22.7		0.0320	[197]
3.	TiO ₂	Sol-gel	81.48		0.2298	[Present study]

4.2 Impact of Solar Irradiation on Dye Removal in Absence of Photocatalyst

Dye removal under solar irradiation without photocatalyst was investigated. Even after 4 h of exposure of dye under solar irradiation, we didn't find a substantial change of dye concentration [198] because solar irradiation couldn't produce ([•]OH) radical enough to degrade the dye (Figure 4.7). In an open reactor, the dye concentrations were reduced from 10 ppm to 9.83 ppm after 4 h of exposure. According to the literature, no photocatalytic degradation was observed in the absence of TiO₂ photocatalyst [199].

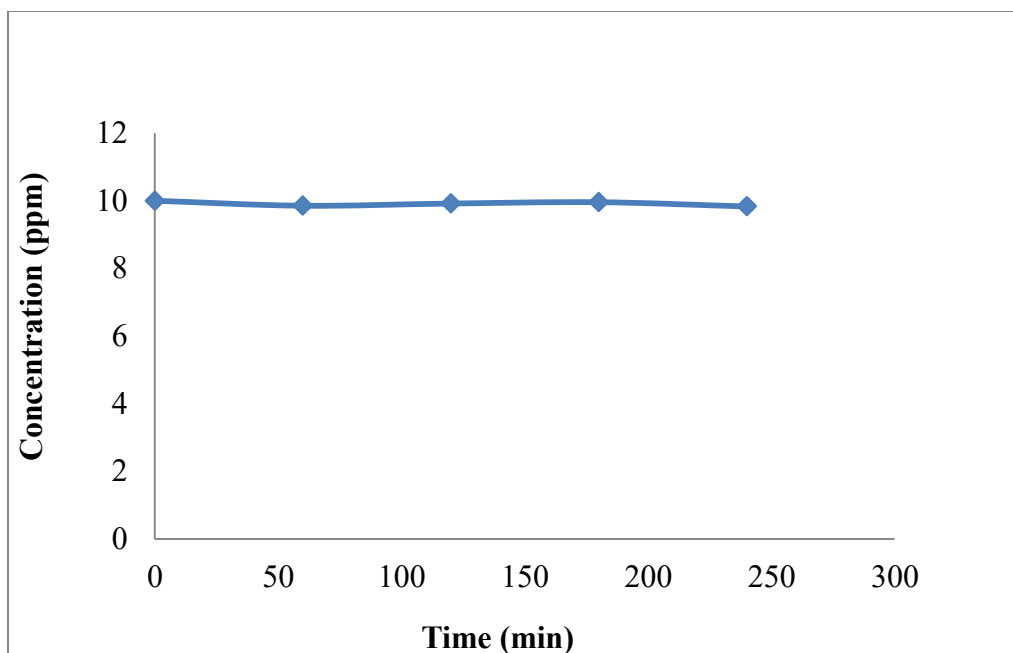


Figure 4.7: Dye concentration under solar irradiation at open reactor in absence photocatalyst

4.3 Effect of Evaporation on Dye Degradation in Absence of Photocatalyst

Evaporation is an important factor in dye degradation under solar irradiation because it has an inverse effect on dye degradation which means with the increase of evaporation, dye concentration is increased in the solution. Besides, with the increase of temperature, the organic adsorption capacity of the photocatalyst is decreased; and thus, a decrease of the photocatalytic reactor performance [139]. Therefore, three types of reactor design were considered for this study: open reactor, closed with aluminum foil reactor, and glass cover reactor. A 125 mL MO dye solution containing a concentration of 10 ppm was placed under solar irradiation without photocatalyst up to 4 hours and the results showed that the 21, 2, and 3 ml of water evaporated from open, aluminum foil-covered and glass-covered reactors, respectively. This was formed due to the evaporation of the solvent (water) from the MO dye solution under solar irradiation. The results are shown in Figure 4.8. This implies that the photocatalytic degradation process is closely associated with evaporation and that the evaporation rate can affect the photocatalytic degradation rate [200]. In the study, the concentrations were decreased with respect to time on a different model of reactors under solar irradiation without photocatalyst were investigated. The concentrations were changed from 10.00 ppm to 9.831, 9.407, and 9.334 ppm for the open

reactor, aluminum foil-covered reactor, and glass-covered reactor, respectively, after 4 hours of contact time.

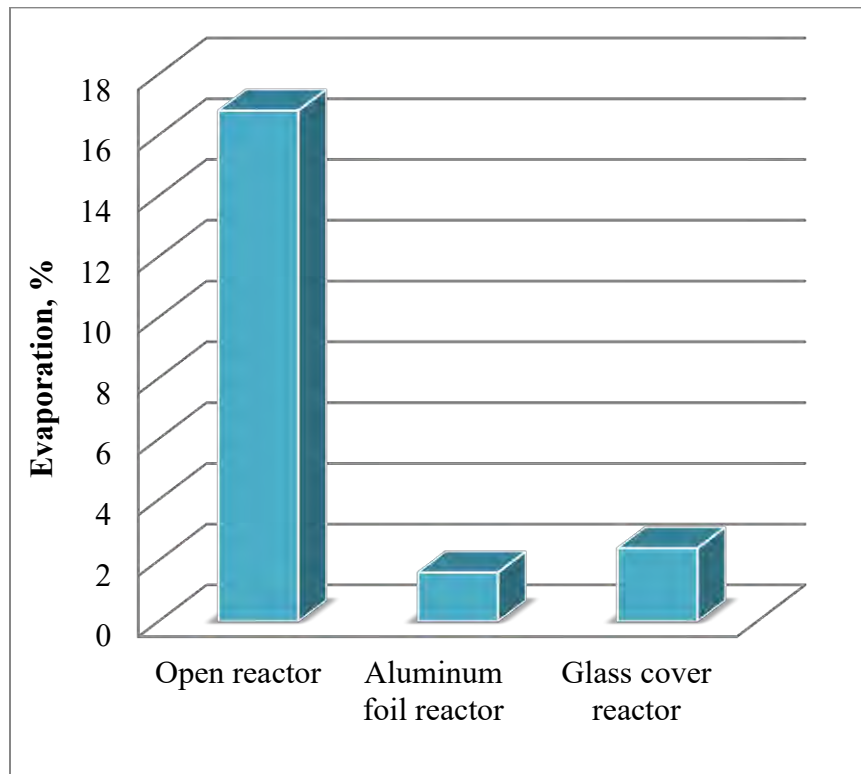


Figure 4.8: Effect of evaporation at different reactor model

4.4 Photocatalytic Activity Assessment

Based on the surface characterization analyses, we observed that the TiO₂ nanoparticles synthesized with hydrolysis are anatase, smaller crystal size, have lower bandgap and higher surface area. Therefore, the TiO₂ nanoparticle with hydrolysis preparation was tested for photocatalytic assessment study. The applied immobilization dosages of TiO₂ nanoparticles were 0.060, 0.090, 0.120, and 0.150 g known as 1st, 2nd, 3rd and 4th layer dosages on borosilicate glass, cement coated borosilicate glass, and steel wire mesh surfaces were investigated in the degradation of MO dye under solar irradiation with 5 h contact time. Initially, 10 ppm dye concentration at pH 6.2 was used for all the immobilized reactors.

4.4.1 Effect of Thickness of TiO₂-Immobilization on Dye Degradation

The effect of thickness of TiO₂-immobilization on the borosilicate glass reactor in the degradation of dye in the presence of solar irradiation was investigated and the results are shown

in Figure 4.9 (a). The concentration of MO dye was decreased from 10.00 ppm to 4.27, 2.978, 0.217, and 0.098 ppm, respectively, for the 1st, 2nd, 3rd and 4th layer of TiO₂ immobilization on borosilicate glass after contact of 5 h of solar irradiation. The maximum solar irradiation was found from 1.00 pm to 2.00 pm. The dye degradation was increased with the increase of TiO₂ immobilization thickness. According to the literature survey, glass is commonly used as the coating substrate, which has high transparency to solar radiation and has the good adhesive property to support TiO₂ nanoparticle without reduction of catalyst activity [201,202]. Therefore, the high degradation rate was observed. Literature reported that MO dye can be removed completely at low concentration with TiO₂ at suspension, but with higher initial concentrations, the removal percentages were declined rapidly, and thus, the removal of MO could not reach a satisfying level [203]. Similarly, the effect of TiO₂-immobilization thickness on cement coated borosilicate glass reactor in the presence of solar irradiation was investigated and the results are shown in Figure 4.9 (b). The concentration of MO dye was decreased from 10.00 ppm to 5.443, 5.042, 1.642, and 1.137 ppm respectively for 1st, 2nd, 3rd and 4th layer of TiO₂-immobilization on cement coated borosilicate glass after 5 h of solar irradiation. We have noticed that a similar effect was found between the 2nd and 3rd layers from 1.00 pm to 2.00 pm due to the higher intensity of solar irradiation. The decreasing concentration rate was slightly lower than TiO₂-immobilized borosilicate glass due to comparatively lower light transparent capacity and lower free radical production than only used borosilicate glass reactor. According to the literature survey, cement is also used as the coating materials and can be incorporated into glass substrate for photocatalytic degradation purposes. It can be seen that the concentration was decreased due to the formation of a monolayer of cement coating on the borosilicate glass and huge free active sites would be available and therefore, further reduction of concentration was observed [204]. But the major limitation of the cement coated borosilicate glass reactor was not feasible in catalyst separation [205] and thus further treatment will be needed.

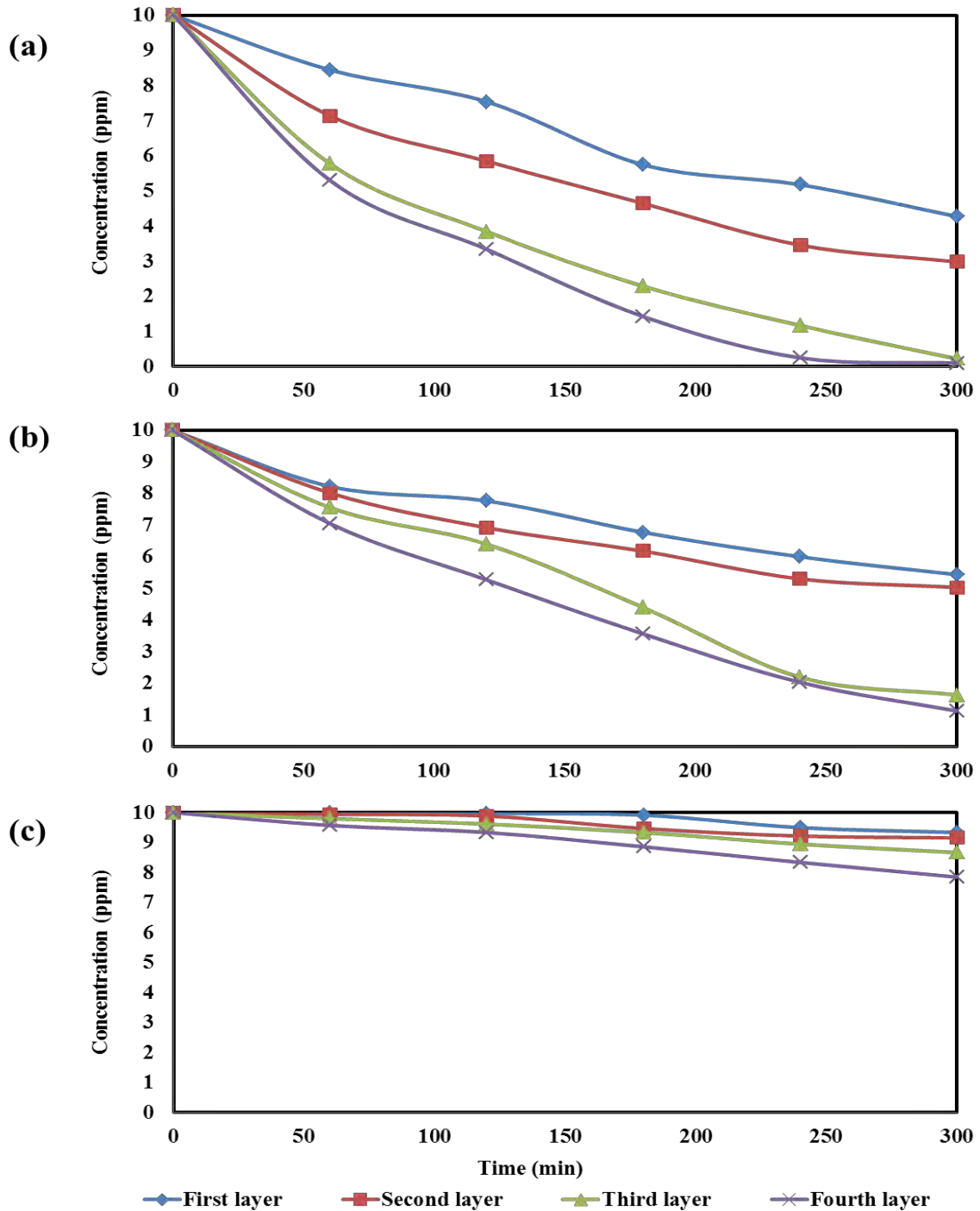


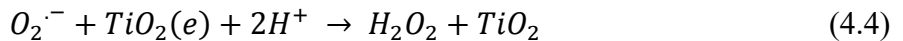
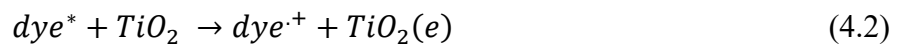
Figure 4.9: Concentration change of MO dye under solar irradiation (1st, 2nd, 3rd, and 4th layer of TiO₂ immobilized reactors: 60 mg, 90 mg, 120 mg, and 150 mg, pH:6.2, initial MO dye conc.: 10 ppm) (a) borosilicate glass reactor, (b) cement coated borosilicate glass reactor and (c) steel wire mesh reactor.

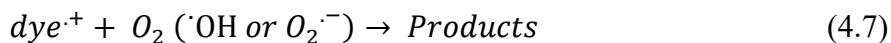
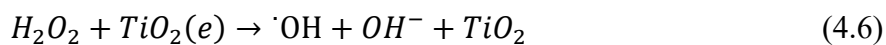
Finally, the effect of thickness of TiO₂-immobilization on steel wire mesh reactor in the presence of solar irradiation was investigated and the results are shown in Figure 4.9 (c). The concentration of MO dye was decreased from 10.00 ppm to 9.334, 9.155, 8.665, and 7.849 ppm, respectively, for the 1st, 2nd, 3rd, and 4th layers of TiO₂-immobilization on steel wire mesh glass after 5 h of solar irradiation. It can be seen that there was a homogeneous change of removal between in all layers. A significant decreased of concentration was not observed in TiO₂-immobilized on steel wire mesh up to the 4th layer after 5 h of solar irradiation due to the formation of metal alloy in high temperature of calcination (more than 500°C) and poor adhesion with the substrate [206,207]. In 500°C calcination temperature, the steel wire mesh determines the diffusion of the alloy that was responsible for decreasing effects on the photocatalytic activity [208]. Generally, when the dye concentration increases, the process efficiency decreases due to the photon penetration through dye molecules to reach the catalyst surface decreases, consequently leads to the formation of a lower amount of hydroxyl radicals that degrade the dye molecules structure [209].

4.4.2 Reactors Performance Evaluation

In photocatalytic reaction, the optimum catalyst dose must be determined to avoid excessive catalyst loss and to ensure the total absorption of efficient photons. The effect of dye removal of TiO₂-immobilization on the borosilicate glass reactor in the presence of solar irradiation was investigated and the results are shown in Figure 4.10 (a). It can be seen that photocatalytic removal of MO dye was found 57.3%, 70.22%, 97.83%, and 99.02% for the 1st, 2nd, 3rd and 4th layer of TiO₂ immobilization on borosilicate glass reactor, respectively, after 5 h of solar irradiation. The plot showed more than 97% dye was removed after the 3rd layer immobilization at an exposure time of 3-4 h. According to literature, it can be seen that by increasing the TiO₂ loading with the substrate, the removal efficiency increases, but further increasing of TiO₂ loading will decrease the dye removal efficiency due to the aggregation of TiO₂ on the substrate surface which results in lowering of the surface area [209]. Previously, it has been reported that a sufficient amount of catalysts with multilayer coatings is required for effective dye removal from the photocatalytic system [210], however, light scattering and the reduction of light penetration into the solution may be executed with an excess amount of photocatalyst loading [204]. Therefore, TiO₂-immobilization dose with a removal efficiency of MO dye of 97.83% was

considered as an optimum catalyst dose. Similarly, Figure 4.10 (b) represents the effect of doses of TiO₂-immobilized on cement coated borosilicate glass reactor on MO dye removal. It can be seen that photocatalytic removal of MO dye was found to be 45.57%, 49.58%, 83.58%, and 88.63% for 1st, 2nd, 3rd and 4th layer of TiO₂ immobilization on cement coated borosilicate glass reactor respectively. The experimental results showed that the increasing layer of TiO₂-immobilization on CCBG increases the photocatalytic removal efficiency, however longer solar irradiation time was required to attain the maximum dye removal efficiency as compared to BG reactor [211]. The removal rate was slightly lower due to comparatively lower light transparent capacity and lower free radical production than the TiO₂-immobilized BG reactor. However, this reactor system is not feasible where catalyst separation is required [205]. Finally, Figure 4.10 (c) indicates the photocatalytic removals of MO dye were 6.66%, 8.45%, 13.35%, and 21.51% for 1st, 2nd, 3rd and 4th layer of TiO₂-immobilization on steel wire mesh respectively. The experimental results showed that there was a consistent reduction of removal efficiency between all the layers as compared with borosilicate glass and cement coated borosilicate glass reactors. The lowest removal efficiency was obtained from steel wire mesh reactor due to non-transparency of steel wire mesh, poor adhesion of nanoparticles with the substrate, and the reduction of nanoparticles reactivity by the attachment process [212]. Besides, the diffusion of alloy elements from the substrate to the layer was formed due to calcined at 500°C that also inhibited on the photocatalytic activity [213]. The involved mechanism of dye removal was the excitation of visible light photons by absorbing dye molecules on the TiO₂ photocatalyst surface and produce single or triplet states Eq. (4.1). The removal occurs quickly using charge injection from the dye molecule to the TiO₂ semiconductor. The electron from the excited dye molecule is injected into the conduction band of the TiO₂ and reacts with oxygen to form radicals at the surface is likely to be the major reactive one Eq. (4.2-4.3). Then the superoxyl radical anion reacts with a proton to form hydroperoxyl radical and further react with the conduction band of the TiO₂ to form hydroxyl radical that quickly undergoes degradation to yield stable products Eq. (4.4-4.7) [214,215].





dye^* : excited single or triplet states of the dye

dye^+ : dye having loss an electron charge

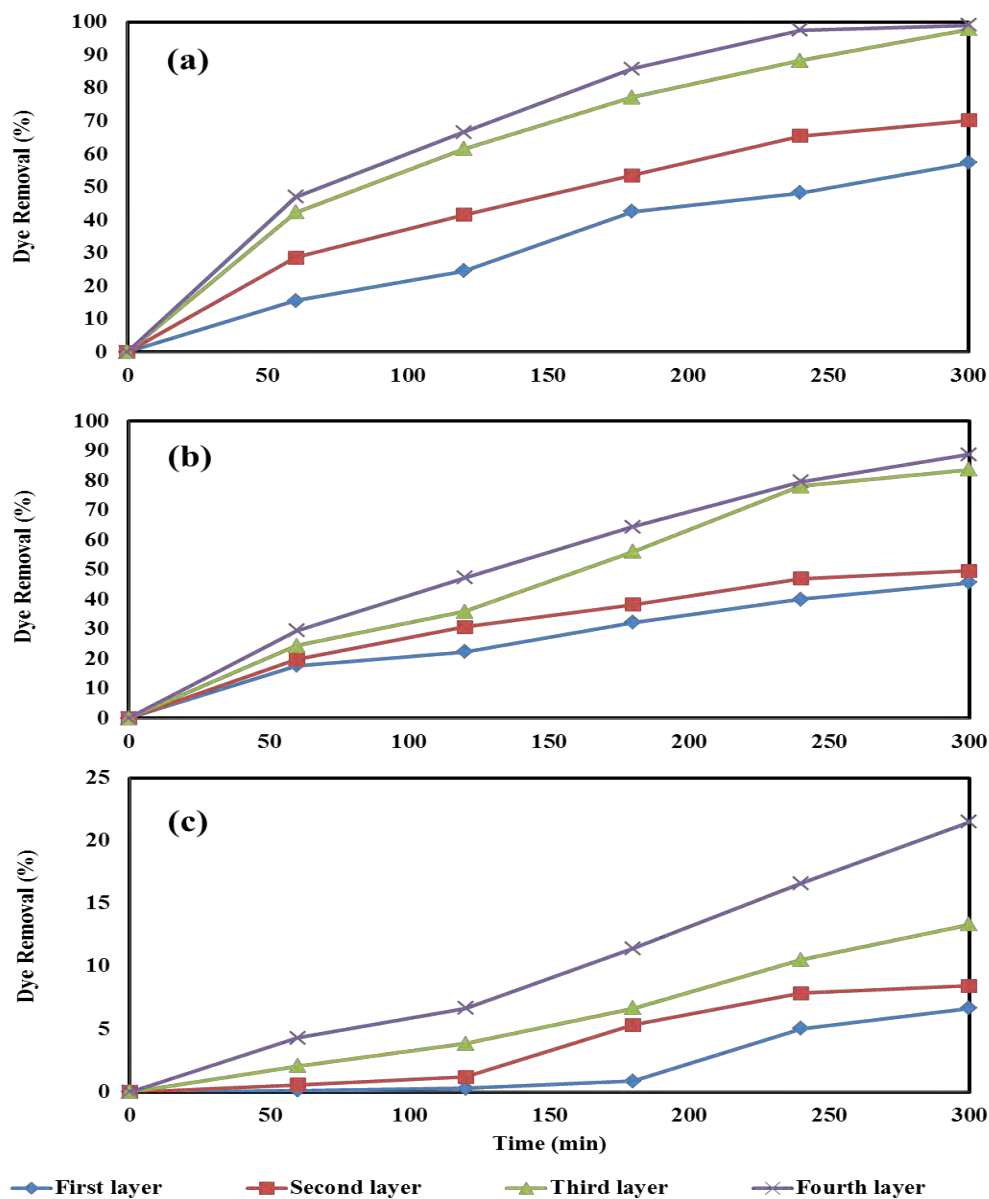


Figure 4.10: MO dye removal under solar irradiation (1st, 2nd, 3rd, and 4th layer of TiO₂ immobilized reactors: 60 mg, 90 mg, 120 mg, and 150 mg, pH:6.2, initial MO dye conc.: 10 ppm) (a) borosilicate glass reactor, (b) cement coated borosilicate glass reactor and (c) steel wire mesh reactor.

4.4.3 Reaction Kinetics Study

The decisive clarification is done by studying the photocatalytic reaction kinetics with the calculation of rate constant. The obtained rate constant value was used for evaluation and explanation of photocatalytic reaction. Based on experimental data, zero-order, pseudo-first-order and second-order reaction models were fitted. Based on regression coefficients R^2 value, we found that the pseudo-first-order fitted the best with the experimental data, which demonstrates that the straight lines almost fit the experimental values. The plots for zero order, pseudo-first-order, and second-order reaction kinetics are shown in Appendix B (Figure B1-3) and the kinetics parameters are summarized in Table B-4 (Appendix B). The corresponding graphs for TiO_2 -immobilized borosilicate glass reaction kinetics are plotted as shown in Figure 4.11 (a). The respective photocatalytic reaction rate constants were calculated from the slope of the linear trend-line plot. The respective rate constants for photocatalytic dye degradation of TiO_2 immobilized borosilicate glass with 1st, 2nd, 3rd, and 4th layers were found to be 0.0029 min^{-1} , 0.004 min^{-1} , 0.0117 min^{-1} , 0.0158 min^{-1} respectively. The correlation coefficients (R^2) were 0.9893, 0.9913, 0.9197, and 0.9551 for 1st, 2nd, 3rd, and 4th layer, respectively. It can be seen that the rate constant values were increased with the addition of photocatalyst layers and thus, decreasing the dye concentration has formulated. This was formed due to the increased number of photogenerated electron-hole pairs and thus, hydroxyl radicals were increased and resulting dye removal was increased [216]. In contrast, the decreasing trend of rate constant was observed with the increase of dye concentration in the treatment. This decrease in the rate of reaction might be executed from the reduction of active sites on the catalyst surface and interference of the solar light to reach the catalyst surface. The slight deviations might be performed due to operating conditions like light intensity, pH, dye concentration, and oxygen concentration or interfering intermediates [196]. Similarly, the corresponding graphs for TiO_2 immobilized on cement coated borosilicate glass reaction kinetics are plotted as shown in Figure 4.11 (b). The respective photocatalytic reaction rate constants were calculated from the slope of the linear trend-line plot. The respective rate constants for photocatalytic dye degradation of TiO_2 immobilized cement coated borosilicate glass with 1st, 2nd, 3rd, and 4th layers were found to be 0.002 min^{-1} , 0.0023 min^{-1} , 0.0062 min^{-1} , 0.0071 min^{-1} , respectively. The correlation coefficients (R^2) were 0.986, 0.972, 0.9597, and 0.9797 for 1st, 2nd, 3rd, and 4th layer, respectively. It can be seen that the rate constant values were increased with the addition of photocatalyst layers and

thus decreasing the dye concentration has formulated. It demonstrates that the straight lines almost fit the experimental values.

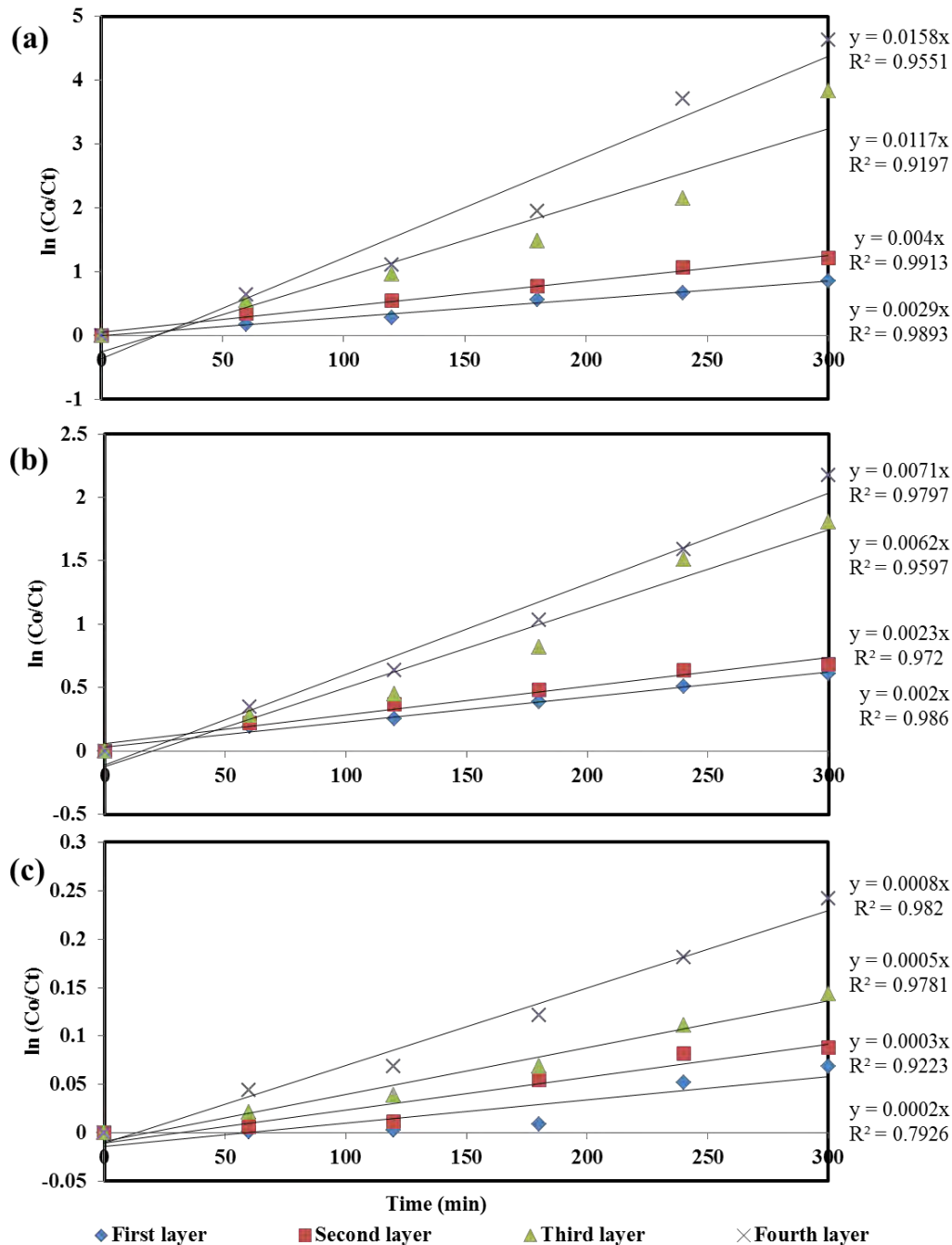


Figure 4.11: Pseudo first-order reaction kinetics of MO dye removal in presence of solar irradiation (1st, 2nd, 3rd, and 4th layer of TiO₂ immobilized reactors: 60 mg, 90 mg, 120 mg, and 150 mg, pH:6.2, initial MO dye conc.: 10 ppm) (a) borosilicate glass, (b) cement coated borosilicate glass and (c) steel wire mesh

Finally, the corresponding graphs for TiO₂ immobilized on steel wire mesh reaction kinetics are plotted as shown in Figure 4.11 (c). The respective photocatalytic reaction rate constants are calculated from the slope of the linear trend-line plot. The respective rate constants for photocatalytic dye degradation of TiO₂ immobilized borosilicate glass with 1st, 2nd, 3rd, and 4th layer found to be 0.0002 min⁻¹, 0.0003 min⁻¹, 0.0005 min⁻¹, 0.0008 min⁻¹, respectively. The correlation coefficients (R²) are 0.7926, 0.9223, 0.9781, and 0.982 for 1st, 2nd, 3rd, and 4th layer, respectively. It demonstrates that the straight lines almost fit the experimental values.

4.5 Comparison of different Reactor Models and Weight Loss from different reactors

Firstly, the comparison of TiO₂-immobilized on borosilicate glass, cement coated borosilicate glass, and steel wire meshes were measured in a layer by layer. Secondly, the weights of TiO₂-immobilized in all reactors were calculated before and after photocatalytic treatment. In all experiments of the reactor model, the initial dye concentration and pH were 10 ppm and 6.2, respectively.

4.5.1 Comparison of Reactors Performance

The reactor's performance was compared for 1st, 2nd, 3rd, and 4th layers, and Figure 4.12 (a) and (b) shows the contribution of each layer in dye concentration and dye degradation for borosilicate glass, cement coated borosilicate glass and steel wire mesh. The maximum dye concentration was reduced at the 4th layer of supporting immobilized reactors due to photocatalyst doses, lower initial dye concentration, and solar intensity. The borosilicate reactor models were shown that the maximum amount of dye concentration was reduced than other reactor models from 1.00 pm to 2.00 pm due to higher light transparency and adhesion of TiO₂ on borosilicate glass reactor. For similar reasons, the maximum dye removal was observed at the 4th layer of supporting immobilized reactors. The borosilicate reactor model was showed that the maximum amount of dye removal than other reactor models due to higher light transparency and adhesion of TiO₂ on the borosilicate glass reactor.

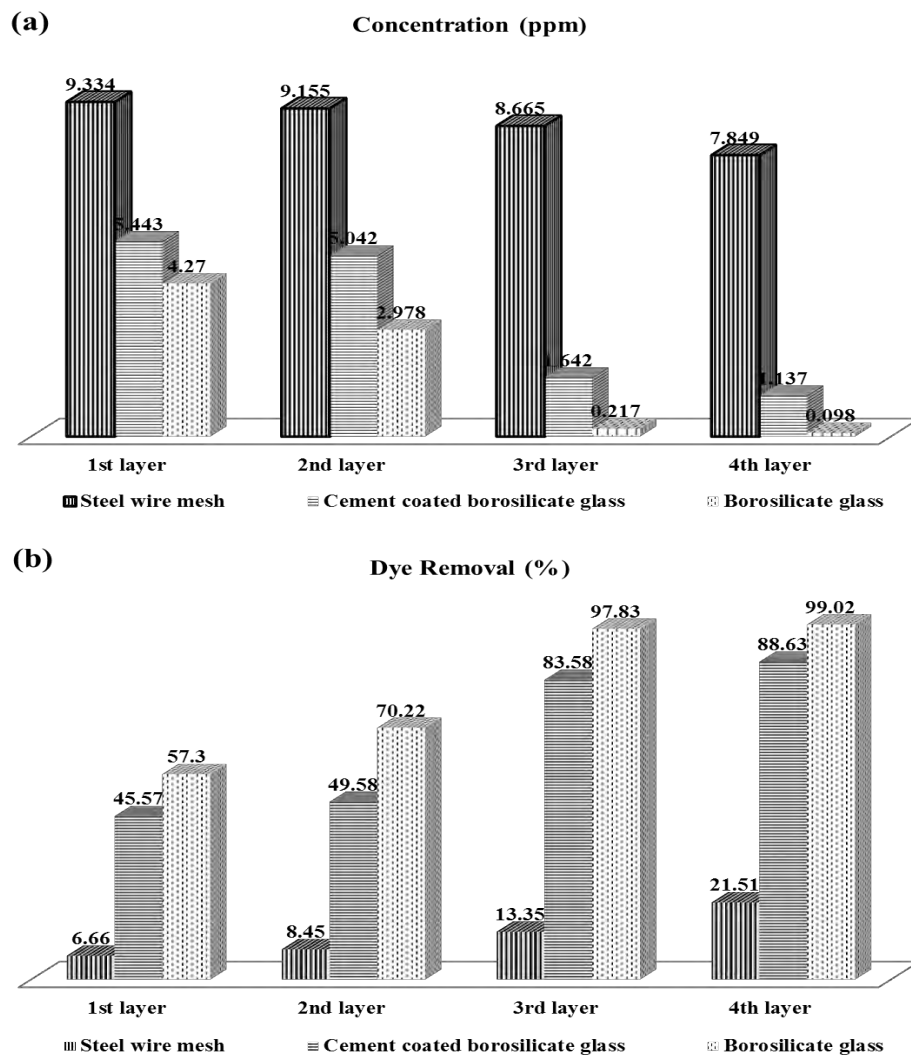


Figure 4.12: Comparison of TiO_2 -immobilized different reactors on a layer by layer (a) change of concentration and (b) change of dye removal

4.5.2 Weight Loss Measurement

The mechanical stability and reusability of TiO_2 nanoparticles are crucial properties for a realistic application of a structured photocatalytic reactor [217]. The photocatalytic performance is greatly influenced by the stability and recycles the ability of photocatalyst [218]. The weights of TiO_2 immobilized on borosilicate glass, cement coated borosilicate glass and steel wire mesh was measured before and after calcined at 500°C . The desired weight was calculated before photocatalytic removal of MO dye in the presence of solar irradiation. After 5 h of contact time with the dye solution, the TiO_2 nanoparticles were lost from the supporting materials were

calculated. After treatment, the immobilized TiO_2 losses from borosilicate glass were found 0.006, 0.008, 0.019, and 0.012 g for 1st, 2nd, 3rd, and 4th layer, respectively. Similarly, the immobilized TiO_2 losses from cement coated borosilicate glass were found 0.0133, 0.0081, 0.0114, and 0.0256 g for 1st, 2nd, 3rd, and 4th layer, respectively.

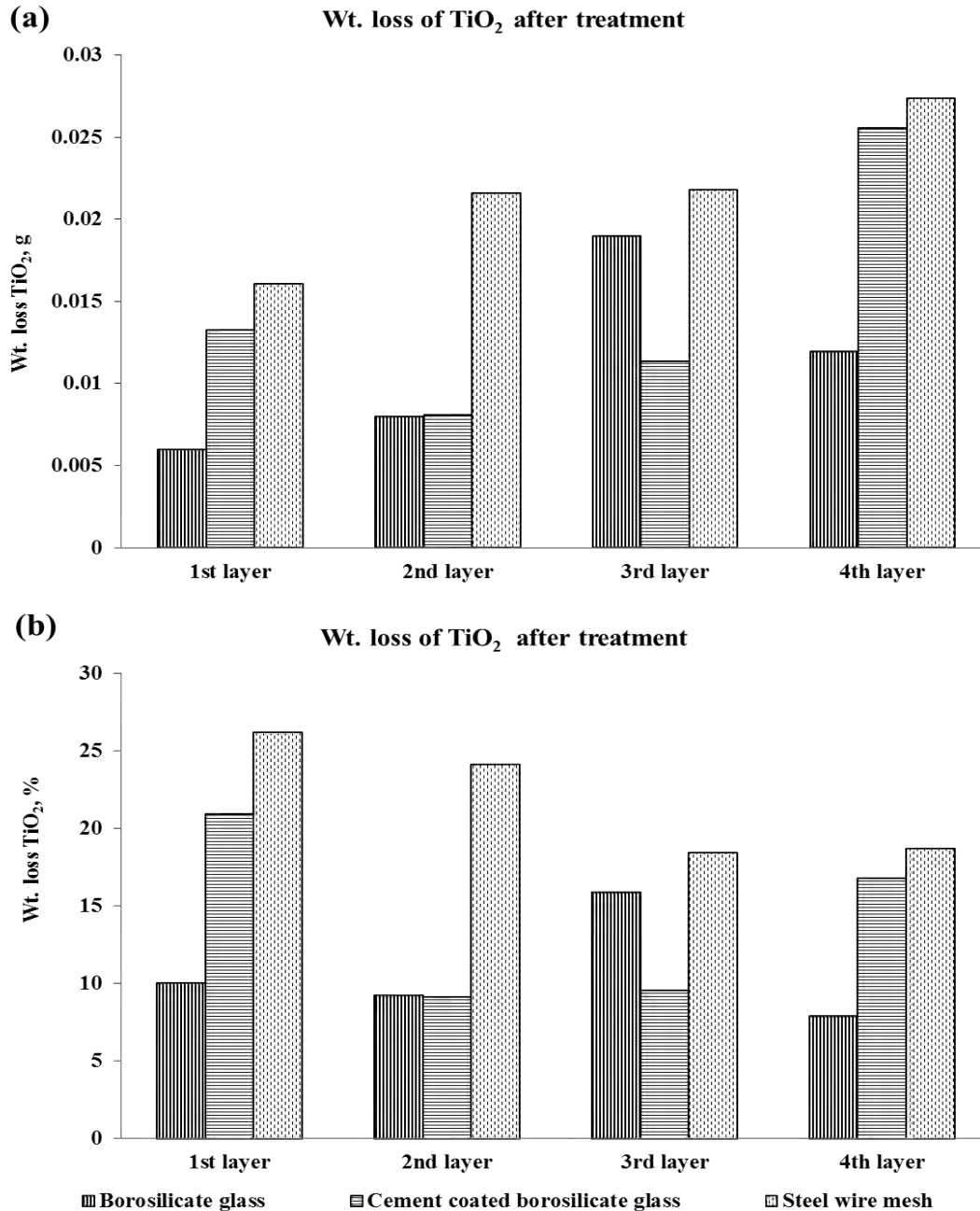


Figure 4.13: Weight loss measurement from borosilicate glass, cement coated borosilicate glass, and steel wire mesh supporting materials (a) unit is g and (b) unit is percent.

Finally, the immobilized TiO₂ losses from steel wire mesh were found 0.0161, 0.0216, 0.0218, and 0.0274 g for 1st, 2nd, 3rd, and 4th layer, respectively. The weight losses of TiO₂ immobilized with supporting materials are shown in Figure 4.13 (a). The minimum loss of photocatalyst was found in borosilicate glass after 5 h contact time. According to the literature, the activities of coated layers after 4 cycles of reuse were slightly decreased, resulting from the degradation of MO dye compared to those of the freshly coated layers [219]. However, the fouling phenomena on the catalyst surface were caused by the formation of by-products and their accumulation in the cavities and on the active surface sites of the catalyst [169]. Though the TiO₂ photocatalyst was immobilized on supporting materials as layers by layer were of approximately closer to the desired value, the percentage of weight loss of TiO₂ photocatalyst was found to be 10.03, 20.94 and 26.22% of 1st layer of borosilicate glass, cement coated borosilicate glass, and steel wire mesh, respectively, after 5 h of contact time. For 2nd layer, the losses were 9.23, 9.16, and 24.13%, for 3rd layer, the losses were 15.91, 9.59, and 18.47%, and finally, for 4th layer, the losses were 7.92, 16.82, and 18.72%, respectively. The weight losses of TiO₂ immobilized on borosilicate glass, cement coated borosilicate glass, and steel wire mesh supporting materials are shown in Figure 4.13 (b).

4.6 Impact of Dye Concentration and Hydrogen Peroxide Concentration on Reactors Performance

As we observed more than 99% degradation of 10 ppm MO dye using a borosilicate glass reactor within 5 h of solar irradiation, we increased dye concentration to evaluate the reactor performance for higher dye concentration. Besides, in this section, we also studied the impact of the addition of hydrogen peroxide in the reactor to observe the change of reactor performance. The optimum photocatalyst dose (0.120 g TiO₂) and natural solution of pH (6.2) were used to construct a TiO₂ immobilized borosilicate glass reactor. The impact of dye concentration on reactor performance was observed for 10.0 ppm, 20.0 ppm and 30.0 ppm MO dye. Two doses (0.1 mL and 0.25 mL) of hydrogen peroxide concentrations were used to investigate the impact of hydrogen peroxide on reactor performance.

4.6.1 Impact of Dye concentration

Studying the dependence of the removal efficiency on the initial dye concentration is important from an application point of view [220]. The initial MO concentrations used in this study were 10, 20, and 30 ppm. A volume of 125 mL of each dye initial concentration was treated with the 3rd layer of immobilized TiO₂ photocatalyst of 120 mg in the normal condition (natural solution pH of 6.2).

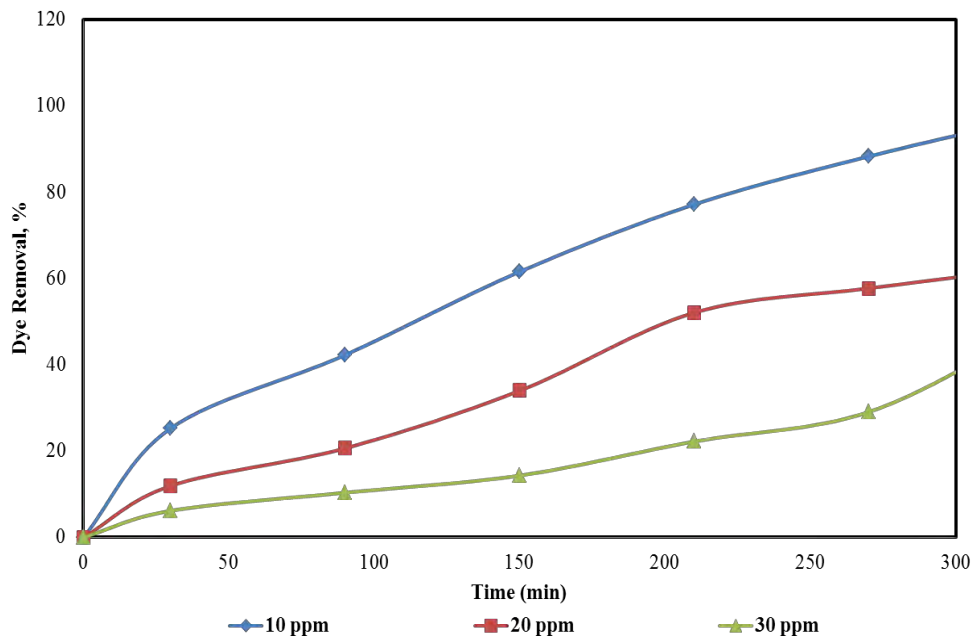


Figure 4.14: Impact of initial MO concentration on the removal efficiency (The third layer of TiO₂-immobilized coated borosilicate glass: 120 mg, pH: 6.2).

As shown in Figure 4.14, the MO removal obtained after 5 h of irradiation was 97.8%, 62.8%, and 49.25% for the initial MO concentrations of 10, 20, and 30 ppm respectively, indicating the decrease of reactor performance with the increase of dye concentration in the reactor. This is because (i) the decrease of the active sites on the catalyst surface by adsorption of more dye molecules with the increase of dye concentration while the catalyst loading is kept constant, and this is very crucial for the catalysis reaction to decompose dye, and (ii) the color of the solution turns into intense color with the increase of dye concentration, which interferes the solar light to reach the catalyst surface and thereby allowing fewer photons to reach the surface of the catalyst [211]. As a result, the generation of hydroxyl and peroxide might be reduced leading to negligible photo-degradation of dye [221]. However, to overcome this limitation, it requires

higher light intensity, more nanoparticles dose on the reactor surface, longer irradiation time, reduce the path of light, and addition of oxidant externally [222].

4.6.2 Impact of the addition of H₂O₂ in the Reactor

The impact of the addition of H₂O₂ (two doses: 0.1 mL and 0.25 mL containing 0.5 M concentration) on the reactor performance were also studied. H₂O₂ itself cannot generate OH radicals; however, in the presence of the TiO₂ catalyst, it can enhance the generation of hydroxyl radicals and thus, increase the performance of the photocatalytic reactor. As shown in Figure 4.16(a), more than 99% dye removal was observed for both 0.1 and 0.25 mL H₂O₂ doses, however, the H₂O₂ contribution to removal was not significant as the TiO₂-immobilized BG reactor alone could remove 97.8% of 10 mg/L dye concentration. For 20 mg/L dye concentration (Figure 4.16b), the addition of H₂O₂ into the reactor has pronounced impact on MO dye removal and the removal efficiency was increased from 63.7% to 77.95% and 92.65%, respectively, after the addition of 0.1 and 0.25 mL of H₂O₂ into the reactor. A similar impact was also observed for 30 mg/L dye concentration (Figure 4.16c) where the removal efficiency was increased from 27.6% to 60.23% and 86.93%, respectively, after the addition of 0.1 and 0.25 mL of H₂O₂ into the reactor. The removal efficiency was enhanced as the concentration of H₂O₂ was increased from 0.1 to 0.25 mL. There is no effect of H₂O₂ when the reaction is carried out in the absence of photocatalyst [223], however, the addition of H₂O₂ increases oxidation rates of organic molecules in photocatalytic processes due to three reasons: (i) It is a strong oxidant, which scavenges conduction band electrons that were excited by irradiation of the catalyst and generates highly oxidative $h\nu_{VB}^+$ on catalyst surface [224], (ii) The H₂O₂ reacts with the electrons that were emitted from the valence band of the photocatalyst to generate hydroxyl radicals and hydroxide anions while inhibiting the $e_{CB}^-/h\nu_{VB}^+$ recombination process [225], and (iii) also, H₂O₂ may be split photolytically to produce hydroxyl radicals directly [226].

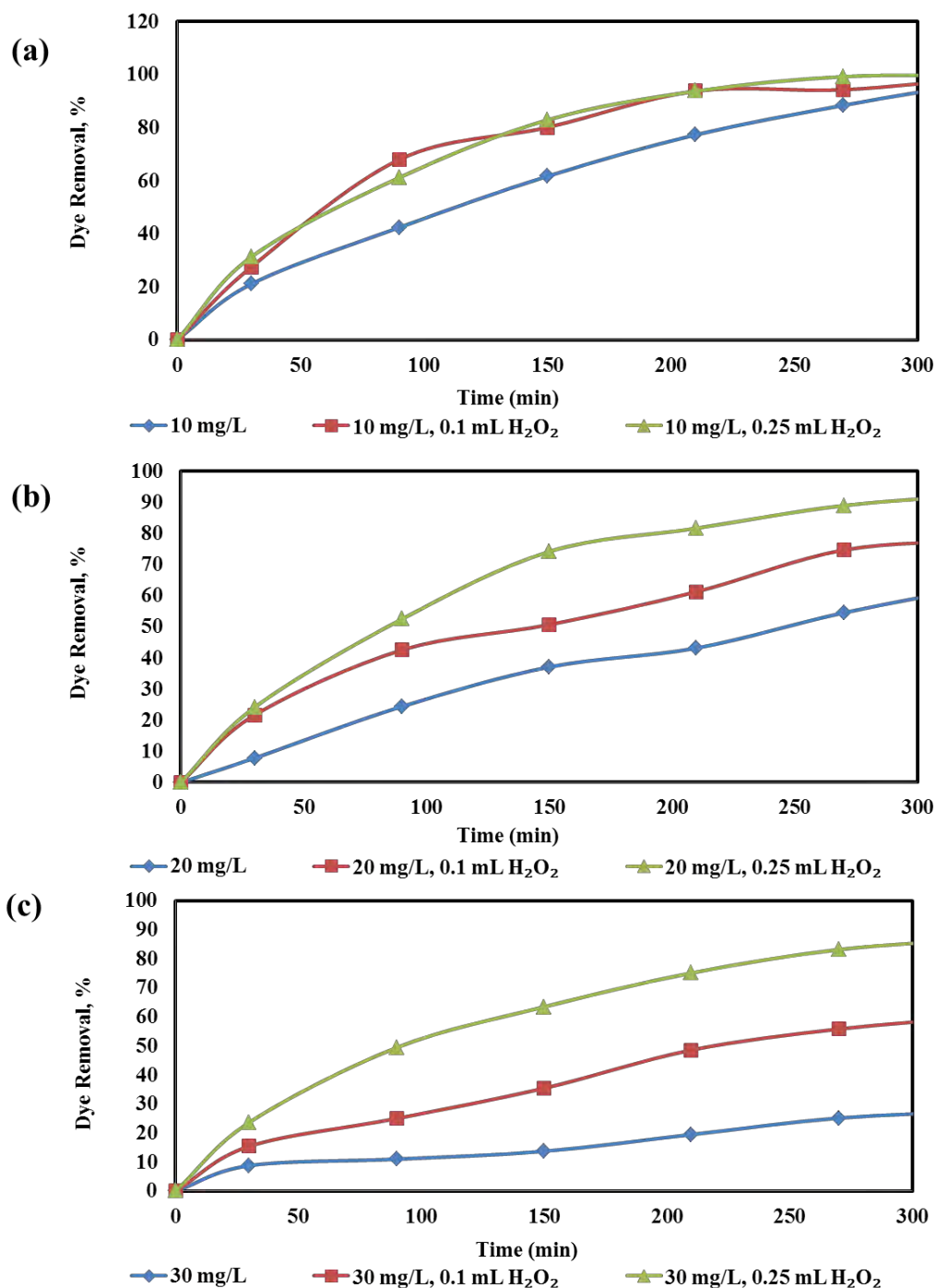


Figure 4.16: Impact of H₂O₂ concentration on the removal efficiency (The third layer of TiO₂-immobilized coated borosilicate glass: 120 mg, pH: 6.2). (a) 10 ppm initial dye concentration with addition of 0.1 and 0.25 mL H₂O₂ concentration, (b) 20 ppm initial dye concentration with addition of 0.1 and 0.25 mL H₂O₂ concentration, and (c) 30 ppm initial dye concentration with addition of 0.1 and 0.25 mL H₂O₂ concentration.

CHAPTER 5

CONCLUSION

5.1 Conclusion

In this study, the TiO₂ nanoparticle was synthesized by sol-gel and thermal treatment method for the treatment of methyl orange dye solution in aqueous water. The photocatalytic treatment of methyl orange dye was performed using TiO₂ immobilized borosilicate glass, cement coated borosilicate glass, and steel wire meshes reactors. The following conclusions can be drawn from the study:

- (i) The XRD results showed that the TiO₂ nanoparticle was preferentially anatase.
- (ii) The SEM images showed higher surface roughness of TiO₂ nanoparticle synthesized by hydrolysis. Besides, the average estimated particle size was smaller of TiO₂ nanoparticle synthesized by hydrolysis as compared with TiO₂ nanoparticle synthesized in the absence of water.
- (iii) The FT-IR results showed peaks around 1300-1400 cm⁻¹ and 700-800 cm⁻¹ were attributed to Ti-O-Ti stretching vibration and Ti-O bond in the TiO₂ lattice, respectively.
- (iv) UV-Vis results showed that TiO₂ nanoparticle with hydrolysis assisted to shift absorption edge towards longer wavelength. The estimated band gap energies (E_g) were calculated to be 3.066 eV, and 5.29 eV for TiO₂ nanoparticle synthesized from hydrolysis and without hydrolysis, respectively.
- (v) BET surface analysis suggested that the specific area of TiO₂ nanoparticle synthesized with hydrolysis was found 67 times larger than the surface area for TiO₂ nanoparticle prepared without hydrolysis. The pore volume of TiO₂ nanoparticle synthesized with hydrolysis was higher than the pore volume of TiO₂ nanoparticle synthesized without hydrolysis.
- (vi) Photocatalytic treatment of MO dye revealed that the preparation of TiO₂ nanoparticle with hydrolysis was very effective in the presence of solar irradiation. The fourth layer of TiO₂-immobilized photoreactor showed the highest photocatalytic degradation. The dye degradation results were found 97.8%, 88.6%, and 21.5% for TiO₂-immobilized on borosilicate glass, cement coated borosilicate glass, and steel

wire mesh, respectively. The degradation rate constants were measured by using pseudo-first-order steady reaction kinetics and the results were 0.0158 min^{-1} , 0.0071 min^{-1} , and 0.0008 min^{-1} for TiO_2 -immobilization on borosilicate glass, cement coated borosilicate glass, and steel wire mesh, respectively.

- (vii) The optimum conditions were found to be 0.120 g dose of photocatalyst, 20.0 ppm dose of dye concentration and 0.25 mL dose of H_2O_2 , respectively.
- (viii) The photocatalytic removal of dye was decreased with the increase of dye concentration because of the decreasing of available active sites on the catalyst surface and increase of light interference from the increase of color of the solution. In contrast, the photocatalytic performance was increased with the addition of H_2O_2 due to the increase of hydroxyl radical formation and reduction of electron-hole recombination on the catalyst surface. The study indicates that a solar TiO_2 -immobilized reactor can be a great option for the sustainable management of textile wastewater.

REFERENCES

- [1] Streeter, H. W., and Phelps, E. B. (1925) *A study of the pollution and natural purification of the Ohio river*. Public Health Bulletin, U.S. Public Health Service, Washington DC.
- [2] Saini, K., and Malhotra, S., –“Environmental Pollution,” *Int. J. Eng. Res. & Appl.*, vol. 6, pp. 70-74, 2016.
- [3] Seung, H. H. (2011) *Physics and Application of Graphene-Experiments*. In. Tech. Ltd., Rijeka.
- [4] Lopez, M. P. L., Valverde, J. L., Sanchez-Silva, L., and Romero, A., –“Solvent-based exfoliation via sonication of graphitic materials for graphene manufacture,” *Ind. Eng. Chem. Res.*, vol. 55, pp. 845-855, 2016.
- [5] Vymazal, J., –“The use constructed wetlands with horizontal sub-surface flow for various types of wastewater,” *Ecolog. Eng.*, 35, pp. 1-17, 2009.
- [6] Cameselle, C., Pazos, M., and Sanroman, M. A., –“Selection of an Electrolyte to Enhance the Electrochemical Decolourization of Indigo Optimization and Scale-up,” *Chemosp.*, vol. 60, pp. 1080, 2005.
- [7] Caner, N., Kiran, I., Ilhan, S., and Iscen, C.F. –“Isotherm and Kinetic Studies of Burazol Blue ED Dye Biosorption by Dried Anaerobic Sludge,” *J. Hazard. Mater.*, vol. 165, pp. 279, 2009.
- [8] Chacó, J. M., Leal, M. T., Sánchez, M., and Bandala, E. R., –“Solar photocatalytic degradation of azo-dyes by photo-Fenton process,” *Dy. Pigmt.*, vol. 69, pp. 144–150, 2006.
- [9] Villanueva, S. F., and Martínez, S. S., –“TiO₂-assisted degradation of acid orange 7 textile dye under solar light,” *Sol. Eng. Mater. Sol. C.*, vol. 91, pp. 1492–1495, 2007.
- [10] Hossain, L., Sajib, M., and Enamul, H. (2017) *Readymade garment industries going green*. The Financial Express. International Publications Ltd.
- [11] Masum, M., –“The Bangladesh textile-clothing industry: a demand-supply review,” *Soc. Syst. Stud.*, vol. 9, pp. 109-139, 2016.
- [12] Holkar, C. R., Jadhav, A. J., Pinjari, D. V., Mahamuni, N. M., and Pandit, A. B., –“A critical review on textile wastewater treatments: Possible approaches,” *J. Environ. Manage.*, vol. 182, pp. 351-366, 2016.

- [13] Miguel, R., Victor, S., Santiago, E., and Cesar, P., "Photo-Fenton treatment of a bio-recalcitrant wastewater generated in textile activities: biodegradability of the photo-treated solution," *J. Photochem. Photobiol. A: Chem.*, vol. 151, pp. 129-135, 2002.
- [14] Ledakowicz, S., Solecka, M., and Zylla, R., "Biodegradation, decolourisation and detoxification of textile wastewater enhanced by advanced oxidation processes," *J. Biotechnol.*, vol. 89, pp. 175-184, 2001.
- [15] Punzi, M., Nilsson, F., Anbalagan, A., Svensson, B. M., Jönsson, K., Mattiasson, B., and Jonstrup, M., "Combined anaerobic-ozonation process for treatment of textile wastewater: Removal of acute toxicity and mutagenicity," *J. Hazard. Mater.*, vol. 292, pp. 52-60, 2015.
- [16] Ganesh, R., Boardman, G. D., and Michelson, D., "Fate of azo dyes in sludges," *W. Wat. Res.*, vol. 28, pp. 1367-1376, 1994.
- [17] Weber, E. J., and Adams, R. L., "Chemical and sediment mediated reduction of the azo dye disperse blue 79," *Environ. Sci. Technol.*, vol. 29, pp. 1163-1170, 1995.
- [18] Gümüş, D., and Akbal, F., "Photocatalytic Degradation of Textile Dye and Wastewater," *W. A. Soi. Poll.*, vol. 216, pp. 117-124, 2011.
- [19] Mathur, N., Bhatnagar, P., Nagar, P., and Bijarnia, M. K., "Mutagenicity assessment of effluents from textile/dye industries of Sanganer, Jaipur (India): a case study," *Ecotoxicol. Environ. Saf.*, vol. 61, pp. 105-113, 2005.
- [20] Ibhaddon, A. O., and Fitzpatrick, P., "Heterogeneous Photocatalysis: Recent Advances and Applications," *Catal.*, vol. 3, pp. 189-218, 2013.
- [21] Souza, R. P., Freitas, T. K. F. S., Domingues, F. S., Pezoti, O., Ambrosio, E., Ferrari-Lima, A. M., and Garcia, J. C., "Photocatalytic activity of TiO₂, ZnO and Nb₂O₅ applied to degradation of textile wastewater," *J. Photochem. Photobiol. A: Chem.*, vol. 329, pp. 9-17, 2016.
- [22] Groff, K. A., and Byung, R. K., "Textiles waste," *J. WPCF.*, vol. 61, pp. 872-875, 1989.
- [23] Groff, K. A., "Textiles Waste," *Res. J. WPCF.*, vol. 63, pp. 459-460, 1991.
- [24] Sue, C. A., and Groff, K.A., "Textile waste," *Res. J. WPCF.*, vol. 62, pp. 473-475, 1990.
- [25] Neppolian, B., Choi, H. C., Sakthivel, S., Arabindoo, B., and Murugesan, V., "Solar light induced and TiO₂ assisted degradation of textile dye reactive blue 4," *Chemosp.*, vol. 46, pp. 1173-1181, 2002.

- [26] Wang, Y., –Solar photocatalytic degradation of eight commercial dyes in TiO₂ suspension,” *W. Res.*, vol. 34, pp. 990-994, 2000.
- [27] Silva, D. C. G., and Faria, J. L., –Photochemical and photocatalytic degradation of an azo dye in aqueous solution by UV irradiation,” *J. Photochem. Photobiol. A: Chem.*, vol. 155, pp. 133-143, 2003.
- [28] Mahmoodi, N., Arami, M., Limaee, N., and Tabrizi, N., –Kinetics of heterogeneous photocatalytic degradation of reactive dyes in an immobilized TiO₂ photocatalytic reactor,” *J. Coll. Inter. Sci.*, vol. 295, pp. 159-164, 2006.
- [29] Nakata, K., and Fujishima, A., –TiO₂ Photocatalysis: Design and Applications,” *J. Photochem. Photobiol. C: Photochem. Rev.*, vol. 13, pp. 169-189, 2012.
- [30] Swarnakar, P., Kanel, S. R., Nepal, D., Jiang, Y., Jia, H., Kerr, L., Goltz, M. N., Levy, J., and Rakovan, J., –Silver deposited titanium dioxide thin film for photocatalysis of organic compounds using natural light,” *Sol. Ener.*, vol. 88, pp. 242-249, 2013.
- [31] Rapsomanikis, A., Apostolopoulou, A., Stathatos, E., and Lianos, P., –Ceriummodified TiO₂ nanocrystalline films for visible light photocatalytic activity,” *J. Photoch. Photobio. A*, vol. 280, pp. 46-53, 2014.
- [32] Umebayashi, T., Yamaki, T., Sumita, T., Yamamoto, S., Tanaka, S., and Asai, K., –UV-ray photoelectron and ab initio band calculation studies on electronic structures of Cr or Nb-ion implanted titanium dioxide,” *Nucl. Instrum. Metho. Phys. Res., Sect. B*, vol. 206, pp. 264-267, 2003.
- [33] Choi, H. P., and Hoffmann, M. R., –Effects of Single Metal-Ion Doping on the Visible-Light Photoreactivity of TiO₂,” *J. Phys. Chem. C*, vol. 114, pp. 783-792, 2010.
- [34] Zhou, W., and Fu, H., –Mesoporous TiO₂: Preparation, doping, and as a composite for photocatalysis,” *Chem. Catal. Chem.*, vol. 5, pp. 885-894, 2013.
- [35] Bhattacharyya, K., Majeed, J., Dey, K. K., Ayyub, P., Tyagi, A. K., and Bharadwaj, S. R., –Effect of Mo-Incorporation in the TiO₂ Lattice: A Mechanistic Basis for Photocatalytic Dye Degradation,” *J. Phys. Chem. C*, vol. 118, pp. 15946-15962, 2014.
- [36] Nasir, M., Bagwasi, S., Jiao, Y., Chen, F., Tian, B., and Zhang, J., –Characterization and activity of the Ce and N co-doped TiO₂ prepared through hydrothermal method,” *Chem. Eng. J.*, vol. 236, pp. 388-397, 2014.

- [37] Wu, Y., Xing, M., and Zhang, J., –Gel-hydrothermal synthesis of carbon and boron co-doped TiO₂ and evaluating its photocatalytic activity,” *J. Hazard. Mater.*, vol. 192, pp. 368-373, 2011.
- [38] Bagwasi, S., Tian, B., Zhang, J., and Nasir, M., –Synthesis, characterization and application of bismuth and boron Co-doped TiO₂: A visible light active photocatalyst,” *Chem. Eng. J.*, vol. 217, pp. 108-118, 2013.
- [39] El-Mekkawi, D., and Galal, H. R., –Removal of a synthetic dye –Direct Fast Blue B2RL” via adsorption and photocatalytic degradation using low cost rutile and Degussa P25 titanium dioxide,” *J. Hydro-environ. Res.*, vol. 7, pp. 219–226, 2013.
- [40] Sampaio, M. J., Silva, C. G., Marques, R. R. N., Silva, A. M. T., and Faria, J. L., –Carbon nanotube–TiO₂ thin films for photocatalytic applications,” *Catal. Tod.*, vol. 161, pp. 91–96, 2011.
- [41] Rachel, A., Subrahmanyam, M., and Boule, P., –Comparison of photocatalytic efficiencies of TiO₂ in suspended and immobilised form for the photocatalytic degradation of nitro benzene sulfonic acids,” *Appl. Catal. B: Environ.*, vol. 37, pp. 301-308, 2002.
- [42] Löfberg, A., Giornelli, T., Paul, S., and Richard, E. B., –Catalytic coatings for structured supports and reactors: VO_x/TiO₂ catalyst coated on stainless steel in the oxidative dehydrogenation of propane,” *Chem. Eng. J.*, vol. 171, pp. 692-702, 2011.
- [43] Shan, A. Y., Ghazi, T. I. M., and Abdul, R. S., –Immobilisation of titanium dioxide onto supporting materials in heterogeneous photocatalysis: a review,” *Appl. Catal. A: Gen.*, vol. 389, pp. 1-8, 2010.
- [44] Coleman, H. M., Vimonses, V., Leslie, G., and Amal, R., –Removal of contaminants of concern in water using advanced oxidation techniques,” *W. Sci. Technol.*, vol. 55, pp. 301-306, 2007.
- [45] Lam, S. W., Hermawan, M., Coleman, H. M., Fisher, K., and Amal, R., –The role of copper (II) ions in the photocatalytic oxidation of 1,4-dioxane,” *J. Mol. Catal. A-Chem.*, vol. 278, pp. 152-159, 2007..
- [46] Youn, N. K., Heo, J. E., Joo, O. S., Lee, H., Kim, J., and Min, B. K., –The effect of dissolved oxygen on the 1,4-dioxane degradation with TiO₂ and Au–TiO₂ photocatalysts,” *J. Hazard. Mater.*, vol. 177, pp. 216-221, 2010.

- [47] Simonsen, M. E., Jensen, H., Li, Z., and Sogaard, E. G., –Surface properties and photocatalytic activity of nanocrystalline titania films,” *J. Photochem. Photobiol. A: Chem.*, vol. 200, pp. 192-200, 2008.
- [48] Malato, S., Fernandez, I. P., Maldonado, M. I., Blanco, J., and Gernjak, W., –MONOGRAPH: Decontamination and disinfection of water by solar photocatalysis: Recent overview and trends,” *Catal. Tod.*, vol. 147, pp. 1-59, 2009.
- [49] Soares, P. A., Silva, T. F. C. V., Manenti, D. R., Souza, S. M. A. G. U., Boaventura, R. A. R., and Vilar, V. J. P., –Electrooxidation of industrial wastewater containing 1,4-dioxane in the presence of different salts,” *Environ. Sci. Poll. Res.*, vol. 21, pp. 932-945, 2014.
- [50] Al-Mamun, M. R., Kader, S., Islam, M. S., and Khan, M. Z. H., –Photocatalytic activity improvement and application of UV-TiO₂ photocatalysis in textile wastewater treatment: A review,” *J. Environ. Chem. Eng.*, vol. 7, pp. 103248, 2019.
- [51] Gutierrez, M. A. G., Velazquez, M. S., Alberto, A., Gallegos, M., Ahmadi, M., Jose, A. H. P., F., Ghanbari, F., and Silva, M. S., –Recent Overview of Solar Photocatalysis and Solar Photo-Fenton Processes for Wastewater Treatment,” *Int. J. Photoener.*, vol. 8528063, pp. 27, 2017.
- [52] Hossain, L., Sarker, S. K., and Khan, M. S., –Evaluation of present and future wastewater impacts of textile dyeing industries in Bangladesh,” *Environ. Develop.*, vol. 26, pp. 23-33, 2018.
- [53] Ribeiro, M. C. M., Starling, M. C. V. M., Leo, M. M. D., and Amorim, C. C. D., –Textile wastewater reuse after additional treatment by Fenton’s reagent,” *Environ. Sci. Poll. Res.*, vol. 24, pp. 6165-6175, 2017.
- [54] Bisschops, I. A. E., and Spanjers, H., –Literature review on textile wastewater characterization,” *Environ. Technol.*, vol. 24, pp. 1399-1411, 2003.
- [55] Orhon, D., Babuna, F. G., and Insel, G., –Characterization and modelling of denimprocessing wastewaters for activated sludge,” *J. Chem. Technol. Biotech.*, vol. 76, pp. 919-931, 2001.
- [56] Muruganandham, S. M., –Decolorisation of Reactive Orange 4 by Fenton and photo-Fenton oxidation technology,” *Dy. Pigmt.*, vol. 63, pp. 315-21, 2004.

- [57] Aleboye, A., Aleboye, H., and Moussa, Y., "Decolorisation of Acid Blue 74 by ultraviolet/H₂O₂," *Environ. Chem. Lett.*, vol. 1, pp. 161-164, 2003.
- [58] Mohr, U. K. (1992) *Textile treatments and ecological aspects in future South Africa*. Textile Industries Dyegest SA.
- [59] Zongping, W., Miaomiao, X., Kai, H., and Zizheng, L. (2011) *Textile Dyeing Wastewater Treatment, Advances in Treating Textile Effluent*. Prof. Peter Hauser (Ed.), ISBN: 978-953-307-704-8, In Tech.
- [60] Amin, N. K., "Removal of direct blue-106 dye from aqueous solution using new Activated carbons developed from pomegranate peel: Adsorption equilibrium and Kinetics," *J. Hazard. Mater.*, vol. 165, pp. 52, 2009.
- [61] Wellington, S., Pereira, S., Renato, S., and Freire, S., "Azo Dye Degradation by Recycled Waste Zero-Valent Iron Powder," *J. Braz. Chem. Soc.*, vol. 17, pp. 832, 2006.
- [62] Chen, C. C., Chaudhary, A. J., and Grimes, S. M., "Photodegradation of Acid Blue 29 and Ethyl Violet in the Presence/Absence of Sodium Hydroxide and Aluminium Ions," *Environ. Infor. Arch.*, vol. 3, pp. 111, 2005.
- [63] Ranghu, S., and Ahmed, B. C., "Dye Destruction and Simultaneous Generation of Sodium Hydroxide Using a Divided Electrochemical Reactor," *Ind. Eng. Chem. Res.*, vol. 47, pp. 5277, 2008.
- [64] Ghaly, A., Ananthashankar, R., Alhattab, M., and Ramakrishnan, V., "Production, characterization and treatment of textile effluents: a critical review," *J. Chem. Eng. Proc. Technol.*, vol. 5, pp. 1-18, 2014.
- [65] Kehinde, F. O., and Aziz, H. A., "Textile waste water and the advanced oxidative treatment process, an overview," *Int. J. Innovat. Res. Sci. Eng. Technol.*, vol. 3, pp. 15310-15317, 2014.
- [66] Hussein, F. H., "Chemical properties of treated textile dyeing wastewater," *Asi. J. Chem.*, vol. 25, pp. 9393-9400, 2013.
- [67] Upadhye, V. B., and Joshi, S. S., "Advances in wastewater treatment—a review," *Int. J. Chem. Sci. Appl.*, vol. 3, pp. 264-268, 2012.
- [68] Turhan, K., and Turgut, Z., "Decolorization of direct dye in textile wastewater by ozonization in a semi-batch bubble column reactor," *Desalination*, vol. 242, pp. 256-263, 2009.

- [69] Eswaramoorthi, S., Dhanapal, K., and Chauhan, D. S. (2008) *Advances in textile wastewater treatment: the case for UV-Ozonation and membrane bioreactor for common effluent treatment plants in Tirupur*. Tamil Nadu, India.
- [70] Aziz, M. A., –A Text Book of Water Supply Engineering,” pp. 178-182, Hafij book centre, 125 Dhaka, 1994.
- [71] Ayad, M. M., and El-Nasr, A. A., –Adoption of Cationic Dye (Methylene Blue) from Water Using Polyaniline Nanotubes Base,” *J. Phys. Chem. C*, vol. 114, pp. 14377-14383, 2010.
- [72] Bafana, A., Devi, S. S., and Chakrabarti, T., –Azo dyes: past, present and the future,” *Environ. Rev.*, vol. 19, pp. 350–370, 2011.
- [73] Hasnat, M. A., Siddiquey, I. A., and Nuruddin, A., –Comparative Photocatalytic Studies of Degradation of a Cationic and an Anionic Dye,” *Dy. Pigmt.*, vol. 66, pp. 185-188, 2005.
- [74] Athawale, V. D., and Lele, V., –Graft Copolymerization onto Starch. II. Grafting of Acrylic Acid and Preparation of it’s Hydrogels,” *Carbohy. Poly.*, vol. 35, pp. 21-27, 1998.
- [75] Shahid, M., Islam, M., and Mohammad, F., –Recent advancements in natural dye applications: a review,” *J. Clean. Prod.*, vol. 53, pp. 310-331, 2013.
- [76] Robinson, T., McMullan, G., Marchant, R., and Nigam, P., –Remediation of dyes in textile effluent: a critical review on current treatment technologies with a proposed alternative,” *Biores. Technol.*, vol. 77, pp. 247-255, 2001.
- [77] Wu, T., Liu, G., Zhao, J., Hidaka, H., and Serpone, N., –Evidence for H₂O₂ Generation during the TiO₂-Assisted Photodegradation of Dyes in Aqueous Dispersions under Visible Light Illumination,” *J. Phys. Chem. B*, vol. 103, pp. 4862-4863, 1999.
- [78] Brüsweiler, B. J., Küng, S., Bürgi, D., Mural, L., and Nyfeler, E., –Identification of non-regulated aromatic amines of toxicological concern which can be cleaved from azo dyes used in clothing textiles,” *Regul. Toxicol. Pharmacol.*, vol.69, pp. 263-272, 2014.
- [79] Deepak, R., Vandana, M., and Radhey, S. S., –Detoxification of azo dyes in the context of environmental processes,” *Chemosp.*, vol. 155, pp. 591-605, 2016.
- [80] Wai, S., Chi, W. K., Yuen, C. W. M., Shun, W. C., and Kim, H. L., –Effective Photodegradation of Methyl Orange Using Fluidized Bed Reactor Loaded with Cross-

- Linked Chitosan Embedded Nano-CdS Photocatalyst” *Int. J. Chem. Eng.*, vol. 2014, pp. 270946, 2014.
- [81] Konstantinou, I., and Albanis, T., “TiO₂-assisted photocatalytic degradation of azo dyes in aqueous solution: kinetic and mechanistic investigations,” *Appl. Catal. B: Environ.*, vol. 49, pp. 1-14, 2004.
- [82] Fair, G. M., Geyer, J. C., and Okum, D. A. (1966) *Water and Wastewater Engineering*. Wiley, New York.
- [83] Carmen, Z. and Daniela S. (2012) *Textile Organic Dyes Characteristics, Polluting Effects and Separation/Elimination Procedures from Industrial Effluents – A Critical Overview*. Organic Pollutants Ten Years after the Stockholm Convention- Environmental and Analytical Update.
- [84] Naveed, S., Bhatti, I., and Ali, K., “Membrane technology and its suitability for treatment of textile waste water in Pakistan,” *J. Res.(Sci.)*, vol. 17, pp. 155-164, 2006.
- [85] Ramesh, B., Parande, A. K., Raghu, S., and Prem, K. T., “Textile technology. Cotton Textile Processing: Waste Generation and Effluent Treatment,” *J. Cott. Sci.*, Vol.11, pp. 141-153, 2007.
- [86] Blackburn, R. S., “Natural Polysaccharides and their Interactions with Dye Molecules: Applications in Effluent Treatment,” *Environ. Sci. Technol.*, vol. 38, pp. 4905-4909, 2004.
- [87] Matsui, Y., Murase, R., Sanogawa, T., Aoki, N., Mima, S., Inoue, T., and Matsushita, T., “Rapid adsorption pretreatment with submicrometre powdered activated carbon particles before microfiltration,” *W. S. Technol.*, vol.51, pp. 249-256, 2005.
- [88] Bornick H. and Schmidt T. C. (2006) *Amines, In: Organic pollutants in the water cycle. Properties, occurrence, analysis and environmental relevance of polar compounds*. Wiley, Weinheim, Germany.
- [89] Anjaneyulu, Y., Sreedhara, N., and Suman, D. S., “Decolourization of industrial effluents – available methods and emerging technologies – A review,” *Rev. Environ. Sci. Bio/Technol.*, vol. 4, pp. 245-273, 2005.
- [90] Birch, R. R., Biver, C., Campagna, R., Gledhill, W. E., Pagga, U., Steber, J., Reust, H., and Bontinck, W. J., “Screening of chemicals for anaerobic biodegradability,” *Chemosp.*, vol. 19, pp. 1527-1550, 1989.

- [91] Dos, S. A. B., Cervantes, F. J., and Van, L. J. B., –Azo dye reduction by thermophilic anaerobic granular sludge, and the impact of the redox mediator AQDS on the reductive biochemical transformation,” *Appl. Microbiol. Biotechnol.*, vol. 64, pp. 62-69, 2004.
- [92] Tan, N. C. G., Borger, A., Slenders, P., Svitelskaya, A., Lettinga, G., and Field, J. A., –Degradation of azo dye mordant yellow 10 in a subsequential anaerobic and bioaugmented aerobic bioreactor,” *W. Sci. Technol.*, vol.42, pp. 337-344, 2000.
- [93] Gogate, P. R., and Pandit, A. B., –A review of imperative technologies for wastewater treatment I: oxidation technologies at ambient conditions,” *Adv. Environ. Res.*, vol. 8, pp. 501-551, 2004.
- [94] Andreozzi, R., Caprio, V., Insola, A., and Marotta, R., –Advanced oxidation processes (AOP) for water purification and recovery,” *Catal. Tod.*, vol. 53, pp. 51–59, 1999.
- [95] Malato, S., Blanco, J., Maldonado, M. I., Oller, I., Gernjak, W., and Pérez-Estrada, L., –Coupling solar photo-Fenton and biotreatment at industrial scale: Main results of a demonstration plant,” *J. Hazard. Mater.*, vol. 146, pp. 440-446, 2007.
- [96] Oussi, D., Asmae, M., and Esplugas, S., –Removal of aromatic compounds using UV/H₂O₂,” *Rec. Res. Develop. Photochem. Photobiol.*, vol. 1, pp. 77-83, 1997.
- [97] Kopplin, P. S., and Hertkorn, N. K. A., –Structural changes in dissolved soil humic matter during photochemical degradation processes under nitrogen and oxygen atmospheres,” *Environ. Sci. Technol.*, vol. 32, pp. 2531-2541, 1998.
- [98] Benitez, F. J., Heredia, J. B., Acero, J. L., and Rubio, F. J., –Contribution of free radicals to chlorophenols decomposition by several advanced oxidation processes,” *Chemosp.*, vol. 41, pp. 1271-1277, 2000.
- [99] Beltrán, F. J., González, M., and Álvarez, P., –Tratamiento de aguas mediante oxidación avanzada (II): Procesos con peróxido de hidrógeno,” *Ing. Quím.*, vol. 332, pp. 165-169, 1997.
- [100] Glaze, W. H., Kang, J. W., and Chapin, D. H., –The chemistry of water treatment processes involving ozone, hydrogen peroxide and ultraviolet radiation,” *Ozo. Sci. Eng.*, vol. 9, pp. 335-342, 1987.
- [101] Hirvonen, A., Trapido, M., Hentunen, J., and Takharen, J., –Formation of hydroxylated and dimeric intermediates during oxidation of chlorinated phenols in aqueous solution,” *Chemosp*, vol. 41, pp. 1211-1218, 2000.

- [102] Mohamed, A. H., and Ahmed, E. N., "Advanced Oxidation Processes for Textile Wastewater Treatment," *Int. J. Photochem. Photobiol.*, vol. 2, pp. 85-93, 2017.
- [103] Rodríguez, M., Ben, A. N., Contreras, S., Chamarro, E., Gimenez, J., and Esplugas, S., "Iron (III) photooxidation of organic compounds in aqueous solutions," *Appl. Catal. B: Environ.*, vol. 37, pp. 131-137, 2002.
- [104] Malato, S., Blanco, J., Compos, A., Caceres, J., Guillard, C., Herrmann, J. M., and Fernández-Alba, A. R., "Effect of operating parameters on the testing of new industrial titania catalysts at solar pilot plant scale," *Appl. Catal. B: Environ.*, vol. 42, pp. 349-357, 2003.
- [105] Kormann, C., Bahnemann, D. W. and Hoffman, M. R., "Photocatalytic Production of H₂O₂ and Organic Peroxides in Aqueous Suspensions of TiO₂, ZnO and Desert sand," *Environ. Sci. Technol.*, vol. 22, pp. 798-806, 1988.
- [106] Chao, M. T., and Abdul, R. M., "Roles of titanium dioxide and ion-doped titanium dioxide on photocatalytic degradation of organic pollutants (phenolic compounds and dyes) in aqueous solutions: A review," *J. Allo. Comp.*, vol. 509, pp. 1648-1660, 2011.
- [107] Khaki, M. R. D., Shafeeyan, M. S., Raman, A. A. A., Ashri, W. M., and Daud, W., "Application of doped photocatalysts for organic pollutant degradation- A review," *J. Environ. Manage.*, vol. 198, pp. 78-94, 2017.
- [108] Banerjee, S., Dionysiou, D. D., and Pillai, S. C., "Self-Cleaning Applications of TiO₂ by Photo-Induced Hydrophilicity and Photocatalysis," *Appl. Catal. B Environ.*, vol. 176-177, pp. 396-428, 2015.
- [109] Elsalamony, R. A., "Advances in Photo-catalytic Materials for Environmental Applications," *Res. Rev.: J. Mater. Sci.*, vol. 4, pp. 26-50, 2016.
- [110] Gerischer, H., and Heller, A., "Photocatalytic Oxidation of Organic Molecules at TiO₂ Particles by Sunlight in Aerated Water," *J. Electrochem. Sci.*, vol. 139, pp. 113-118, 1992.
- [111] Shavisi, Y., Sharifnia, S., and Mohamadi, Z., "Solar-light-harvesting degradation of aqueous ammonia by CuO/ZnO immobilized on pottery plate: Linear kinetic modeling for adsorption and photocatalysis process," *J. Environ. Chem. Eng.*, vol. 4, pp. 2736-2744, 2016.

- [112] Mitoraj, D., and Kisch, H., –On the mechanism of urea-induced titania modification,” *Chem. A Eur. J.*, vol. 16, pp. 261-269, 2010.
- [113] Özkan, A., Özkan, M. H., Gürkan, R., Akçay, M., and Sökmen, M., –Photocatalytic degradation of a textile azo dye, Sirius Gelb GC on TiO₂ or Ag-TiO₂ particles in the absence and presence of UV irradiation: the effects of some inorganic anions on the photocatalysis,” *J. Photochem. Photobiol. A: Chem.*, vol. 163, pp. 29-35, 2004.
- [114] Mukhlis, M. Z. B., Najnin, F., Rahman, M. M., and Uddin, M. J., –Photocatalytic Degradation of Different Dyes Using TiO₂ with High Surface Area: A Kinetic Study,” *J. Sci. Res.*, vol. 5, pp. 301-314, 2013.
- [115] Ameta, R., Benjamin, S., and Ameta, A., –Photocatalytic degradation of organic pollution: A review,” *Mater. Sci. For.*, vol. 734, pp. 247-272, 2013.
- [116] Lee, S. Y., and Park, S. J., –TiO₂ photocatalyst for water treatment applications,” *J. Ind. Eng. Chem.*, vol. 19, pp. 1761-1769, 2013.
- [117] Xiang, Q., Yu, J., and Wong, P. K., –Quantitative characterization of hydroxyl radicals produced by various photocatalysts,” *J. Coll. Interf. Sci.*, vol. 357, pp. 163-167, 2011.
- [118] Grabowska, E., Reszczyńska, J., and Zaleska, A., –Mechanism of phenol photodegradation in the presence of pure and modified-TiO₂: A review,” *W. Res.*, vol. 46, pp. 5453-5471, 2012.
- [119] Chong, M., Jin, B., Chow, C. and Saint, C., –Recent developments in photocatalytic water treatment technology: A review,” *W. Res.*, vol. 44, pp. 2997-3027, 2010.
- [120] King, D. S., and Nix, R. M., –Thermal Stability and Reducibility of ZnO and Cu/ZnO Catalysts,” *J. Catal.*, vol. 76, pp. 160, 1996.
- [121] Corradi, A. B., –Conventional and Microwave-hydrothermal Synthesis of TiO₂ Nanopowders,” *J. Am. Ceram. Soc.*, vol. 88, pp. 2639-2641, 2005.
- [122] Yan, W., Yiming, H., Qinghua, L., and Maohong, F., –Review of the progress in preparing nano TiO₂: An important 3 environmental engineering material,” *J. Environ. Sci.*, vol. 26, pp. 2139-2177, 2014.
- [123] Nasirian, M., Lin, Y. P., Bustillo, L. C. F., and Mehrvar, M., –Enhancement of photocatalytic activity of titanium dioxide using non-metal doping methods under visible light: a review,” *Int. J. Environ. Sci. Technol.*, vol. 15, pp. 2009, 2032, 2018.

- [124] Varshney, G., Kanel, S. R., Kempisty, D., Varshney, V., Agrawal, A., Sahle, D, Varma, R. S., and Nadagouda, M. N., –Nanoscale TiO₂ films and their application in remediation of organic pollutants,” *Coord. Chem. Rev.*, vol. 306, pp. 43-64, 2016.
- [125] Mukherjee, P. S., and Ray, A. K., –Major Challenges in the Design of a Large-Scale Photocatalytic Reactor for Water Treatment,” *Chem. Eng. Technol.*, vol. 22, pp. 253-260, 1999.
- [126] Serpone, N., Borgarello, E., Harris, R., Cahill, P., and Borgarello, M., –Photocatalysis over TiO₂ supported on a glass substrate,” *Sol. Eng. Mater.*, vol. 14, pp. 121-127, 1986.
- [127] Azeddine, B., and Mostefa, Z., –Photocatalytic activities of TiO₂ layers immobilized on glass substrates by dip-coating technique toward the decolorization of methyl orange as a model organic pollutant,” *J. Environ. Chem. Eng.*, vol. 5, pp. 1565-1574, 2017.
- [128] Byrne, J. A., Eggins, B. R., Brown, N. M. D., McKinney, B., and Rouse, M., –Immobilisation of TiO₂ powder for the treatment of polluted water,” *Appl. Catal. B: Environ.*, vol. 17, pp. 25-36, 1998.
- [129] Fretwell, R., and Douglas, P., –An active, robust and transparent nanocrystalline anatase TiO₂ thin film —preparation, characterisation and the kinetics of photodegradation of model pollutants,” *J. Photochem. Photobiol. A: Chem.*, vol. 143, pp. 229-240, 2001.
- [130] Meiting, G., Hong, Y. H., James, R. B., and Mohamed, G. E. D., –Comparison of Low- and Medium-Pressure Ultraviolet Lamps: Photoreactivation of Escherichia Coli and Total Coliforms in Secondary Effluents of Municipal Wastewater Treatment Plants,” *W. Res.*, vol. 43, pp. 815-21, 2009.
- [131] Halen, W., and Waltar, H., –A very large stereoelectronic effect on acetal cleavage,” *Am. Chem. Soc.*, vol. 104, pp. 4630-4, 1982.
- [132] Fenton, H. J. H., –Oxidation of tartaric acid in presence of iron,” *Chem. Soc.*, vol. 65, pp. 899-910, 1894.
- [133] Stickler, Greg. (2016) *Educational Brief-Solar Radiation and the Earth System*. National Aeronautics and Space Administration.
- [134] Esparza, P., Hernández, T., Borges, M. E., Álvarez-Galván, M. C., Ruiz-Morales, J. C., and Fierro, J. L. G., –TiO₂ modifications by hydrothermal treatment and doping to improve photocatalytic behavior under visible light,” *Catal. Tod.*, vol. 210, pp. 135-141, 2013.

- [135] Cassano, A. E., and Alfano, O. M., "Reaction engineering of suspended solid heterogeneous photocatalytic reactors," *Catal. Tod.*, vol. 58, pp. 167-197, 2000.
- [136] Gaya, U. I., and Abdullah, A. H., "Heterogeneous photocatalytic degradation of organic contaminants over titanium dioxide: A review of fundamentals, progress and problems," *J. Photochem. Photobiol. C: Photochem. Rev.*, vol. 9, pp. 1-12, 2008.
- [137] Nam, W., Kim, J., and Han, G., "Photocatalytic oxidation of methyl orange in a three-phase fluidized bed reactor," *Chemosp.*, vol. 47, pp. 1019-1024, 2002.
- [138] Merabet, S., Bouzaza, A., and Wolbert, D., "Photocatalytic degradation of indole in a circulating upflow reactor by UV/TiO₂ process—Influence of some operating parameters," *J. Hazard. Mater.*, vol. 166, pp. 1244-1249, 2009.
- [139] Wang, Z. C., and Shui, H. F., "Effect of PO₄³⁻ and PO₄³⁻-SO₄²⁻ modification of TiO₂ on its photocatalytic properties," *J. Mol. Catal., A: Chem.*, vol. 263, pp. 20-25, 2007.
- [140] Mozia, S., "Photocatalytic membrane reactors (PMRs) in water and wastewater treatment. A review," *Sep. Purif. Technol.*, vol. 73, pp. 71-91, 2010.
- [141] Tang, C., and Chen, V., "The photocatalytic degradation of reactive black 5 using TiO₂/UV in an annular photoreactor," *W. Res.*, vol. 38, pp. 2775-2781, 2004.
- [142] Ji, T., Yang, F., Lv, Y., Zhou, J., and Sun, J., "Synthesis and visible-light photocatalytic activity of Bi-doped TiO₂ nanobelts," *Mater. Lett.*, vol. 63, pp. 2044-2046, 2009.
- [143] Habibi, M. H., Hassanzadeh, A., and Mahdavi, S., "The effect of operational parameters on the photocatalytic degradation of three textile azo dyes in aqueous TiO₂ suspensions," *J. Photoch. Photobio. A*, vol. 172, pp. 89-96, 2005.
- [144] Rauf, M. A., Meetani, M. A., and Hisaindee, S., "An overview on the photocatalytic degradation of azo dyes in the presence of TiO₂ doped with selective transition metals," *Desal.*, vol. 276, pp. 13-27, 2011.
- [145] Daneshvar, N., Salari, D., and Khataee, A. R., "Photocatalytic degradation of azo dye Acid Red 14 in water: investigation of the effect of operational parameters," *J. Photochem. Photobiol. A: Chem.*, vol. 157, pp. 111-116, 2003.
- [146] Ollis, D. F., Pelizzetti, E., and Serpone, N., "Photocatalyzed Destruction of Water Contaminants," *Environ. Sci. Technol.*, vol. 25, pp. 1523, 1991.

- [147] Muruganandham, M., and Swaminathan, M., –TiO₂–UV photocatalytic oxidation of Reactive Yellow 14: Effect of operational parameters,” *J. Hazard. Mater. B*, vol. 135, pp. 78-86, 2006.
- [148] Songfeng, P., and Hui-Meng, C., –The reduction of graphene oxide”, *Carb.*, vol. 50, pp. 3210-3228, 2012.
- [149] Hummers, W. S., and Offeman, R. E., –Preparation of graphitic oxide”, *J. Am. Chem. Soc.*, vol. 80, pp. 1339-1339, 1958.
- [150] Dreyer, D. R., Park, S., Bielawski, C. W., and Ruoff, R. S., –The chemistry of graphene oxide”, *Chem. Soc. Rev.*, vol. 39, pp. 228-240, 2010.
- [151] Baojun, L., Huaqiang, C., Jin, S., Meizhen, Q., and Jamie, H. W., –Superparamagnetic Fe₃O₄ nanocrystals@graphene composites for energy storage devices”, *J. mater. Chem.*, vol. 21, pp. 5069-5075, 2011.
- [152] Ayrat, M. D., and James, M. T., –Mechanism of graphene oxide formation”, *ACS Nan.*, vol. 8, pp. 3060-3068, 2014.
- [153] Sing, K., –The use of nitrogen adsorption for the characterization of porous materials,” *Coll. Surf. A: Physicochem. Eng. Asp.*, vol. 187-188, pp. 3-9, 2001.
- [154] Ali, M., Parvain, G., and Samad, M. T., –Synthesis of nanosized TiO₂ powder by Sol-Gel method in acidic conditions,” *J. Ir. Chem. Res.*, vol. 2, pp. 145-149, 2009.
- [155] Siti, A. I., and Srimala, S., *Proceedings of ICXRI 2010 International Conference on X-Rays & Related Techniques in Research & Industry*, June 9 –10, 2010, pp. 84-87.
- [156] Sharmila, R. D., Venkatesh, D. R., and Rajeshwari, D. S., –Synthesis of Titanium Dioxide Nanoparticles by Sol-Gel Technique,” *Int. J. Innov. Res. Sci. Eng. Technol.*, vol. 3, pp. 15206-15211, 2014.
- [157] Wetchakun, N., and Phanichphant, S., –Effect of temperature on the degree of anatase–rutile transformation in titanium dioxide nanoparticles synthesized by the modified sol–gel method,” *Curr. Appl. Phys.*, vol. 8, pp. 343-346, 2008.
- [158] Sakthivel, S., Shankar, M. V., Palanichamy, M., Arabindoo, B., Bahnemann, D. W., and Murugesan, V., –Enhancement of photocatalytic activity by metal deposition: characterisation and photonic efficiency of Pt, Au and Pd deposited on TiO₂ catalyst,” *W. Res.*, vol.38, pp. 3001-3008, 2004.

- [159] Madhusudan R. K., Manorama, S. V., and Ramachandra R. A., –Bandgap Studies on Anatase Titanium Dioxide Nanoparticles,” *Mater. Chem. Phys.*, vol. 78, pp. 239-245, 2002.
- [160] Linsebigler, A. L., Lu, G. Q., and Yates, J. T., –Photocatalysis on TiO₂ surfaces: Principles, mechanisms, and selected results,” *Chem. Rev.*, vol. 95, pp. 735-758, 1995.
- [161] Method, U. T., Wongwanwattana, P., Sompan, T., Saipin, T., and Krongkitsiri, P., –Preparation and Characterization of Nano-TiO₂ Thin Films by Sol-gel Dip-coating Method,” *CMU. J. Nat. Sci.*, vol. 7, pp. 129, 2008.
- [162] Rab, N., Chong, F. K., Mohamed, H. I., and Lim, W. H., –Preparation of TiO₂ nanoparticles by hydrolysis of TiCl₄ using water and glycerol solvent system,” *IOP Conf. Ser.: J. Phys.: Conf. Ser.*, vol. 1123, pp. 012065, 2018.
- [163] Kotani, Y., Matoda, T., Marsuda, A., Kogure, T., Tatsumisago, M., and Minami, T., –Anatase nanocrystal-dispersed thin films via sol–gel process with hot water treatment: effects of poly(ethylene glycol) addition on photocatalytic activities of the films,” *J. Mater. Chem.*, vol. 11, pp. 2045-2048, 2001.
- [164] Sebastian, M., Bozena, P., "The influence of heat treatment temperature on the morphology of TiO₂ Sol-Gel coatings," *Adv. Mater. Sci.*, vol. 4, no. 2(4), 2003.
- [165] Cullity, B. D., and Stock. S. R. (2001) *Elements of X-ray Diffraction*. 3rd Ed, Prentice-Hall., New Jersey.
- [166] Wu, C., Yue, Y., and Deng, X., –Investigation on the synergetic effect between anatase and rutile nanoparticles in gas-phase photocatalytic oxidations,” *Catal. Tod.*, vol. 93/95, pp. 863-869, 2004.
- [167] Yahia, C. L., Yahiaoui, I., Aissani, B. F., Madi, K., Benmehdi, N., Fourcade, F., and Amrane, A., –Heat Attachment Method for the Immobilization of TiO₂ on Glass Plates: Application to Photodegradation of Basic Yellow Dye and Optimization of Operating Parameters, Using Response Surface Methodology,” *Ind. Eng. Chem. Res.*, vol. 53, pp. 3813-3819, 2014.
- [168] Vaez, M., Moghaddam, A. Z., Mahmoodi, N. M., and Alijani, S., –Decolorization and degradation of acid dye with immobilized titania nanoparticles,” *Pro.. Saf. Environ. Protect.*, vol. 90, pp. 56-64, 2012.

- [169] Ökte, A. N., and Yılmaz, Ö., –Photodecolorization of methyl orange by yttrium incorporated TiO₂ supported ZSM-5,” *Appl. Catal. B: Environ.*, vol. 85, pp. 92-102, 2008.
- [170] Jiang, W., Joens, J. A., Dionysiou, D. D., and O'Shea, K. E., –Optimization of photocatalytic performance of TiO₂ coated glass microspheres using response surface methodology and the application for degradation of dimethyl phthalate,” *J. Photochem. Photobiol. A: Chem.*, vol. 262, pp. 7-13, 2013.
- [171] Yu, J. C., Yu, J., Zhang, L., and Ho, W., –Enhancing effects of water content and ultrasonic irradiation on the photocatalytic activity of nano-sized TiO₂ powders,” *J. Photochem. Photobiol. A: Chem.*, vol.148, pp. 263-271, 2002.
- [172] Colón, G., Hidalgo, M. C., Munuera, G., Ferino, I., Cutrufello, M. G., and Navío, J. A., –Structural and surface approach to the enhanced photocatalytic activity of sulfated TiO₂ photocatalyst,” *Appl. Catal. B: Environ.*, vol. 63, pp. 45-59, 2006.
- [173] Venkatachalam, N., Palanichamy, M., and Murugesan, V., –Sol-gel preparation and characterization of nanosize TiO₂: Its photocatalytic performance,” *Mater. Chem. Phys.*, vol. 104, pp. 454–459, 2007.
- [174] López, R., and Gómez, R., –Band-gap energy estimation from diffuse reflectance measurements on sol-gel and commercial TiO₂: A comparative study,” *J. Sol-Gel Sci. Technol.*, vol. 61, pp. 1–7, 2012.
- [175] Rab, N., Chong, F. K., Mohamed, H. I., and Lim, W. H., –Preparation of TiO₂ nanoparticles by hydrolysis of TiCl₄ using water and glycerol solvent system,” *J. Phys. Conf. Ser.*, vol. 1123, pp. 012065, 2018.
- [176] Tipparach, U., Wongwanwatthana, P., Sompan, T., and Saipin, T., –Preparation and Characterization of Nano-TiO₂ Thin Films by Sol-gel Dip-coating Method,” *Nanotechnol.*, vol. 7, pp. 129–136, 2008.
- [177] Vijayalakshmi, R., and Rajendran, V., –Synthesis and characterization of nao-TiO₂ via different methods,” *Arch. Appl. Sci. Res.*, vol. 4, pp. 1183–1190, 2012.
- [178] Yang, X., Ma, F., Li, K., Guo, Yingna, Hu, J., Li, W., Huo, M., and Guo, Y., –Mixed phase titania nanocomposite codoped with metallic silver and vanadium oxide: New efficient photocatalyst for dye degradation,” *J. Hazard. Mater.*, vol. 175, pp. 429–438, 2010.

- [179] Zhang, W., Zhang, Y., Yang, K., Yang, Y., Jia, J., and Guo, L., –Photocatalytic performance of SiO₂/CNOs/TiO₂ to accelerate the degradation of rhodamine B under visible light,” *Nanomater.*, vol. 9, pp. 1671, 2019.
- [180] Sugapriya, S., Sriram, R., and Lakshmi, S., –Effect of annealing on TiO₂ nanoparticles,” *Optik- Int. J. Lig. Elect. Opt.*, vol. 124, pp. 4971-5, 2013.
- [181] You, Y. F., Xu, C. H., Xu, S. S., Cao, S., Wang, J. P., Huang, Y. B., and Shi, S. Q., –Structural characterization and optical property of TiO₂ powders prepared by the sol-gel method,” *Ceram. Int.*, vol. 40, pp. 8659–8666, 2014.
- [182] Šegota, S., Čurković, L., Ljubas, D., Svetličić, V., Houra, I.F., and Tomašić, N., –Synthesis, characterization and photocatalytic properties of sol-gel TiO₂ films,” *Ceram. Int.*, vol. 37, pp. 1153–1160, 2011.
- [183] Behnajady, M. A., Eskandarloo, H., Modirshahla, N., and Shokri, M., –Investigation of the effect of sol-gel synthesis variables on structural and photocatalytic properties of TiO₂ nanoparticles,” *Desal.*, vol. 278, pp. 10–17, 2011.
- [184] Park, N. G., Van De Lagemaat, J., and Frank, A. J., –Comparison of dye-sensitized rutile- and anatase-based TiO₂ solar cells,” *J. Phys. Chem. B.*, vol. 104, pp. 8989–8994, 2000.
- [185] Park, N. G., Lagemaat, J. V., and Frank, A. J., –Comparison of dye-sensitized rutile and anatase-based TiO₂ solar cells,” *J. Phys. Chem. B.*, vol. 104, pp. 8989-8994, 2000.
- [186] Park, N. G., Schlichthörl, G., Lagemaat, J. V., Cheong, H. M., Mascarenhas, A., and Frank, A. J., –Dye-sensitized TiO₂ solar cells: structural and photoelectrochemical characterization of nanocrystalline electrodes formed from the hydrolysis of TiCl₄,” *J. Phys. Chem. B.*, vol. 103, pp. 3308-3314, 1999.
- [187] Yu, J. G., Su, Y. R., and Cheng, B., –Template-free fabrication and enhanced photocatalytic activity of hierarchical macro-/mesoporous titania,” *Adv. Funct. Mater.*, vol. 17, pp. 1984-1990, 2007.
- [188] Yin, H., Wada, Y., Kitamura, T., Kambe, S., Murasawa, S., Mori, H., Sakata, T., and Yanagida, S., –Hydrothermal synthesis of nanosized anatase and rutile TiO₂ using amorphous phase TiO₂,” *J. Mater. Chem.*, vol. 11, pp. 1694, 2001.
- [189] Yoldas, B. E., –Hydrolysis of titanium alkoxides and effects of hydrolytic poly condensation parameters,” *J. Mater. Sci.*, vol. 21, pp. 1087-1092, 1984.

- [190] Yoldas, B. E., "Hydrolysis of titanium alkoxide and effects of hydrolytic polycondensation parameters," *J. Mater. Sci.*, vol. 21, pp. 1087–1092, 1986.
- [191] Bosc, F., Lacroix, D. P., and Ayral, A., "TiO₂ anatase-based membranes with hierarchical porosity and photocatalytic properties," *J. Coll. Interf. Sci.*, vol. 304, pp. 545-8, 2006.
- [192] Helen, B., Daphne, H., Changseok, H., Dionysios, D. D., Carlos, N., and Ángeles, B., "Degradation of 1,4-dioxane from industrial wastewater by solar photocatalysis using immobilized NF-TiO₂ composite with monodisperse TiO₂ nanoparticles," *Appl. Catal. B: Environ.*, vol. 180, pp. 44-52, 2016.
- [193] Viana, V.F., and Soares, N.D.S.M., "Synthesis and characterization of TiO₂ Nanoparticles," *Ceram. Int.*, vol. 36, pp. 2047–2053, 2010.
- [194] He, K., Zhao, C., Zhao, G., and Han, G., "Effects of pore size on the photocatalytic activity of mesoporous TiO₂ prepared by a sol–gel process," *J. Sol-Gel Sci. Technol.*, vol. 75, pp. 557–563, 2015.
- [195] Li, J., Xu, J., Dai, W. L., Li, H., and Fan, K., "Direct hydro-alcohol thermal synthesis of special core-shell structured Fe-doped titania microspheres with extended visible light response and enhanced," *Appl. Catal. B: Environ.*, vol. 85, pp. 162-170, 2009.
- [196] Neon, M. H. K., and Islam, M. S., "MoO₃ and Ag co-synthesized TiO₂ as a novel heterogeneous photocatalyst with enhanced visible-light-driven photocatalytic activity for methyl orange dye degradation," *Environ. Nanotechnol., Monitor. & Manage.*, vol. 12, pp. 100244, 2019.
- [197] Hyeok, C., Elias, S., and Dionysios, D. D., "Photocatalytic TiO₂ films and membranes for the development of efficient wastewater treatment and reuse systems," *Desal.*, vol. 202, pp. 199-206, 2007.
- [198] Tawfik, A., Saleh, V., and Gupta, K., "Photo-catalyzed degradation of hazardous dye methyl orange by use of a composite catalyst consisting of multi-walled carbon nanotubes and titanium dioxide," *J. Coll. Interf. Sci.*, vol. 371, pp. 101-106, 2012.
- [199] Veronika, P., Minoo, T., Milada, V., and Urška, L. Š., "Photocatalytic degradation of b-blockers by using immobilized titania/ silica on glass slides," *J. Photochem. Photobiol. A: Chem.*, vol. 305, pp. 19-28, 2015.

- [200] Jian, H., Yurong, H., Li, W., Yimin, H., and Baocheng, J., "Bifunctional Au@TiO₂ core-shell nanoparticle films for clean water generation by photocatalysis and solar evaporation," *Ener. Conver. Manage.*, vol. 132, pp. 452-459, 2017.
- [201] Noorjahan, M., Pratap, R. M., Durga, K. V., Lavédrine, B., Boule, P., and Subrahmanyam, M., "Photocatalytic degradation of H-acid over a novel TiO₂ thin Film fixed bed reactor and in aqueous suspensions," *J. Photochem. Photobiol. A: Chem.*, vol. 156, pp. 179-187, 2003.
- [202] Valtierra, J. M., Servín, J. G., Reyes, C. F., and Calixto, S., "The photocatalytic application and regeneration of anatase thin films with embedded commercial TiO₂ particles deposited on glass microrods," *Appl. Surf. Sci.*, vol. 252, pp. 3600-3608, 2006.
- [203] Niu, P., and Hao, J., "Photocatalytic degradation of methyl orange by titanium dioxide-decatungstate nanocomposite films supported on glass slides," *Coll. Surf. A*, vol. 431, pp. 127-132, 2013.
- [204] Toor, A. P., Verma, A., Singh, V., Jotshi, C. K., and Bajpai, P. K., "Treatment of bleaching effluents from the pulp and paper industry by photocatalytic oxidation," *Tap. J.*, vol. 6, pp. 9-13, 2007.
- [205] Haque, M. M., and Muneer, M., "Heterogeneous photocatalysed degradation of a herbicide derivative, isoproturon in aqueous suspensions of titanium dioxide," *J. Environ. Manage.*, vol. 69, pp. 169-176, 2003.
- [206] Zhu, Y., Zhang, L., Wang, L., Fu, Y., and Cao, L., "The preparation and chemical structure of TiO₂ film photocatalyst supported on stainless steel using the sol-gel method," *J. Mater. Chem.*, vol. 11, pp. 1864-1868, 2001.
- [207] Chen, Y., and Dionysiou, D. D., "Effect of calcination temperature on the photocatalytic activity and adhesion of TiO₂ films prepared by the P-25 powder-modified sol-gel method," *J. Mol. Catal. A: Chem.*, vol. 244, pp. 73-82, 2006.
- [208] Chen, Y., and Dionysiou, D. D., "A comparative study on physicochemical properties and photocatalytic behavior of macroporous TiO₂-P25 composite films and macroporous TiO₂ films coated on stainless steel substrate," *Appl. Catal. A: Gen.*, vol. 317, pp. 129-137, 2007.
- [209] Elmira, P., Mehdi, R., and Mokhtar, A., "Carbon and CNT fabricated carbon substrates for TiO₂ nanoparticles immobilization with industrial perspective of continuous

- photocatalytic elimination of dye molecules,” *J. Indus. Eng. Chem.*, vol.55, pp. 149-163, 2017.
- [210] Sampaio, M. J., Silva, C. G., Silva, A. M. T., Vilar, V. J. P., Boaventura, R. A. R., and Faria, J. L., –Photocatalytic activity of TiO₂-coated glass raschig rings on the degradation of phenolic derivatives under simulated solar light irradiation,” *Chem. Eng. J.*, vol. 224, pp. 32–38, 2013.
- [211] Kaur, J., and Singhal, S., –Heterogeneous photocatalytic degradation of rose bengal: Effect of operational parameters,” *Phys. B: Condens. Matter.*, vol. 450, pp. 49–53, 2014.
- [212] Chen, Y., and Dionysiou, D. D., —A comparative study on physicochemical properties and photocatalytic behavior of macroporous TiO₂-P25 composite films and macroporous TiO₂ films coated on stainless steel substrate,” *Appl. Catal. A: Gen.*, vol. 317, pp. 129–137, 2007.
- [213] Bestetti, M., Sacco, D., Brunella, M. F., Franz, S., Amadelli, R., and Samiolo, L., –Photocatalytic degradation activity of titanium dioxide sol-gel coatings on stainless steel wire meshes,” *Mater. Chem. Phys.*, vol. 124, pp. 1225–1231, 2010.
- [214] Zayani, G., Bousselmi, L., Mhenni, F., and Ghrabi, A., –Solar photocatalytic degradation of commercial textile azo dyes: Performance of pilot plant scale thin film fixed-bed reactor,” *Desal.*, 246, 344–352, 2009.
- [215] Zuo, R., Du, G., Zhang, W., Liu, L., Liu, Y., Mei, L., and Li, Z., –Photocatalytic degradation of methylene blue using TiO₂ impregnated diatomite,” *Adv. Mater. Sci. Eng.*, vol. 2014, pp. 170148, 2014.
- [216] Kaur, J., and Singhal, S., –Heterogeneous photocatalytic degradation of rose bengal: effect of operational parameters,” *Physica. B*, vol. 450, pp. 49-53, 2014.
- [217] Espino, E. M. R., Fernandez, R. C., Gonzalez, D. O. M., Fernandez, H. D., and Dona, R. J. M., –Enhancement of stability and photoactivity of TiO₂ coatings on annular glass reactors to remove emerging pollutants from water,” *Chem. Eng. J.*, vol. 279, pp. 488-497, 2015.
- [218] Wang, Q., Chen, X., Yu, K., Zhang, Y., and Cong, Y., –Synergistic photosensitized removal of Cr(VI) on amorphous TiO₂ under visible light irradiation,” *J. Hazard. Mater.*, vol. 246–247, pp.135-144, 2013.

- [219] Leghari S. A. K., Shamaila, S., Tian, B., Chen, F., and Zhang, J., –Comparative studies of operational parameters of degradation of azo dyes in visible light by highly efficient WO_x/TiO₂ photocatalyst,” *J. Hazard. Mater.*, vol. 177, pp. 781-791, 2010.
- [220] Zhu, H., Jiang, R., Fu, Y., Guan, Y., Yao, J., Xiao, L., and Zeng, G., –Effective photocatalytic decolorization of methyl orange utilizing TiO₂/ZnO/chitosan nanocomposite films under simulated solar irradiation,” *Desal.*, vol. 286, pp. 41-48, 2012.
- [221] Jiang, W., Joens, J.A., Dionysiou, D.D., and O’Shea, K.E., –Optimization of photocatalytic performance of TiO₂ coated glass microspheres using response surface methodology and the application for degradation of dimethyl phthalate,” *J. Photochem. Photobiol. A: Chem.*, vol. 262, pp. 7–13, 2013.
- [222] Niu, P., and Hao, J., –Photocatalytic degradation of methyl orange by titanium dioxide-decatungstate nanocomposite films supported on glass slides,” *Coll. Surf. A: Physicochem. Eng. Asp.*, vol. 431, pp. 127–132, 2013.
- [223] Dionysiou, D. D., Suidan, M. T., Bekou, E., Baudin, I., and Laîné, J. M., –Effect of ionic strength and hydrogen peroxide on the photocatalytic degradation of 4-chlorobenzoic acid in water,” *Appl. Catal. B: Environ.*, vol. 26, pp. 153–171, 2000.
- [224] Daneshvar, N., Salari, D., and Khataee, A. R., –Photocatalytic degradation of azo dye acid red 14 in water: Investigation of the effect of operational parameters,” *J. Photochem. Photobiol. A: Chem.*, 157, 111–116, 2003.
- [225] Daneshvar, N., Hejazi, M. J., Rangarany, B., and Khataee, A. R., –Photocatalytic Degradation of an Organophosphorus Pesticide Phosalone in Aqueous Suspensions of Titanium Dioxide,” *J. Environ. Sci. Heal. - Part B Pestic. Food Contam. Agric. Wastes*, vol. 39, pp. 285–296, 2004.
- [226] Daneshvar, N., Rabbani, M., Modirshahla, N., and Behnajady, M. A., –Photooxidative degradation of acid red 27 (AR27): Modeling of reaction kinetic and influence of operational parameters,” *J. Environ. Sci. Heal. – P. A Toxic/Hazar. Subst. Environ. Eng.*, vol. 39, pp. 2319–2332, 2004.

APPENDIX

Appendix A: BET Isotherm Study

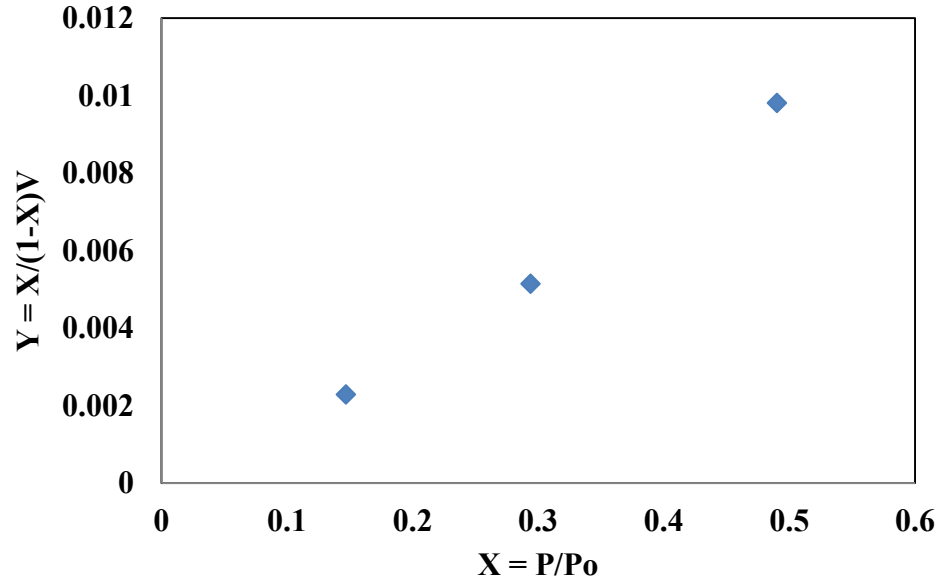


Figure A-1: Plot of BET isotherm of standard silica-alumina ($\text{SiO}_2\text{-Al}_2\text{O}_3$)

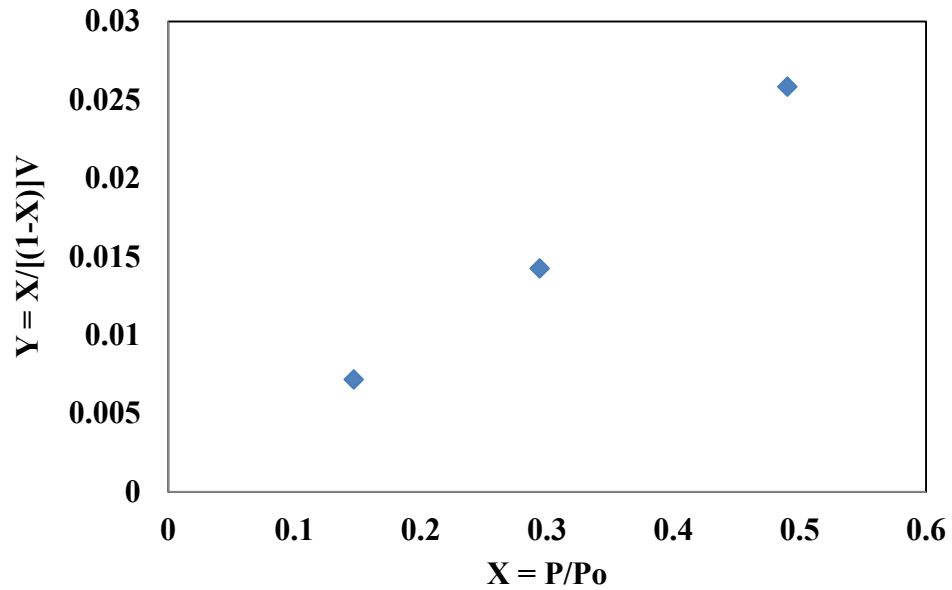


Figure A-2: Plot of BET isotherm of TiO_2 nanoparticle with hydrolysis

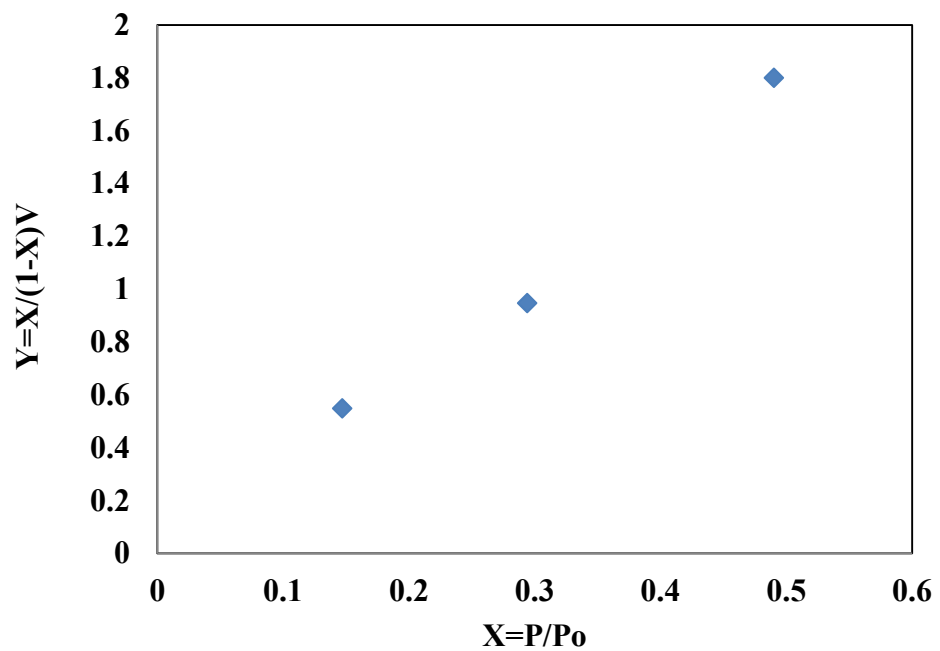


Figure A-3: Plot of BET isotherm of TiO₂ nanoparticle without hydrolysis

Appendix B: Reaction Kinetic Study

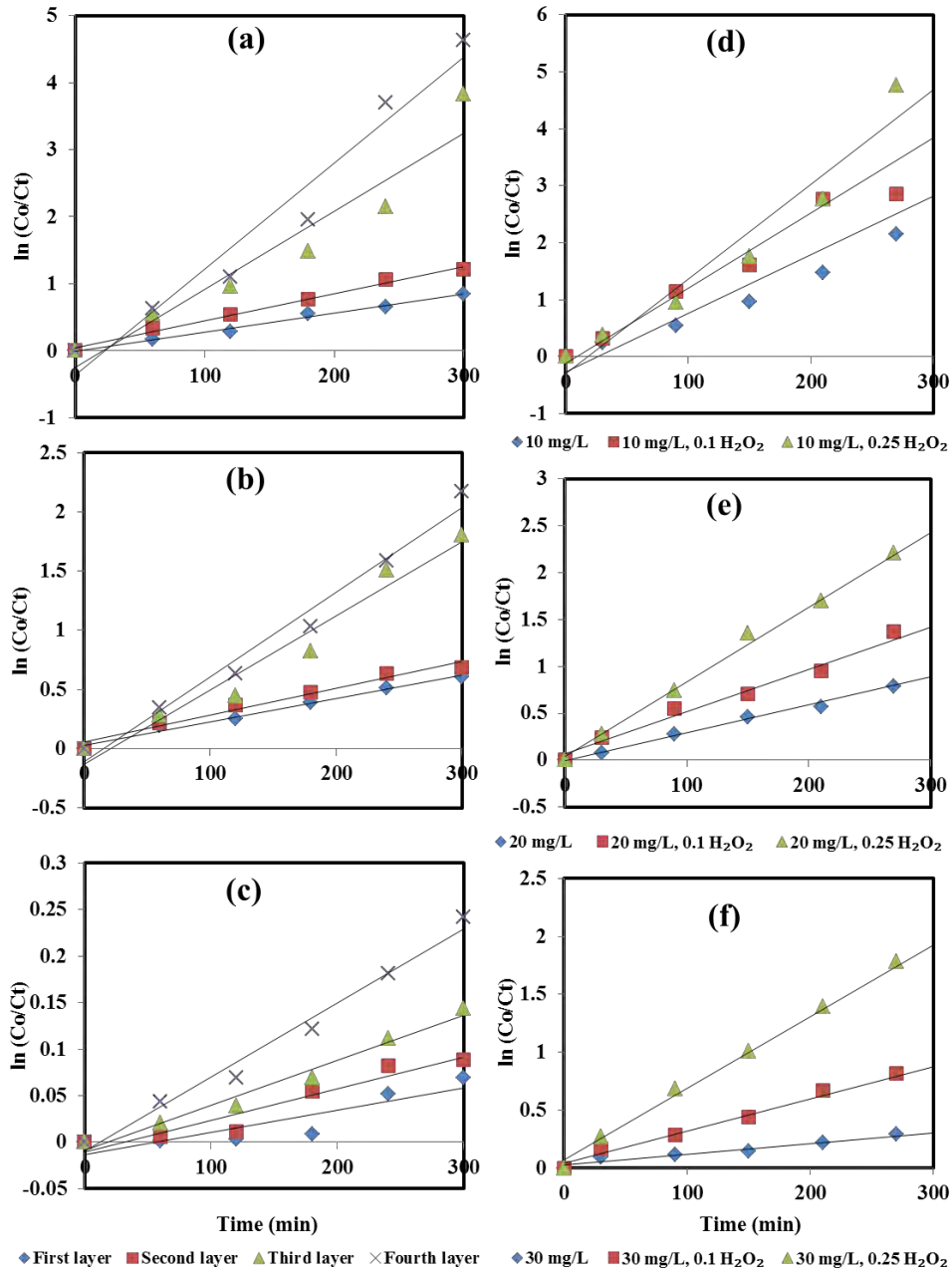


Figure B-1: Pseudo-first-order reaction kinetics of MO dye removal in presence of solar irradiation (a) BG reactor, (b) CCBG reactor, and (c) SWM (Experimental condition: 1st, 2nd, 3rd, and 4th layer of TiO₂ immobilized in all reactors: 60 mg, 90 mg, 120 mg, and 150 mg, pH:6.2, initial MO dye conc.: 10 mg/L); BG reactor (d), (e), and (f) (Experimental condition: 3rd layer of TiO₂ immobilized: 120 mg, pH:6.2, MO dye conc.: 10, 20, and 30 mg/L, H₂O₂: 0.1 mL, and 0.25 mL)

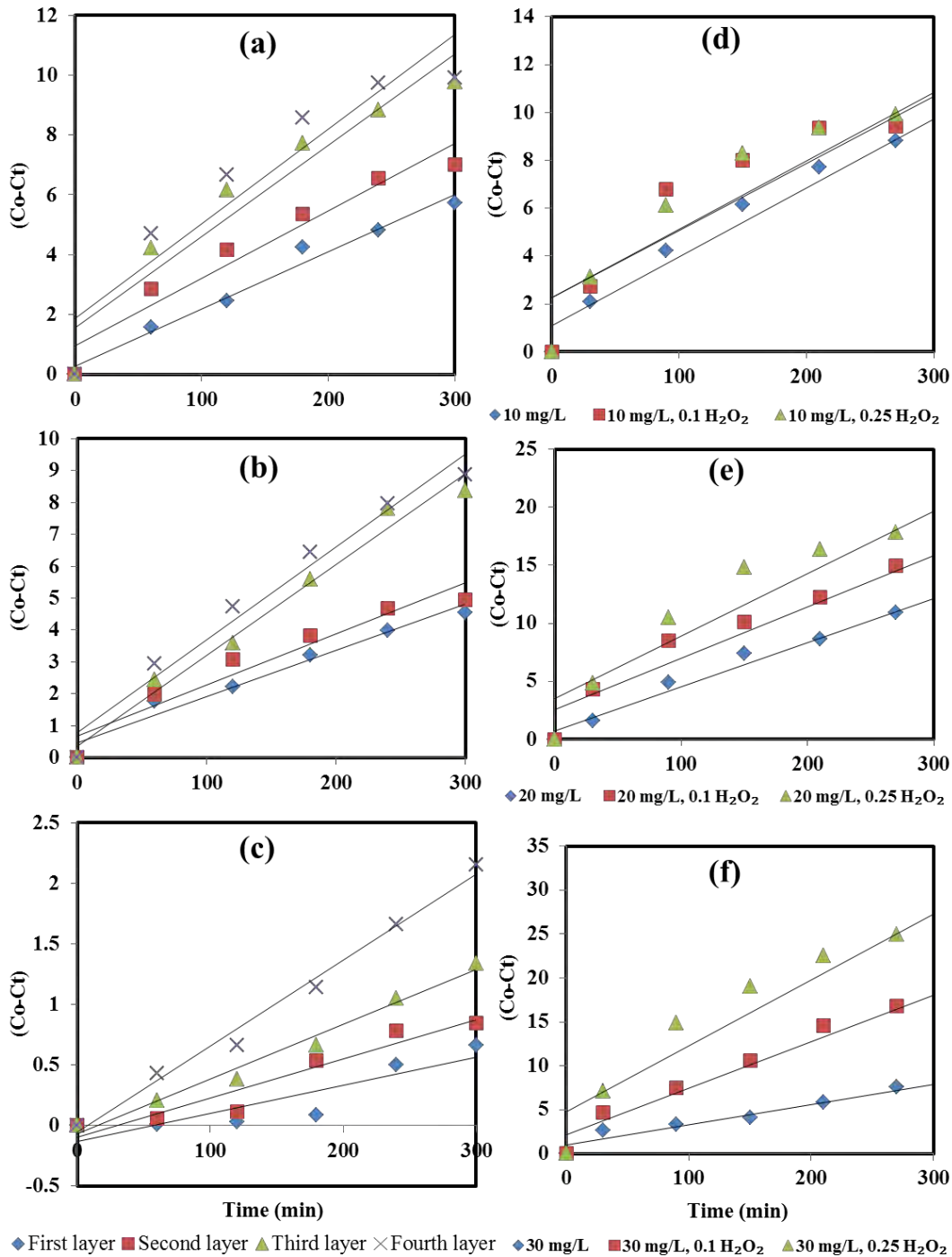


Figure B-2: Zero-order reaction kinetics of MO dye removal in presence of solar irradiation (a) BG reactor, (b) CCBG reactor, and (c) SWM (Experimental condition: 1st, 2nd, 3rd, and 4th layer of TiO₂ immobilized in all reactors: 60 mg, 90 mg, 120 mg, and 150 mg, pH:6.2, initial MO dye conc.: 10 mg/L); BG reactor (d), (e), and (f) (Experimental condition: 3rd layer of TiO₂ immobilized: 120 mg, pH:6.2, MO dye conc.: 10, 20, and 30 mg/L, H₂O₂: 0.1 mL, and 0.25 mL)

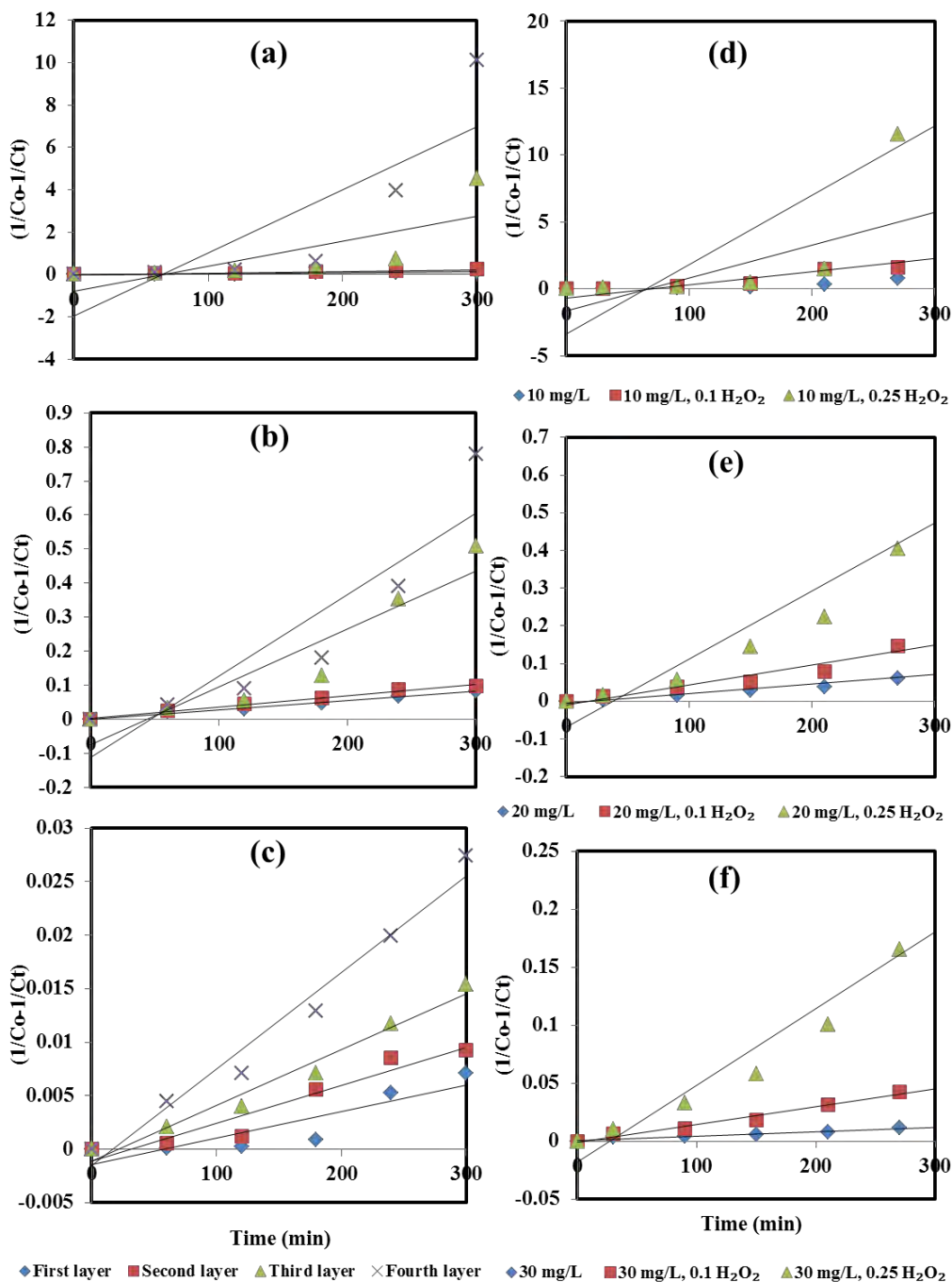


Figure B-3: Second-order reaction kinetics of MO dye removal in presence of solar irradiation (a) BG reactor, (b) CCBG reactor, and (c) SWM (Experimental condition: 1st, 2nd, 3rd, and 4th layer of TiO₂ immobilized in all reactors: 60 mg, 90 mg, 120 mg, and 150 mg, pH:6.2, initial MO dye conc.: 10 mg/L); BG reactor (d), (e), and (f) (Experimental condition: 3rd layer of TiO₂ immobilized: 120 mg, pH:6.2, MO dye conc.: 10, 20, and 30 mg/L, H₂O₂: 0.1 mL, and 0.25 mL)

Table B-4: Summary of kinetic parameters of MO dye removal

Surface	Immobilized condition	Operating condition	Zero-order		First-order		Second-order	
			R ²	k _o (mg/L . 1/min)	R ²	k ₁ (1/min)	R ²	k ₂ (L/mg.1/min)
BG	1 st layer TiO ₂ (g)	10 mg/L, pH 6.2	0.979	0.0192	0.989	0.0029	0.974	4×10 ⁻⁴
	2 nd layer TiO ₂ , (g)	10 mg/L, pH 6.2	0.938	0.0226	0.991	0.004	0.982	8×10 ⁻⁴
	3 rd layer TiO ₂ , (g)	10 mg/L, pH 6.2	0.917	0.0306	0.919	0.0117	0.571	118×10 ⁻⁴
	4 th layer TiO ₂ , (g)	10 mg/L, pH 6.2	0.880	0.0317	0.955	0.0158	0.691	298×10 ⁻⁴
CCBG	1 st layer TiO ₂ (g)	10 mg/L, pH 6.2	0.964	0.0145	0.986	0.002	0.989	3×10 ⁻⁴
	2 nd layer TiO ₂ , (g)	10 mg/L, pH 6.2	0.933	0.016	0.972	0.0023	0.991	3×10 ⁻⁴
	3 rd layer TiO ₂ , (g)	10 mg/L, pH 6.2	0.982	0.0285	0.959	0.0062	0.869	17×10 ⁻⁴
	4 th layer TiO ₂ , (g)	10 mg/L, pH 6.2	0.971	0.0291	0.979	0.0071	0.829	24×10 ⁻⁴
SWM	1 st layer TiO ₂ (g)	10 mg/L, pH 6.2	0.794	0.0023	0.793	0.0002	0.791	0.22×10 ⁻⁴
	2 nd layer TiO ₂ , (g)	10 mg/L, pH 6.2	0.923	0.0032	0.922	0.0003	0.922	0.4×10 ⁻⁴
	3 rd layer TiO ₂ , (g)	10 mg/L, pH 6.2	0.983	0.0045	0.978	0.0005	0.973	0.5×10 ⁻⁴
	4 th layer TiO ₂ , (g)	10 mg/L, pH 6.2	0.988	0.0071	0.982	0.0008	0.973	0.9×10 ⁻⁴
BG	3 rd layer TiO ₂ , (g)	20 mg/L, pH 6.2	0.982	0.0379	0.994	0.003	0.959	3×10 ⁻⁴
	3 rd layer TiO ₂ , (g)	30 mg/L, pH 6.2	0.955	0.0231	0.965	0.0009	0.969	0.4×10 ⁻⁴
	3 rd layer TiO ₂ , (g)	10 mg/L, pH 6.2, 0.1 mL H ₂ O ₂	0.818	0.028	0.958	0.0132	0.549	246×10 ⁻⁴
	3 rd layer TiO ₂ , (g)	10 mg/L, pH 6.2, 0.25 mL H ₂ O ₂	0.842	0.0287	0.966	0.0166	0.721	517×10 ⁻⁴

3 rd layer TiO ₂ , (g)	20 mg/L, pH 6.2, 0.1 mL H ₂ O ₂	0.926	0.0443	0.985	0.0045	0.951	5×10 ⁻⁴
3 rd layer TiO ₂ , (g)	20 mg/L, pH 6.2, 0.25 mL H ₂ O ₂	0.875	0.0538	0.997	0.0079	0.911	18×10 ⁻⁴
3 rd layer TiO ₂ , (g)	30 mg/L, pH 6.2, 0.1 mL H ₂ O ₂	0.961	0.0531	0.989	0.0028	0.987	2×10 ⁻⁴
3 rd layer TiO ₂ , (g)	30 mg/L, pH 6.2, 0.25 mL H ₂ O ₂	0.897	0.075	0.995	0.0062	0.954	7×10 ⁻⁴
